ESCOLA DE CIÊNCIAS
PROGRAMA DE PÓS-GRADUAÇÃO EM BIOLOGIA CELULAR E MOLECULAR
MESTRADO EM BIOLOGIA CELULAR E MOLECULAR

JÚLIA CRISPIM DA FONTOURA

DETERMINAÇÃO DE EFEITO DE DROGAS ANTITUMORAIS *IN VITRO* EM DIFERENTES ESTRATÉGIAS DE CULTURA CELULAR

Porto Alegre
2019

Júlia Crispim da Fontoura

Determinação de efeito de drogas antitumorais *in vitro* em diferentes estratégias de cultura celular

Dissertação apresentada como requisito parcial para a obtenção do grau de Mestre pelo Programa de Pós-Graduação em Biologia Celular e Molecular da Faculdade de Ciências Biológicas da Pontifícia Universidade Católica do Rio Grande do Sul.

Orientador: Prof. Dr. Moisés Bauer

Coorientadores: Profª. Drª. Cristina Bonorino

Drª. Michelle Stumpf Viegas

Porto Alegre

2019

Júlia Crispim da Fontoura

Determinação de efeito de drogas antitumorais *in vitro* em diferentes estratégias de cultura celular

Dissertação apresentada como requisito parcial para a obtenção do grau de Mestre pelo Programa de Pós-Graduação em Biologia Celular e Molecular da Faculdade de Ciências Biológicas da Pontifícia Universidade Católica do Rio Grande do Sul.

Aprovada em: ___ de _____ de _____

Banca Examinadora:

Prof[a]. Dr[a]. Fernanda Morrone – PUCRS

Prof Dr. Guido Lenz – UFRGS

Prof. Dr. José Mauro Granjeiro – UFRJ - INMETRO

Porto Alegre

2019

Ficha Catalográfica

F684d Fontoura, Júlia Crispim da

Determinação de efeito de drogas antitumorais in vitro em diferentes estratégias de cultura celular / Júlia Crispim da Fontoura . – 2019.
94 p.
Dissertação (Mestrado) – Programa de Pós-Graduação em Biologia Celular e Molecular, PUCRS.

Orientador: Prof. Dr. Moisés Bauer.
Co-orientadora: Profa. Dra. Cristina Bonorino.
Co-orientadora: Profa. Dra. Michelle Stumpf Viegas.

1. Câncer. 2. HspBP1. 3. Cultura 3D. 4. Eletrofiação. 5. SCPL. I. Bauer, Moisés. II. Bonorino, Cristina. III. Título.

Elaborada pelo Sistema de Geração Automática de Ficha Catalográfica da PUCRS
com os dados fornecidos pelo(a) autor(a).
Bibliotecária responsável: Salete Maria Sartori CRB-10/1363

AGRADECIMENTOS

Primeiramente gostaria de agradecer a minha orientadora Cristina Bonorino por todo apoio, conhecimento e por ter me trazido para esse mundo da imunologia e biologia celular e molecular. Ao prof. Moisés Bauer pela disponibilidade e suporte.

Ao Christian Viezzer que me mostrou ainda na iniciação cientifica o quão divertida poderia ser a bancada. A Michelle Viegas, que me ensinou muito sobre pesquisa e ciência. A Fabiana e prof. Rosane da química que me ensinaram muito.

Também gostaria de agradecer a todo o pessoal do IPB. Em especial agradeço aos colegas do laboratório 6 (Karina, Dornelles, Gassen, Sofia, Fazolo,...) que deixaram os dias pesados mais leves e divertidos.

Agradeço também a minha família por tudo, graças a ela que tive o apoio necessário para conseguir realizar esse trabalho.

Ao Régis que me ajudou muito ao longo de todos esses anos, me dando suporte quando mais precisava. E aos meus amigos que como um todo me ajudaram nessa trajetória.

Agradeço por fim a PUCRS pelas oportunidades e a CAPES pelo apoio financeiro.

RESUMO

Câncer ainda mata milhões de pessoas a cada ano, se vê então a importância do desenvolvimento de novas terapias e de estratégias para melhorar a testagem de novas drogas. Assim, essas duas abordagens foram consideradas no desenvolvimento deste projeto. Primeiramente foi avaliado o potencial terapêutico de uma proteína que inibe a proteína de choque térmico Hsp70. A chaperona Hsp70 apresenta expressão elevada em tumores, onde pode agir promovendo-o; ela precisa, todavia, de outras proteínas para que consiga exercer suas funções de chaperona. Uma dessas proteínas é a cochaperona Hsp70 Binding Protein-1 (HspBP1), que age inibindo a Hsp70. Experimentos preliminares de nosso grupo demonstraram que tumores que superexpressavam HspBP1 tinham seu crescimento reduzido *in vivo*. Assim, foi analisado o potencial antitumoral da HspBP1 em combinação ou não com quimioterápicos. Para isso, diferentes linhagens celulares foram cultivadas *in vitro* e tratadas por 48 h, após o qual foram avaliadas quanto a viabilidade (MTT), densidade celular (Microscopia óptica estática e ao longo das 48 h), morte celular (LDH) e apoptose (Anexina/PI). O tratamento de HspBP1 não teve ação antitumoral significativa, mostrando que o tratamento *in vitro* dessa proteína não foi nem citotóxico, nem citoestático, assim seu efeito *in vivo* deve ser indireto. Em relação a segunda parte, foi feita uma análise comparativa de diferentes modelos de cultivo *in vitro* tridimensionais (3D), visto que eles conseguem se aproximar mais do que é visto *in vivo*. Assim, crescimento celular, morfologia, resposta a quimioterapia e expressão de RNA foram analisados em diferentes modelos de cultura. Os modelos utilizados foram: clássico 2D; cultivo em gel feito a partir de um extrato tumoral (gel EHS, como Matrigel®); membrana eletrofiada; membrana produzida por *Solvent Casting Particle Leaching* (SCPL); e por fim, tumor *in vivo*. Os arcabouços para cultivo 3D foram analisados por Microscopia Eletrônica de Varredura (MEV) em relação a tamanho de poro. Foi visto que o gel apresentava o menor tamanho de poro, seguido pela membrana eletrofiada e por fim pela SCPL. Células de melanoma B16F10GFP foram cultivadas por 7 dias *in vitro* e 10 dias *in vivo*, após o qual foi feita analise por MEV. Como esperado, células crescidas em lamínula de vidro apresentaram morfologia achatada e alongada, enquanto aquelas em 3D eram mais variadas, incluindo formação de agregados celulares e de esferoides. Essa morfologia encontrada nos modelos 3D se assemelhou mais aquelas *in vivo*. Para analisar resistência a quimioterapia, após os 7 dias em cultura amostras foram tratadas por 48 h com cisplatina, seguida de análise de viabilidade por MTT. No geral, foi possível ver uma tendência a resistência nos modelos 3D, porém apenas células na membrana eletrofiada apresentaram resistência significativa ao tratamento. Por fim, análise

de RNA mostrou similaridades entre os modelos de cultivo 3D, confirmando dados morfológicos. Dessa forma, o cultivo celular em qualquer um dos modelos 3D testados foi capaz de se aproximar mais a um tumor *in vivo*, mostrando que alternativas sintéticas têm o potencial de reduzir o uso de modelos derivados de animais para cultivo 3D.

Palavras-chave: Câncer; HspBP1; Cultura 3D; Eletrofiação; SCPL.

ABSTRACT

Cancer has caused millions of deaths every year across the world, evidencing the importance of drug discovery and improving *in vitro* drug testing. With that in mind, those two approaches have been considered for this work. First, was studied a protein which can inhibit Hsp70, thus potentially acting as a new anticancer therapy. The chaperone Hsp70 has been shown to be upregulated in various tumors, where it can inhibit cell death and promote tumor growth. In order for Hsp70 to work properly, it associates with different cochaperones, one of which is the Hsp70 Binding Protein 1 (HspBP1). Preliminary experiments from our group showed that tumors overexpressing HspBP1 grew considerably less than regular ones. As such, the potential for HspBP1 as an anticancer therapy in combination or not with chemotherapy was analyzed. Cells were cultured *in vitro* and treated for 48 h before analysis of: viability (MTT), cell density (Optical microscopy, static and over 48 h), cell death (LDH) and apoptosis (Annexin/PI). Although there were slight antitumor effects, they were not significant, showing that *in vitro* HspBP1 was unable to promote neither cytotoxic, nor cytostatic effects. For the second part, the usage of three-dimensional (3D) models for *in vitro* culture were studied, since it has been shown that growing cells on scaffolds may approximate *in vitro* to *in vivo* cell growth. Thus, cell growth, morphology, response to chemotherapy and RNA expression were analyzed across different culture models. These models encompassed classical 2D culture; culture on a gel made from a tumor extract (EHS gel, such as Matrigel®); an electrospun; a scaffold produced by Solvent Casting Particle Leaching (SCPL); and cells grown *in vivo*. Through Scanning Electron Microscopy (SEM) 3D scaffolds were analyzed regarding pore size. It could be seen that the gel had the smallest pore diameters, followed by the electrospun and then the SCPL membrane. Melanoma B16F10 GFP cells were cultured *in vitro* for 7 and *in vivo* for 10 days, after which morphology was also analyzed through SEM. As expected, cells grown on a glass slide appeared flat and elongated, while cells on 3D had different morphologies, including the formation of cell aggregates and spheroids. Cells on 3D had morphologies more similar to those grown *in vivo*. When analyzing resistance to chemotherapy, after culture cells were treated for 48h with cisplatin, followed by viability analysis through MTT. Though 3D cultures in general had a tendency for cisplatin resistance, only those grown on electrospun membranes had significant resistance. At last, RNA analysis showed similarities across 3D culture models, confirming morphological results. As it is, cell growth on any of the 3D culture models shown was able to better reproduce *in vivo* culture than the 2D model,

showing the potential of synthetic scaffolds to reduce the usage of animal derived models for 3D growth.

Key words: Cancer; HspBP1; 3D culture; Electrospinning; SCPL;

LISTA DE ILUSTRAÇÕES

Sumário

CAPÍTULO 1

1.1 APRESENTAÇÃO

Nessa dissertação foram realizados dois projetos de pesquisa por questões logísticas. Um associado a um projeto guarda-chuva de avaliação do efeito antitumoral de HspBP1 em tumores *in vitro* e outro focando no desenvolvimento de um modelo tridimensional (3D) de cultura *in vitro*. Para satisfazer os critérios do programa para obtenção do título de mestre, o artigo para publicação é referente ao trabalho com o modelo 3D, cujos resultados se mostraram mais propícios para a publicação.

1.2 INTRODUÇÃO

O câncer é uma das maiores causas de morte no mundo, estimando-se cerca de 9,5 milhões de vítimas de tumores apenas em 2018 (BRAY et al., 2018) Considerando apenas tumores de pulmão, foram mais de 1,7 milhão de falecimentos, constituindo a principal causa de óbito por câncer (BRAY et al., 2018). No Brasil, estima-se 600 mil casos novos da doença para cada ano do biênio 2018-2019, com mortalidade acima de 200 mil em 2017 (INCA, 2017; SIM, 2017). Essa elevada taxa de mortalidade é atribuída à natureza heterogênea da doença, visto que embora a maioria dos tumores tenha origem epitelial, cada tecido apresenta diferentes características e necessidades. Além disso, para que tumores cresçam, precisam subverter alguns mecanismos de controle da homeostasia de tecidos saudáveis. Comumente denominados de "*Hallmarks*" (HANAHAN; WEINBERG, 2011; WEINBERG, 2013), esses mecanismos alterados incluem a sustentação de sinais de proliferação, resistência à morte celular programada, imortalidade replicativa, indução angiogênica, evasão da resposta imune, instabilidade e mutação genômica, entre outros (HANAHAN; WEINBERG, 2011). Cada uma dessas "*hallmarks*" pode ser adquirida de diferentes maneiras, atuando em diversas vias de sinalização, o que aumenta a dificuldade de tratamento dessa doença. Deste modo, o câncer representa um conjunto de diversas patologias únicas e complexas reduzidas a um mesmo nome. Portanto, devido a essa notável variabilidade observada entre cada tipo tumoral, diferentes estratégias terapêuticas são requeridas.

1.2.1 Tratamentos antitumorais

O desenvolvimento de fármacos capazes de tratar neoplasias é um processo lento, em que é necessário garantir seletividade e eficiência contra o tumor, reduzindo efeitos colaterais em tecidos saudáveis. Uma das estratégias para o desenvolvimento de medicamentos ocorre em

cinco grandes etapas: modelagem *in silico,* testes enzimáticos, experimentação *in vitro* (em modelos celulares), *in vivo* (em animais) e ensaios clínicos. Considerando esse exemplo de processo, a partir da escolha de um alvo terapêutico, os compostos são modelados e otimizados *in silico*, obtendo-se uma biblioteca de compostos. Esses compostos são testados enzimaticamente, para a avaliação do seu potencial de ação em modelos simplificados. Após essa seleção, as substâncias são testadas *in vitro*, em um sistema simplificado composto por tipos celulares mantidos sob condições artificiais. Seguindo a validação do modelo *in vitro,* o produto passa a ser testado em animais, passo fundamental para determinação de características farmacocinéticas e farmacodinâmicas. Por fim, entre os poucos compostos selecionados, aquele que se mostrar mais promissor será submetido a diferentes estágios de ensaios em humanos, para que finalmente haja a comprovação e descrição do efeito esperado (BRESLIN; O'DRISCOLL, 2013). Infelizmente, este longo processo pode apresentar diversas falhas e muitas substâncias acabam sendo descartadas precocemente pelos modelos não conseguirem reproduzir a natureza complexa dos tumores. Modelos *in vitro*, por exemplo, apesar da facilidade de manipulação e baixo custo em relação a modelos *in vivo*, são limitados e não representam a heterogeneidade de células e o modo de dispersão de compostos observados no microambiente tumoral. Por isso, há uma forte demanda científica que visa o aperfeiçoamento dessa etapa, para que seja possível não apenas a obtenção de dados mais confiáveis, mas sobretudo a otimização do processo de seleção de compostos, com o objetivo de reduzirmos o número de animais utilizados na pesquisa pré-clínica.

1.2.1.1 Quimioterápicos

Atualmente, existem diversos medicamentos disponíveis no mercado para o tratamento de tumores. Tradicionalmente, foram desenvolvidos os quimioterápicos, fármacos cuja ação tem efeito em células com altas taxas proliferativas. Apesar de células tumorais estarem em constante replicação e serem o principal alvo desses medicamentos, muitas outras células em nosso organismo estão em constante proliferação, podendo ocasionar diversos efeitos colaterais. Quimioterápicos podem ser administrados por diferentes estratégias de acordo com o tipo de tumor e o estágio da doença. Um tratamento adjuvante se refere àquele em que o quimioterápico é administrado após a cirurgia para reduzir as chances de o câncer reincidir. Esse tratamento pode-se referir também à utilização de outro fármaco juntamente com o quimioterápico, de forma a potencializar a ação desse. Já em um tratamento neoadjuvante o quimioterápico é previamente administrado para reduzir o tamanho do tumor e facilitar a cirurgia. Por fim, a quimiorradioterapia refere-se à utilização de quimioterapia antes ou durante

a radioterapia para aumentar a eficiência desta (WEINBERG, 2013). Adiante, uma rápida descrição dos quimioterápicos mais utilizados para o tratamento dos tumores abordados nesse trabalho.

1.2.1.1.1 Cisplatina

Cisplatina (CDDP) é um quimioterápico utilizado para o tratamento de diversos tipos de tumores, como de cabeça e pescoço, pulmão e melanoma. Um de seus principais modos de ação é pela formação de adutos com DNA, podendo ativar a via intrínseca de apoptose. Além desse, já foi visto que cisplatina pode induzir a formação de espécies reativas de oxigênio (ROS) e inibir a fosforilação oxidativa (SHALOAM; TCHOUNWOU, 2014).

1.2.1.1.2 Doxorrubicina

Doxorrubicina é uma antraciclina usada no tratamento de tumores de mama, ovário, linfomas, sarcomas entre outros. Esse quimioterápico apresenta dois principais mecanismos de ação. Primeiramente, ela age intercalando o DNA, assim como formando um complexo com ele e a topoisomerase II, inibindo o reparo do DNA. Outra maneira de induzir morte celular, se dá pela formação de radicais livres, levando a danos no DNA, na membrana plasmática, estresse oxidativo e indução de apoptose (BRUNTON LAURENCE L, RANDA HILAL-DANDAN, 2018; THORN; ALTMAN, 2011).

1.2.1.1.3 Fluorouracil

Fluorouracila (5FU), é um análogo de timina, sendo utilizado no tratamento de carcinoma de colón e mama. Para que possa exercer seu efeito terapêutico, 5FU precisa ser convertido em fluorodesoxiuridina monofosfato (FdUMP), fluorodesoxiuridina trifosfato (FdUTP) e fluorouridina trifosfato (FUTP). Esse fármaco pode então ser incorporado no RNA ou DNA e inibir a Timidilato Sintase, bloqueando a síntese de desoxitimidina trifosfato (dTTP) e consequentemente a replicação (BRUNTON LAURENCE L, RANDA HILAL-DANDAN, 2018; LONGLEY; HARKIN; JOHNSTON, 2003).

1.2.1.1.4 Paclitaxel

Amplamente utilizado na clínica para o tratamento de diversos tumores como: mama, pulmão de não-pequenas células e ovário. Age na metáfase, ao se ligar na b-tubulina, estabilizando-a, assim Paclitaxel tem ações antitumorais distintas dependendo da concentração a ser utilizada. A estabilização de microtúbulos e formação de estruturas aberrantes leva a parada mitótica e subsequente morte celular; em doses mais baixas de Paclitaxel, todavia, as

células continuam a mitose, fazendo a separação dos cromossomos em diferentes direções, levando a divisões multipolares, consequentemente morte celular mais lenta (BRUNTON LAURENCE L, RANDA HILAL-DANDAN, 2018; WEAVER, 2014).

1.2.1.1.5 Dacarbazina

É um agente alquilante, que após ativado transfere um grupo metil ao DNA prevenindo a multiplicação de células com crescimento exacerbado. Age independente de ciclo celular e é utilizada principalmente no tratamento de melanoma metastático (AL-BADR; ALODHAIB, 2016; BRUNTON LAURENCE L, RANDA HILAL-DANDAN, 2018; SANADA et al., 2007). Além disso, Dacarbazina induziu células NK, levando a um aumento na morte celular (HERVIEU et al., 2013).

1.2.2 Proteínas de choque térmico (HSPs)

Conceitualmente, um câncer refere-se a um crescimento celular exacerbado e descontrolado, desenvolvido em um microambiente tecidual muitas vezes incapaz de fornecer o suporte necessário ao seu crescimento. Assim, as células tumorais precisam modular seu meio a fim de obter suporte e garantir a resistência necessária à sua sobrevivência em condições desfavoráveis, que incluem diferenças na distribuição de nutrientes, oxigênio e resíduos metabólicos. Devido à sua constante exposição a esses fatores de estresse, muitos tumores demonstram um aumento na expressão de chaperonas, como a Hsp70. Chaperonas moleculares são um grupo de proteínas responsáveis por auxiliar no dobramento correto de proteínas desnaturadas ou mal dobradas (CALDERWOOD; PRINCE, 2011; KOSMAOGLOU et al., 2008). As HSPs (*Heat Shock Proteins*), são uma classe extensa de chaperonas relacionadas à resolução dos efeitos do estresse térmico, além de atuarem na manutenção da homeostasia tecidual. Suas funções comportam não apenas o auxílio no redobramento de proteínas, mas também impedem a formação de agregados proteicos e marcam proteínas para degradação (BORGES et al., 2016). Atualmente, estão descritas 5 famílias de HSPs: HSPA (Hsp70), HSPB (*small* HSP), HSPC (Hsp90), HSPD (Hsp60), HSPH (*large* HSP) (CALDERWOOD, 2013). Aqui, focaremos na Hsp70, um importante membro da família HSPA, com 70 kDa, cujo papel é crucial no dobramento de proteínas em situações de estresse celular (WEGELE; MÜLLER; BUCHNER, 2004). A Hsp70, também conhecida como HSPA1, tem sua expressão aumentada em diversos tipos de tumores, além de ter associação com crescimento celular, migração, invasão e expressão alterada de moléculas pró- e antiapoptóticas (BOROUGHS et al., 2011; JAGADISH et al., 2016). Ela apresenta dois domínios proteicos, um N-terminal, ATPásico

(NBD, ou *nucleotide binding domain*), e um C-terminal, de ligação com seu cliente (SDB, ou *substrate binding domain*), que são unidas por um *linker* (Figura 1.1). Quanto a sua localização, embora Hsp70 seja uma proteína intracelular, pode ser encontrada na membrana plasmática de algumas células tumorais associada a "*lipid rafts*" (BROQUET et al., 2003; GEHRMANN et al., 2008). Ademais, Hsp70 e outras chaperonas podem ser secretadas para o meio extracelular, por rotas ainda não completamente elucidadas. Está descrito que essa secreção ocorre por vias não clássicas e que não respondem a inibição por brefeldina (LANCASTER; FEBBRAIO, 2005). A presença de Hsp70 é amplamente observada em exossomos, servindo como um marcador dessas vesículas extracelulares com papel ativo na comunicação intercelular (BORGES et al., 2016; WOLFERS et al., 2001).

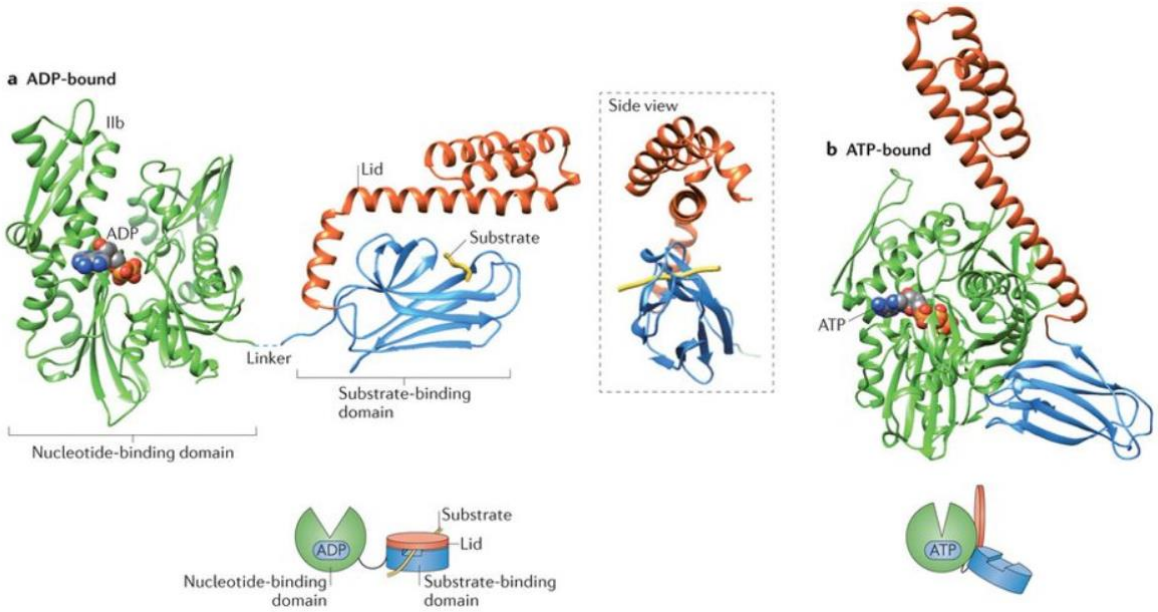

Figura 1.1 Estrutura da Hsp70, em **A** seu estado fechado *(Protein Data Bank*, PDB, *code*: 3HSC porção verde; PDB *code*: 1DKZ porção azul), e em **B** estado aberto da Hsp70 (PDB *code*: 4B9Q) (SAIBIL, 2013).

Para que consigam desempenhar seu papel corretamente, as HSPs contam com o auxílio de cochaperonas, proteínas particularmente essenciais na regulação da atividade de ATPase das chaperonas (CALDERWOOD, 2013). No contexto tumoral, diferentes cochaperonas parecem desempenhar um papel não completamente esclarecido, podendo tanto promover quanto suprimir neoplasias, como mostrado na Figura 1.2 (CALDERWOOD, 2013). Dentre essas diferentes cochaperonas de Hsp70, se encontra a HSP *binding protein* 1 (HspBP1), uma *nucleotide exchanging fator* (NEF). Descoberta em 1998 por Raynes e Guerriero, já foi demonstrado que HspBP1 se liga na porção N-terminal da Hsp70, que sofre uma alteração conformacional e bloqueia a ação ATPásica desta, impedindo a produção de ADP, reduzindo a atividade de redobramento da Hsp70 (MCLELLAN; RAYNES; GUERRIERO, 2003; RAYNES; GUERRIERO, 1998). Assim, a estrutura de HspBP1 pode ser dividida em duas

regiões, a porção principal que contempla o domínio C-terminal, tipo-armadillo, que se liga na região NBD da Hsp70 (Figura 1.3); e domínio N-terminal, de estrutura flexível (GOWDA et al., 2018) (Shomura, 2005). Recentemente, foi visto que essa porção flexível de HspBP1 pode se ligar na porção SBD da Hsp70, de forma a garantir a liberação do cliente (GOWDA et al., 2018).

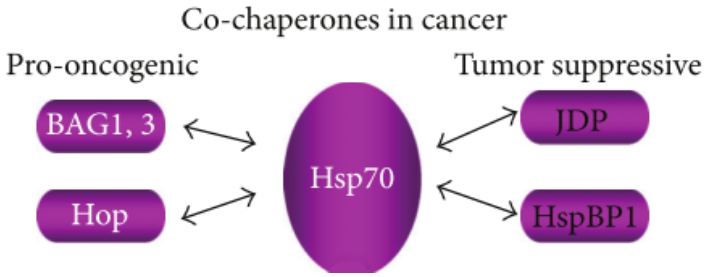

Figura 1.2 Cochaperonas relacionadas a atividade de Hsp70 em um ambiente tumoral. Adaptado de: (CALDERWOOD, 2013)

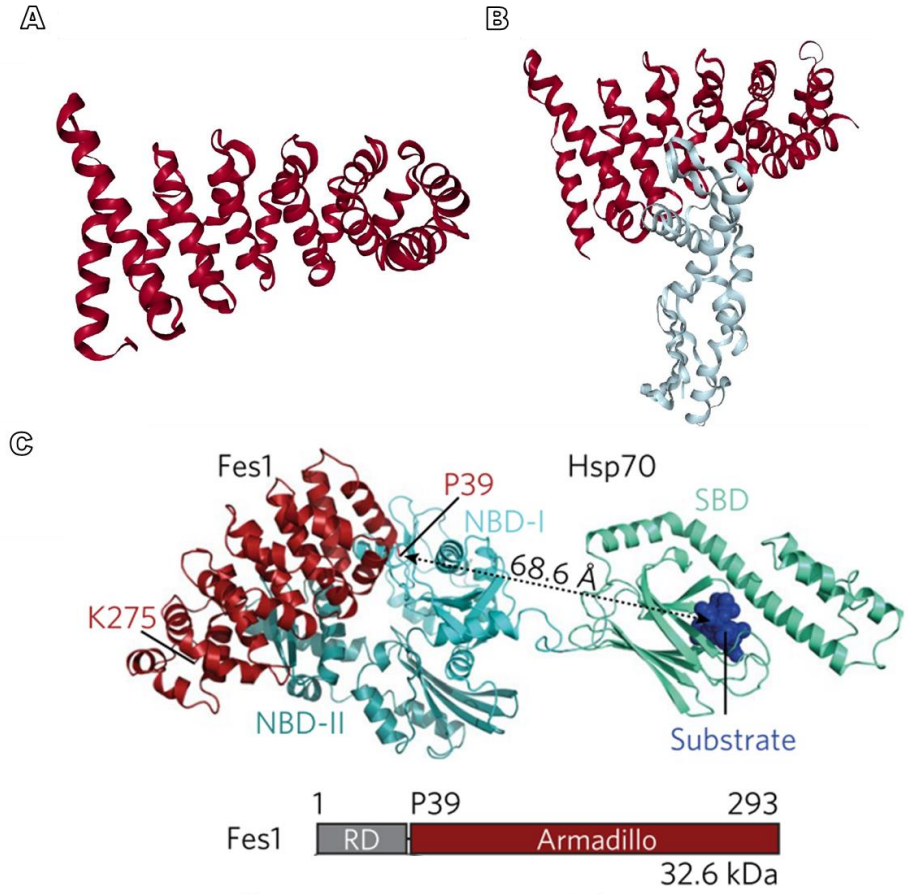

Figura 1.3 Estrutura de HspBP1 e ligação com Hsp70. Estrutura do domínio principal de HspBP1 (A) e domínio principal de HspBP1 (em bordo) em associação com porção NBD de Hsp70 (em azul) (B) (Shomura et al., 2005; Rose and Hildebrand, 2015). Em C vemos novo modelo, com homólogo de HspBP1, a Fes-1 de *Saccharomyces cerevisiae*, novamente o dominio armadillo ligado ao NBD de Hsp70, vemos também a extensão flexivel N-terminal ligada a porção SBD (GOWDA et al., 2018).

Visto que a Hsp70 tem níveis de expressão elevados em tumores e auxilia no correto dobramento de proteínas, sua ação acaba por facilitar a proliferação das células tumorais.

Porém, com o aumento de HspBP1, essa ação protetora da Hsp70 pode ser inibida, podendo resultar na morte das células tumorais. Isso sugere o potencial adjuvante da HspBP1 no tratamento de neoplasias, uma vez que poderia sensibilizar as células tumorais para a morte pela ação de quimioterápicos. Em nosso grupo, foi estudada a expressão de HspBP1 em tumores de mama de pacientes, onde foram verificadas correlações negativas com mortalidade, agressividade e metástase (SOUZA et al., 2009). Dados não publicados de nosso grupo mostram que tumores que superexpressam HspBP1 tem o crescimento inibido *in vivo*. Dados preliminares sugerem ainda que o tratamento com HspBP1 *in vitro* pré-sensibiliza células de linhagens tumorais de melanoma e glioma para morte por quimioterápicos (dados não publicados e ainda confidenciais). Essas análises serviram de base para o depósito de uma patente (WO 2014100883 A1), e para idealização de um projeto científico inovador atualmente financiado pela FINEP, dentro do qual se inserem as atividades descritas na presente dissertação. Os experimentos visam avaliar a atividade antitumoral da proteína HspBP1. Ainda há, todavia, muito a ser elucidado sobre a HspBP1 seja sobre a sua entrada nas células, mecanismos compensatórios ou sua ligação a outras chaperonas. Esses e outros aspectos serão abordados em diversos projetos do grupo.

Nesse trabalho, foram abordados três diferentes tipos tumorais: carcinomas de pulmão, mama, e um modelo murino experimental de melanoma. Como mencionado anteriormente, o estudo científico do câncer de pulmão é de grande relevância devido as suas altas taxas de mortalidade (WORLD HEALTH ORGANIZATION, 2018). Classicamente é dividido em dois grandes grupos: carcinomas de células pequenas e não-pequenas. Tumores pulmonares de células pequenas, são mais comuns em usuários de tabaco e apresentam características de células neuroendócrinas (TRAVIS et al., 2015; WEINBERG, 2013). Já as neoplasias associadas às células não-pequenas abrangem diversos tipos de tumores pulmonares, principalmente adenocarcinoma e carcinoma de células escamosas (CRAPO et al., 1982; INCA, 2017; TRAVIS et al., 2015) (Weinberg, 2014;). Tumores de mama apresentam a maior incidência e mortalidade em mulheres tanto de países desenvolvidos quanto em desenvolvimento (INCA, 2017). Esses tumores são comumente divididos em cinco subtipos: Luminal A, Luminal B, Superexpressão de HER2, tipo-basal e tipo-normal (SUBIK et al., 2010). Além disso, podem também ser classificados em relação à expressão de receptores de estrógenos (ER), progesterona (PR), HER2 (também denominado de Neu ou erbB2) e do fator de crescimento epidérmico (EGFR). Para esses foram desenvolvidos medicamentos que antagonizam suas ações, auxiliando no controle tumoral. Existem, todavia, alguns tumores denominados triplo-

negativos, que não expressam os receptores ER, PR e HER2, considerados por isso ainda mais agressivos e com poucas estratégias efetivas de tratamento. Por fim, neoplasias de pele são as mais comuns no mundo, somando mais de 2 milhões de casos novos por ano (Ultraviolet radiation and the INTERSUN Programme - Skin cancer, 2016). Elas são divididas em tumores de pele não-melanoma e melanomas. O primeiro abrange diversos tipos de neoplasias de alta incidência com baixa mortalidade; enquanto melanomas se caracterizam por baixa incidência, porém com alto risco de metástase e mortalidade quando não tratados rapidamente (GUY et al., 2015; INCA, 2017). Assim, modelos celulares humanos e murinos para estes tipos de tumores foram tratados com HspBP1, que se hipotetiza sensibilizar as células para o tratamento com quimioterápicos.

1.2.3 Cultura tridimensional in vitro

O crescimento de células em um ambiente 3D, é uma maneira de aprimorar experimentos *in vitro* visto que se assemelhem mais corretamente a um tumor *in vivo*. Em uma cultura celular *in vitro* tradicional, se tem o crescimento das células aderidas a uma superfície plana formando uma monocamada. Esse tipo de cultivo promove a interação das células a essa superfície (normalmente um plástico), limitando contato célula-célula e célula-matriz extracelular (ECM). Dessa forma, altera-se inclusive o tipo de adesão exercido pelas células como já foi visto, enquanto em 3D e *in vivo* há colocalização de proteínas de adesão, que é perdida em culturas 2D (CUKIERMAN et al., 2001).

Existem diversos métodos para o crescimento de células em um ambiente 3D, que podem ser classificados em modelos independentes ou dependentes de arcabouço (FANG; EGLEN, 2017; RIMANN; GRAF-HAUSNER, 2012). Ao cultivar células sem um arcabouço, por não terem uma estrutura ao qual se aderir, as células normalmente se agregam levando a formação de esferoides. Isso pode ser obtido a partir de diferentes metodologias, como por exemplo: gota invertida ("*hanging drop*"), um dos mais antigos métodos 3D em que as células crescem em uma gota; "*liquid overlay*", onde é feito um recobrimento (geralmente de agarose ou poly-HEMA) na placa de cultivo, impedindo adesão; hidrogel micromoldado, uma derivação do *liquid overlay* em que se tem um gel não-aderente com poços de tamanho controlado/diminutos, permitindo desenvolver esferoides de tamanhos mais regulares; placas de cultura com baixa aderência; *spinner flasks* e biorreatores, que adicionam movimento a cultura, impedindo adesão ao recipiente; além de outros métodos.

Modelos de cultivo celular em arcabouço, são modelos em que se tem as células crescendo em uma estrutura que tenta mimetizar a matriz extracelular encontrada *in vivo*. Esse

arcabouço pode ser produzido a partir de materiais naturais ou sintéticos. Assim como modelos independentes de arcabouços, podem ser obtidos por diferentes técnicas, podendo ser encontrados em forma de gel ou de matriz "sólida". Hidrogéis, são classicamente feitos a partir de materiais naturais como colágeno, sendo um dos métodos mais utilizados de cultura 3D o crescimento de células em um gel obtido a partir do extrato de tumor murino de Engelbreth-Holm Swarm (Matrigel®, Cultrex®, Geltrex®). Arcabouços sólidos podem ser produzidos a partir de eletrofiação, bioimpressão, evaporação de solvente com lixiviação de porógeno (*Solvent Casting Particle Leaching* – SCPL), entre outros.

1.2.3.1 Extrato de tumor de Engelbreth-Holm Swarm (EHS)

Um dos modelos tridimensionais mais utilizados atualmente, o gel produzido a partir de extrato de tumor de Engelbreth-Holm Swarm (EHS) permite o crescimento das células em uma matriz composta por proteínas encontradas na lamina basal. Esse tumor foi descoberto por J. Engelbreth-Holm da Dinamarca e caracterizado por R. Swarm (BENTON et al., 2014; KLEINMAN; MARTIN, 2005; SWARM, 1963). Apesar de inicialmente ter sido descrito como de origem condrocitária (SWARM, 1963), mais recentemente foi definido por análise de expressão genica como um tumor de origem na endoderme parietal (FUTAKI et al., 2003). Assim, esse tumor produz uma variedade de proteínas, principalmente laminina, colágeno de tipo IV, entectina, fibronectina e proteoglicano de sulfato de heparan, além de diversos fatores de crescimento. Células cultivadas nesse modelo formam esferoides, aumentando então contato célula-célula e célula-ECM. Além disso, após o cultivo de um painel de linhagens de tumor de mama, foi possível fazer uma categorização dessas linhagens em relação a agressividade e organização celular, diferenças que não foram vistas quando cultivadas em modelo de monocamada (KENNY et al., 2007).

1.2.3.2 Eletrofiação

A técnica de eletrofiação foi desenvolvida no começo do século XX, porém apenas nos últimos anos que sua utilização para culturas celulares aumentou. Essa técnica produz membranas ao sujeitar o polímero de escolha a uma alta fonte de voltagem, esticando-o enquanto ele solidifica e o solvente evapora (TEO; RAMAKRISHNA, 2006). Apesar de simples, a eletrofiação produz membranas muito versáteis, que podem ser utilizadas em diversas áreas (HAIDER; HAIDER; KANG, 2018). Considerando cultivo *in vitro*, observou-se que células tumorais crescidas em membranas eletrofiadas podem formar esferoides (GIRARD et al., 2013), levando a um crescimento celular mais semelhante àquele visto *in vivo*.

Na engenharia tecidual, arcabouços eletrofiados quando implantados como enxerto de tendão em camundongos se mostraram muito semelhantes ao controle autoenxerto (BHASKAR et al., 2017). Em “drug delivery”, carregar arcabouços com um fármaco pode reduzir a taxa de dissolução deste, aumentando eficácia, enquanto possivelmente reduz toxicidade. Como visto por Yan et tal., membranas com núcleo de Doxorrubicina apresentaram liberação controlada e gradual do quimioterápico, mantendo sua ação antitumoral (YAN et al., 2014). Considerando a área ambiental, membranas eletrofiadas feitas a partir de filtros de cigarro tiveram alta eficácia na filtragem de diversas misturas de óleo/água (incluindo querosene, diesel e éter de petróleo) (LIU et al., 2019).

1.2.3.3 Solvent Casting Particle Leaching (SCPL)

SCPL é uma técnica em que, após a solubilização do polímero de interesse, ele é misturado com porógenos, como grãos de sal ou açúcar, e então mantido em um molde enquanto o solvente evapora. Após, é feita a lixiviação da amostra para retirada completa do porógeno. Apesar de simples, essa técnica vem sendo utilizada desde 1994, principalmente em engenharia tecidual (MIKOS et al., 1994). Marycz etl al, demonstrou a possibilidade de criar membranas de poliuretano (PU) e polilactido com hidroxiapatita para regeneração óssea e cartilaginosa, que induzissem colonização e diferenciação desses dois tipos celulares *in vitro* (MARYCZ et al., 2016). Enquanto outro tipo de membrana de polilactido apresentou boa biocompatibilidade e infiltração por fibroblastos após implantação subdermal por 7 dias em ratos (XIE et al., 2018). A técnica SCPL também é utilizada na cicatrização de feridas, onde membranas de PU recobertas com extrato de própolis não só aumentaram viabilidade celular *in vitro*, como também promoveram cicatrização *in vivo* (KHODABAKHSHI et al., 2019).

1.2.3.4 Polihidroxibutirato

Polihidroxibutirato (PHB) é um biopolímero da família dos Polihidroxialcanoatos, primeiramente descoberto como uma fonte de energia para bactérias crescendo em ambientes hostis (DEDKOVA; BLATTER, 2014). Atualmente, já foi encontrado em diversos organismos, inclusive em compartimentos subcelulares de células de mamíferos (ELUSTONDO et al., 2013; ELUSTONDO; ZAKHARIAN; PAVLOV, 2012). Quando é utilizado para estocagem de energia é encontrado na forma de cadeia longa, porém também é visto em média ou curta (REUSCH, 2012). Ele é utilizado atualmente em diversas áreas seja em *drug delivery* (WANG et al., 2017), como embalagem biodegradável (CHEE et al., 2018) e engenharia tecidual (REIS et al., 2010).

1.3 JUSTIFICATIVA

O câncer se mantém como uma das doenças de maior impacto no mundo, fazendo milhões de vítimas a cada ano. Apesar do grande número de medicamentos disponibilizados pela indústria, pacientes muitas vezes adquirem resistência ou desenvolvem um fenótipo tumoral intratável. Os tratamentos mais amplamente utilizados na clínica consistem em fármacos cujo alvo são células com altos índices proliferativos, o que vem acompanhado de baixa especificidade e consequentemente a indesejados efeitos colaterais. Essa problemática reforça a importância do desenvolvimento de novos tratamentos antitumorais, principalmente para tumores como de pulmão, melanoma e mama, cujo número de estudos relacionados não representa a grande variabilidade tumoral. Nossa proteína de interesse, a HspBP1, um possível inibidor da Hsp70, age de maneira a reduzir o crescimento tumoral. Visto que muitos tumores apresentam elevada expressão de Hsp70, propomos aqui a análise dos efeitos antitumorais da HspBP1 para o desenvolvimento de fármacos mais seletivos e de maior valor terapêutico. Assim, uma maneira de auxiliar no desenvolvimento de novos medicamentos é a utilização de modelos que consigam mais fielmente retratar o ambiente tumoral *in vivo*. A utilização de culturas tridimensionais é capaz de melhorar a experimentação *in vitro* por permitir que as células interajam mais entre si e com uma matriz extracelular do que quando crescidas em monocamada 2D. Todavia, um dos modelos mais utilizados para o cultivo 3D é o de Matrigel (gel EHS), um gel produzido a partir de um extrato de tumor murino. Assim se constata a importância da utilização de modelos alternativos para cultivo 3D, que não sejam de origem animal.

1.4 OBJETIVOS

1.4.1 Objetivo geral

Determinar o efeito de drogas antitumorais *in vitro* em diferentes estratégias de cultura celular.

1.4.2 Objetivos específicos

Avaliar o potencial antitumoral da cochaperona HspBP1 sozinha ou em combinação com quimioterápicos *in vitro*, quanto a viabilidade e tipo de morte celular

Comparar a eficiência de dois modelos 3D *in vitro* com uma cultura 2D e outra *in vivo*, quanto a crescimento celular, expressão gênica e resposta a quimioterapia

CAPÍTULO 2

AVALIAÇÃO DO POTENCIAL ANTITUMORAL DE HspBP1

2.1 MATERIAIS E MÉTODOS

2.1.1 Cultura celular

Como modelos tumorais de mama, foram utilizadas linhagens tanto ER/PR$^{+/+}$ e Her2^{-} (**MCF7**), quanto triplo negativas para estes receptores (**MDA-MB-231** e **4T1**) para abordar a variabilidade de subtipos em resposta a HspBP1 (Subik *et al.*, 2010; Luo *et al.*, 2015). Já para os modelos tumorais de pulmão, abordamos carcinoma alveolar (**A549**), carcinoma mucoepidermoide (**H292**) e carcinoma pulmonar de Lewis (**LL/2)**. Para nosso modelo de melanoma, utilizamos **B16F10** (Tabela 1). A troca de meio foi realizada três vezes por semana, e as culturas expandidas conforme necessário. Meios de cultivo utilizados para cada tipo celular, assim como referência e origem se encontram na Tabela 1. As culturas celulares foram mantidas em uma incubadora a 37ºC, 5% CO2 e umidade controlada.

Tabela 2.1. Linhagens celulares e suas características de origem, cultivo e tratamentos.

Código	Nome da linhagem	Tecido	Tipo de tumor / celular	Organismo	Linhagem/ Sexo e idade	Meio (10% SFB)	Quimioterápicos
CCL-185	**A549**	Pulmão	Carcinoma	*Homo sapiens*, humano	Macho, 58 anos	F12K	Cisplatina e Paclitaxel
CRL-1848	**H292**	Pulmão	Carcinoma pulmonar Mucoepidermoide	*Homo sapiens*, humano	Fêmea, 32 anos	RPMI-1640,	Cisplatina e Paclitaxel
CRL-1642	**LL/2 (LLC1)**	Pulmão	Carcinoma pulmonar de Lewis	*Mus musculus*, camundongo	C57BL/6	DMEM high glucose	Cisplatina e Paclitaxel
HTB-22	**MCF7**	Glândula mamária	Adenocarcinoma	*Homo sapiens*, humano	Fêmea, 69 anos	DMEM low glucose,	5FU, Doxorrubicina e Paclitaxel
HTB-26	**MDA-MB-231**	Glândula mamária	Adenocarcinoma	*Homo sapiens*, humano	Fêmea, 51 anos	DMEM high glucose	5FU, Doxorrubicina e Paclitaxel
CRL-2539	**4T1**	Glândula mamária	Câncer de mama Estágio IV	*Mus musculus*, camundongo	BALB/cfC3H	RPMI-1640,	5FU, Doxorrubicina e Paclitaxel
CRL-6475	**B16F10**	Pele	Melanoma	*Mus musculus*, camundongo	C57BL/6J	DMEM high glucose	Cisplatina, Dacarbazina e Paclitaxel

2.1.2 Ensaios de curva dose-resposta de quimioterápicos

Visto que nosso agente poderia atuar de maneira a sensibilizar as células tumorais para o tratamento com quimioterápico, primeiramente foram selecionados os fármacos para utilizar em combinação com a proteína. A escolha dos quimioterápicos se baseou naqueles utilizados com maior sucesso clínico nos tipos tumorais que iremos abordar. Logo, as linhagens de mama foram tratadas com Doxorrubicina (Dx), Paclitaxel e Fluouracil (5FU); linhagens de pulmão com Cisplatina (CDDP) e Paclitaxel, e melanoma com Dacarbazina, Cisplatina e Paclitaxel (Tabela 1).

2.1.2.1 Curvas de dose-resposta para análise da citotoxicidade por MTT

Para determinar quais fármacos tinham mais eficiência nessas linhagens celulares, realizamos curvas de dose-resposta, analisando seus efeitos citotóxicos por MTT em comparação com células não tratadas. Assim, ao atingirem 80% de confluência as células foram destacadas da garrafa de cultura, contadas e semeadas 10^4 (para A549, H292, MCF7, MDA-MB-231, 4T1) ou $0{,}5x10^4$ (B16F10 e LL/2) células por poço, em placas de 96 poços. Após 24 horas, foram realizadas as diluições seriadas dos quimioterápicos em seus respectivos meios. O tratamento foi feito com troca parcial de meio, seguido de incubação por 48 horas a 37 ºC, 5% CO_2 e umidade controlada. Finalizado o tempo de incubação, obtivemos imagens representativas dos poços por um microscópio óptico invertido com um sistema de captura de imagem digital, utilizando-se o *software* Qcapture. O MTT (3-(4,5-dimethylthi-azol-2-yl)-2,5-diphenyltetrazolium bromide) 5 mg/ml foi adicionado às culturas de células tratadas e incubado por 3 horas a 37 ºC. Durante esse período, ocorre a entrada do MTT nas células, que sendo metabolicamente ativas e viáveis, reduzem o MTT, formando cristais de formazan. Os cristais foram solubilizados em DMSO (dimetil sulfóxido) e a densidade óptica das amostras lida entre 570 e 620 nm por um leitor de absorbância de placas (Anthos Zenyth 340r) (JAEGER et al., 2017).

2.1.3 Avaliação do efeito citotóxico e adjuvante de HspBP1 em tratamento com quimioterápicos

Foram feitas culturas de cada um dos tipos celulares mencionados, variando a concentração de HspBP1 e do quimioterápico selecionado. A proteína recombinante utilizada foi produzida pelo nosso grupo. Dados preliminares de nosso laboratório indicavam 100 µg/ml de proteína como dose com possível efeito antitumoral. Visto que não foi possível manter a proteína numa concentração alta suficiente para sua diluição apropriada, foram feitas curvas de

50 µg/ml até 0,78 µg/ml. Diferentes aspectos foram então avaliados, como morte celular e viabilidade.

2.1.3.1 Avaliação de morte celular por apoptose (Anexina V/PI)

Em solução, o Iodeto de Propídeo (PI) se difunde para o interior de células que já perderam a integridade de suas membranas (em apoptose tardia ou necróticas), onde irá se intercalar com as bases do DNA. Por outro lado, a anexina apresenta alta afinidade pela fosfatidilserina, um fosfolipídeo externalizado no início do processo apoptótico, permitindo a ligação de anexina enquanto as membranas celulares ainda se encontram intactas. Assim, essa marcação permite a distinção entre células apoptóticas precoces, tardias ou necróticas. Após tratamento com HspBP1 e/ou quimioterápicos, as células foram soltas, lavadas com PBS, mantidas em buffer de ligação para então serem marcadas com anexina/PI. Após 15 minutos de incubação as amostras foram lidas por citometria de fluxo (BD FACSCantoII™) e analisadas utilizando o *software* Flowjo v10 e Graphpad Prism 5.

2.1.3.2 Avaliação de morte celular ao longo do tempo (Incucyte)

De maneira a avaliar a morte celular durante o tempo de cultivo, podendo facilitar a distinção de tipos de morte celular, foram feitos experimentos no equipamento Incucyte, em parceria com Dr. Ricardo Weinlich, pesquisador do Hospital Israelita Albert Einstein, São Paulo. Para marcação de células com danos na membrana plasmática, juntamente com o tratamento, foi adicionado um marcador de morte celular (Sytox green) na cultura. A placa foi acondicionada no equipamento Incucyte e 5 imagens por poço foram obtidas a cada 45 minutos por 96 horas. As imagens foram avaliadas quanto a marcação de Sytox green e quanto a porcentagem de confluência ao longo do tempo.

2.1.4 Análise estatística

Todos os experimentos foram repetidos pelo menos três vezes, em triplicata, as diferenças estatísticas entre os grupos avaliadas por análise de variância (ANOVA) de duas vias, com pós-teste de Tuckey. Análises foram feitas no GraphPad Prism 5 e dados considerados estatisticamente significativos quando tivessem valor de $p<0,05$

2.2 RESULTADOS E DISCUSSÃO

2.2.1 Curvas de dose-resposta com quimioterápicos por MTT

Primeiramente foram feitas curvas com os quimioterápicos para selecionar aqueles que tivessem melhores resultados para cada linhagem celular (Figura 2.1). As curvas foram obtidas a partir da avaliação de viabilidade por MTT, teste amplamente utilizado na pesquisa e que permite uma análise rápida de diversos compostos. Deve-se considerar, todavia as limitações dessa análise, assim os dados foram combinados com densidade celular, obtida a partir de imagens de cada tratamento (Figura 2.2, Tabela 2.1). Nesses experimentos foram encontrados dois tipos de resposta aos quimioterápicos: 1º quando há redução equivalente na viabilidade por MTT com a densidade celular por microscopia, logo o quimioterápico foi capaz de agir de forma esperada (Figura 2.1A); e 2º Resultados discordantes, quando há pela microscopia alteração no número de células e na morfologia celular, porém pelo ensaio de MTT não há redução de viabilidade celular (Figura 2.1B). Essa diferença de eficácia de tratamento entre métodos de análise já foi vista anteriormente. Sabe-se que o MTT apresenta diversas limitações visto que é uma maneira indireta de detectar viabilidade celular. Atualmente, ainda é discutido onde ocorre a redução do tetrazólio em formazan ao se tratar uma cultura com MTT (STOCKERT et al., 2012; SURIN et al., 2017). Essa redução pode ser feita não só por dinucleotídeo de nicotinamida e adenina (NADH) presente em mitocôndrias, como também em desidrogenases presentes no retículo endoplasmático, citoplasma e membrana plasmática (STOCKERT et al., 2012). Assim, alterações que afetem desidrogenases podem levar a resultados alterados (JABBAR; TWENTYMAN; WATSON, 1989; WANG; HENNING; HEBER, 2010). Isso também é visto na utilização de compostos que alterem metabolismo (VAN TONDER; JOUBERT; CROMARTY, 2015) e em alterações de pH (RISS et al., 2004). O próprio MTT pode ser reduzido diretamente por uma substância química, como visto por Ulukaya et al, a incubação de MTT apenas com quimioterápico, sem células, levou a alterações na absorbância (ULUKAYA; COLAKOGULLARI; WOOD, 2004). Assim, dados obtidos a partir de análises de MTT devem ser considerados com cuidado, sendo preferivelmente comparado a outro teste de viabilidade.

Como mencionado no tópico 1.2.1.1.4, Paclitaxel apresenta dois modos de ação distintos em concentrações altas e baixas. Zasadil em 2014, avaliou a concentração plasmática e intracelular de tumores de pacientes, onde viu que apesar de no plasma Paclitaxel variar entre 80 - 280 nM, havia acúmulo do quimioterápico no tumor, onde a concentração se mantinha

entre 1,1 - 9 µM (ZASADIL et al., 2014). Vimos que nos tratamentos de B16, MCF7, MDA-MB-231 e H292 com Paclitaxel, há uma redução na densidade celular, com IC50 variando entre 2,5 e 31,25 nM, enquanto viabilidade por MTT não é reduzida (Tabela 2.1). Essa discrepância ocorre possivelmente pelo Paclitaxel induzir morte ao promover anomalias na separação dos cromossomos, quando em baixas concentrações. Dessa forma, as células conseguem terminar a mitose e podem apenas progredir mais lentamente pelo ciclo, sem que haja alteração no número de mitocôndrias e logo parte da viabilidade por MTT.

Assim, foi selecionado um tratamento por linhagem celular cujos critérios eram ter concordância entre densidade celular e viabilidade por MTT, e ser capaz de matar pelo menos 50% das células (Tabela 2.3). Apesar da linhagem celular LL/2 com cisplatina apresentar essas características, ela foi desconsiderada para os próximos experimentos. Isso se deve a maior dificuldade de cultura dessa linhagem, visto que as células crescem tanto aderidas quanto em suspensão, e após algumas passagens detectou-se uma seleção das células aderentes, o que afetou os experimentos.

2.2.2 Curvas de tratamento simultâneo de HspBP1 com quimioterápicos por MTT

A partir da seleção dos quimioterápicos, foram realizados tratamentos combinando a proteína HspBP1 com o quimioterápico escolhido para aquela linhagem (Figura 2). Desses dados, foram selecionados aqueles pontos que apresentavam maior potencial para subsequentes experimentos de morte celular.

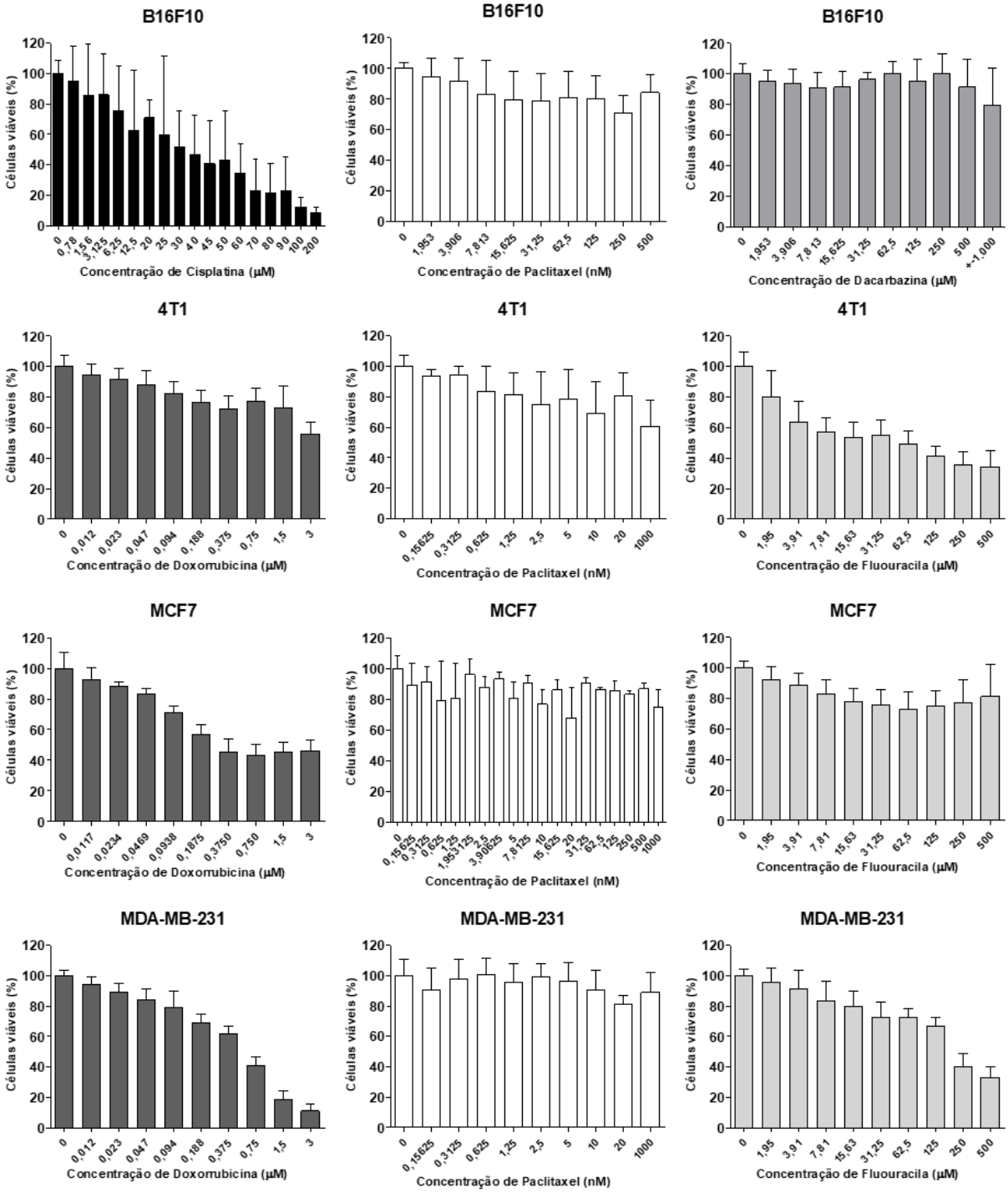

Figura 2.1 Curvas de dose-resposta de quimioterápicos (MTT). Análises de viabilidade em melanoma B16F10 com Cisplatina, Paclitaxel e Dacarbazina, e em linhagens de câncer de mama (4T1, MCF7 e MDA-MB-231) com Doxorrubicina, Paclitaxel e Fluorouracila.

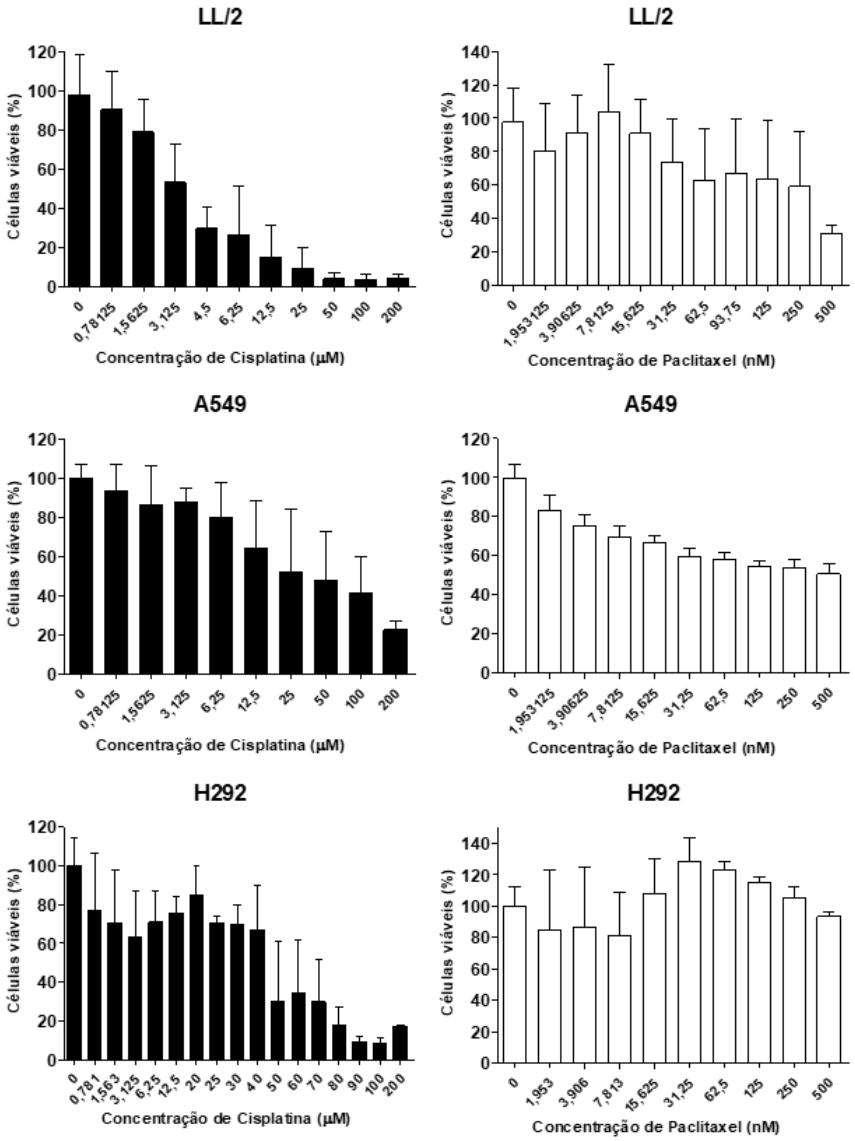

Figura 2.1 (cont.) Curvas de dose-resposta de quimioterápicos (MTT). Análises de viabilidade em linhagens de câncer de pulmão (LL/2, A549 e H292) com Cisplatina e Paclitaxel.

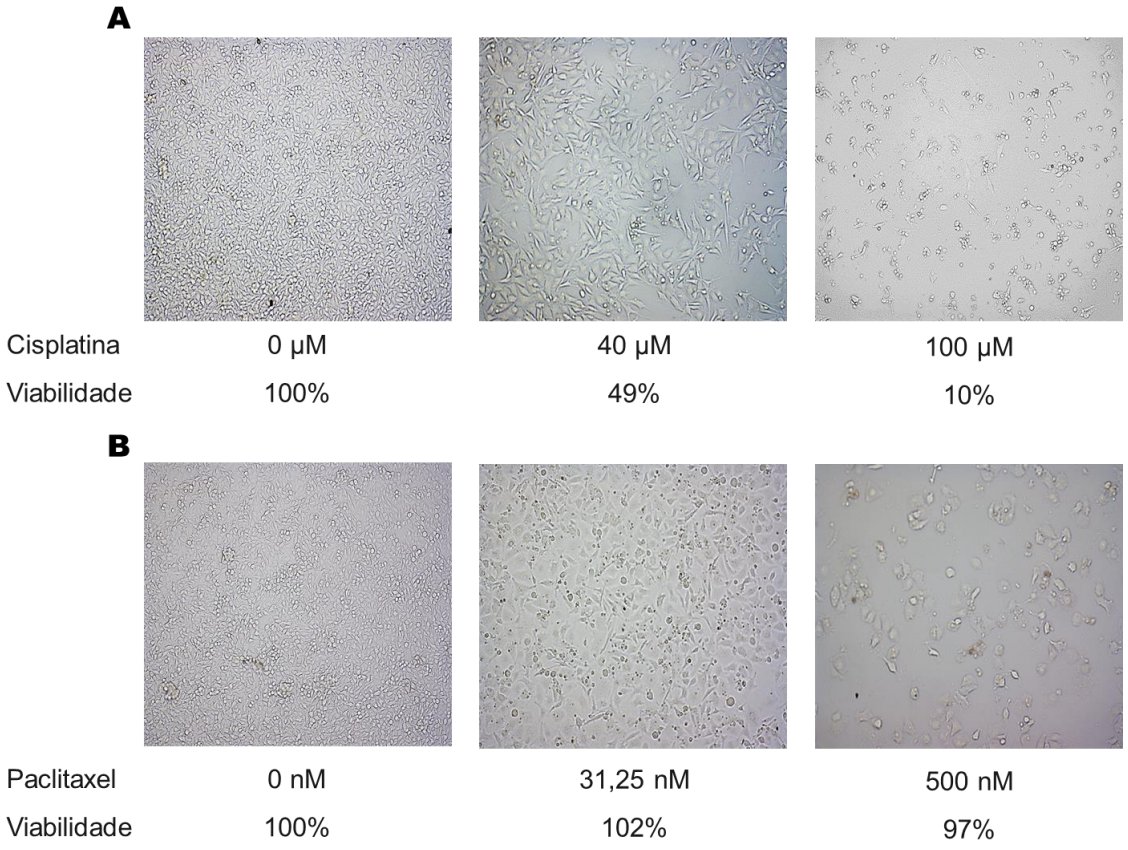

Figura 2.2 Microscopia óptica de B16F10 após tratamento com quimioterápicos, mostrado a dose utilizada e em baixo a porcentagem de células viáveis segundo MTT. Exemplificando os três tipos de resposta encontrados: Em **A,** o quimioterápico é capaz de reduzir densidade e viabilidade celular, vistos por microscopia e MTT, respectivamente; **B** quimioterápico apresenta redução na densidade celular, que não é vista na viabilidade.

Tabela 2.2 Comparação de doses de quimioterápicos obtidas por MTT e microscopia.

Célula	Quimioterápico	IC50	
		MTT	Microscopia
B16F10	Dacarbazina	-	1000 uM
	Cisplatina	40 µM	40 µM
	Paclitaxel	-	31,25 nM
4T1	Doxorrubicina	>3 µM	0,75 µM
	5FU	15,63 µM	7,81 uM
	Paclitaxel	-	1000 nM
MCF7	Doxorrubicina	0,19 µM	0,35 µM
	5FU	-	175 µM
	Paclitaxel	-	2,5 nM
MDA-MB-231	Doxorrubicina	0,56 µM	0,023 µM
	5FU	175 µM	62,5 µM
	Paclitaxel	-	10 nM
LL/2	Cisplatina	3,2 uM	1,6 µM
	Paclitaxel	-	31,2 nM
A549	Cisplatina	25 µM	12,5 µM
	Paclitaxel	125 nM	15,6 nM
H292	Cisplatina	45 µM	45 µM
	Paclitaxel	-	10 nM

Tabela 2.3 Quimioterápicos selecionados para cada linhagem celular

Linhagem Celular	Quimioterápico
B16F10	Cisplatina
4T1	Fluorouracila
MCF7	Doxorrubicina
MDA-MB-231	Doxorrubicina
A549	Cisplatina
H292	Cisplatina

.

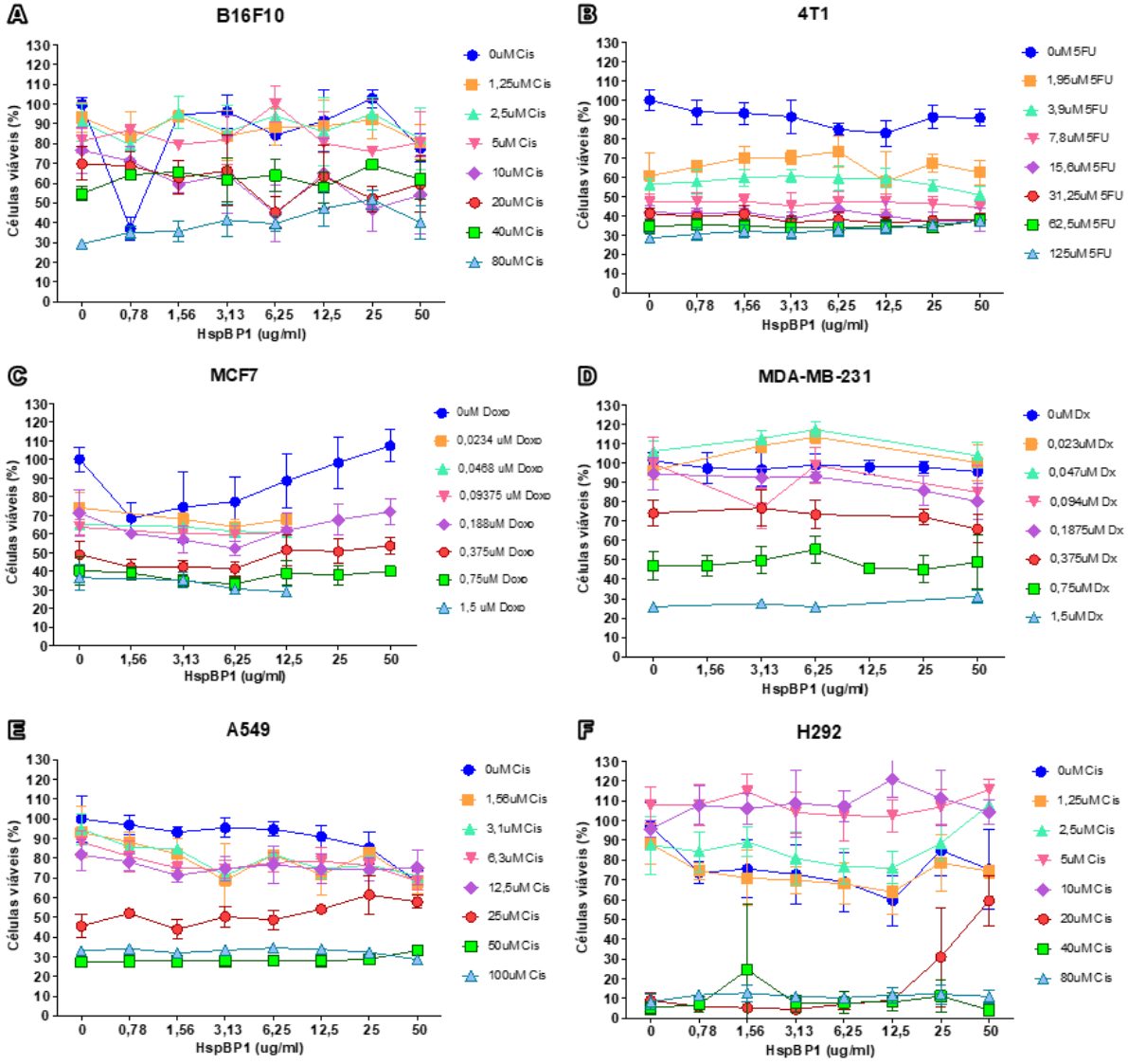

Figura 2.3 Viabilidade celular após tratamento simultâneo de HspBP1 com quimioterápicos em diferentes linhagens. Linhagens e quimioterápicos utilizados juntamente com tratamento de HspBP1: B16F10 com Cisplatina (CDDP), 4T1 com Fluorouracila, MCF7 com Doxorrubicina (Dx), MDA-MB-231 com Doxorrubicina, A549 com Cisplatina e H292 com Cisplatina.

2.2.3 Avaliação de efeito de HspBP1 e/ou quimioterápico ao longo do tempo

De modo a melhor caracterizar os possíveis efeitos da combinação de tratamentos, foram realizados experimentos avaliando morte e morfologia celular pelo equipamento Incucyte. Com essa técnica é possível fazer o acompanhamento da cultura, permitindo não apenas observar alterações morfológicas e comportamentais, como também a marcação de células com danos na membrana plasmática por Sytox, por exemplo. Assim, obter-se-á uma análise mais completa que aquela vista por MTT ou por apenas uma imagem ao final do tratamento. Ao longo das 96 h é possível ver claramente uma alteração na divisão e comportamento celular com o tratamento de cisplatina, além de um aumento na marcação por Sytox (Figura 2.4A; Vídeo 2.1). Também é possível ver essa redução na proliferação na Figura 2.4B, onde foi feita uma análise de confluência ao longo do tempo. Todavia, tanto o tratamento com a proteína HspBP1 sozinha quanto a combinação desta com quimioterápico não alterou nenhum desses aspectos celulares.

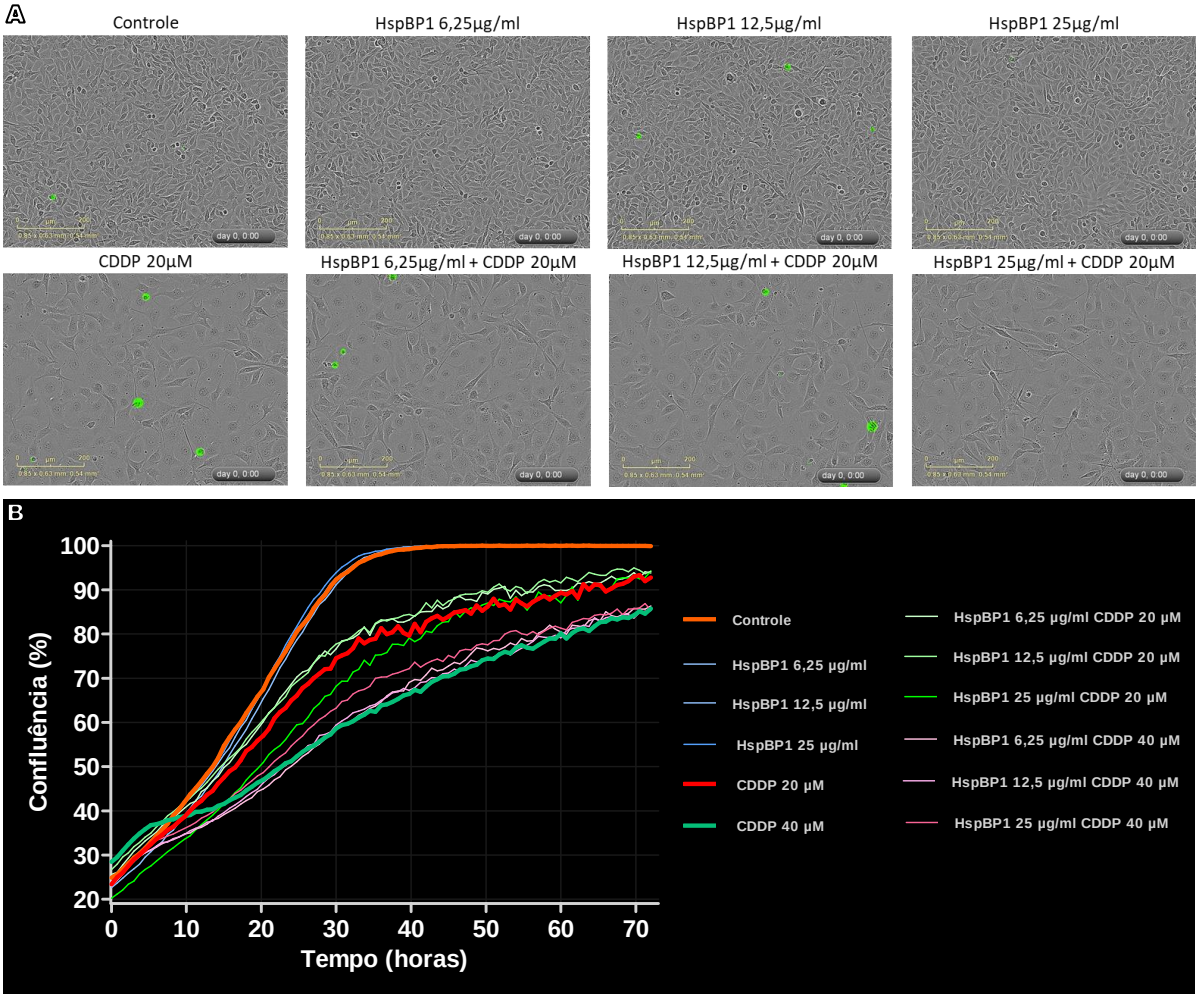

Figura 2.4 Análise pelo equipamento Incucyte de B16F10 após tratamento simultâneo de HspBP1 com Cisplatina. A: Microscopia óptica após 48 h de tratamento, em verde marcação de células mortas com Sytox. **B** Gráfico da confluência ao longo das 72 h de tratamento.

2.2.4 Avaliação de morte após tratamento com HspBP1 e/ou quimioterápico

Com o intuito de confirmar que as células não estariam ainda em estágio inicial de apoptose, foram realizadas análises de morte celular por Anexina V/PI. Para isso foram selecionados pontos a partir dos dados de MTT. Para as linhagens celulares 4T1 e A549 foi feito tratamento somente com HspBP1, visto que a combinação com quimioterápico não pareceu alterar a viabilidade. Todavia, após 48 h de tratamento novamente é visto um aumento de morte celular com a adição de quimioterápicos, e nenhuma alteração significativa ao tratar com HspBP1 (Figura 2.5). Foram feitos também experimentos avaliando morte celular pelo aumento da enzima lactato desidrogenase (LDH) após tratamento com HspBP1 por 12, 24 e 48 h, entretanto também não houve diferenças significativas entre grupos controle e tratado (Figura 2.6).

Assim, vê-se que o tratamento com a proteína HspBP1, seja sozinha ou em combinação com quimioterápicos, não afetou a sobrevivência nem induziu morte celular nas linhagens selecionadas. Resultados preliminares ainda não publicados mostram que o tratamento de tumores de melanoma em camundongos foi capaz de reduzir tamanho tumoral *in vivo*. Estamos estudando atualmente esse resultado, hipotetizando que os efeitos causados pela HspBP1 *in vivo* tenham sido indiretos, possivelmente pela ativação do sistema imune, uma vez que o efeito necessita de um sistema imune intacto para ser observado.

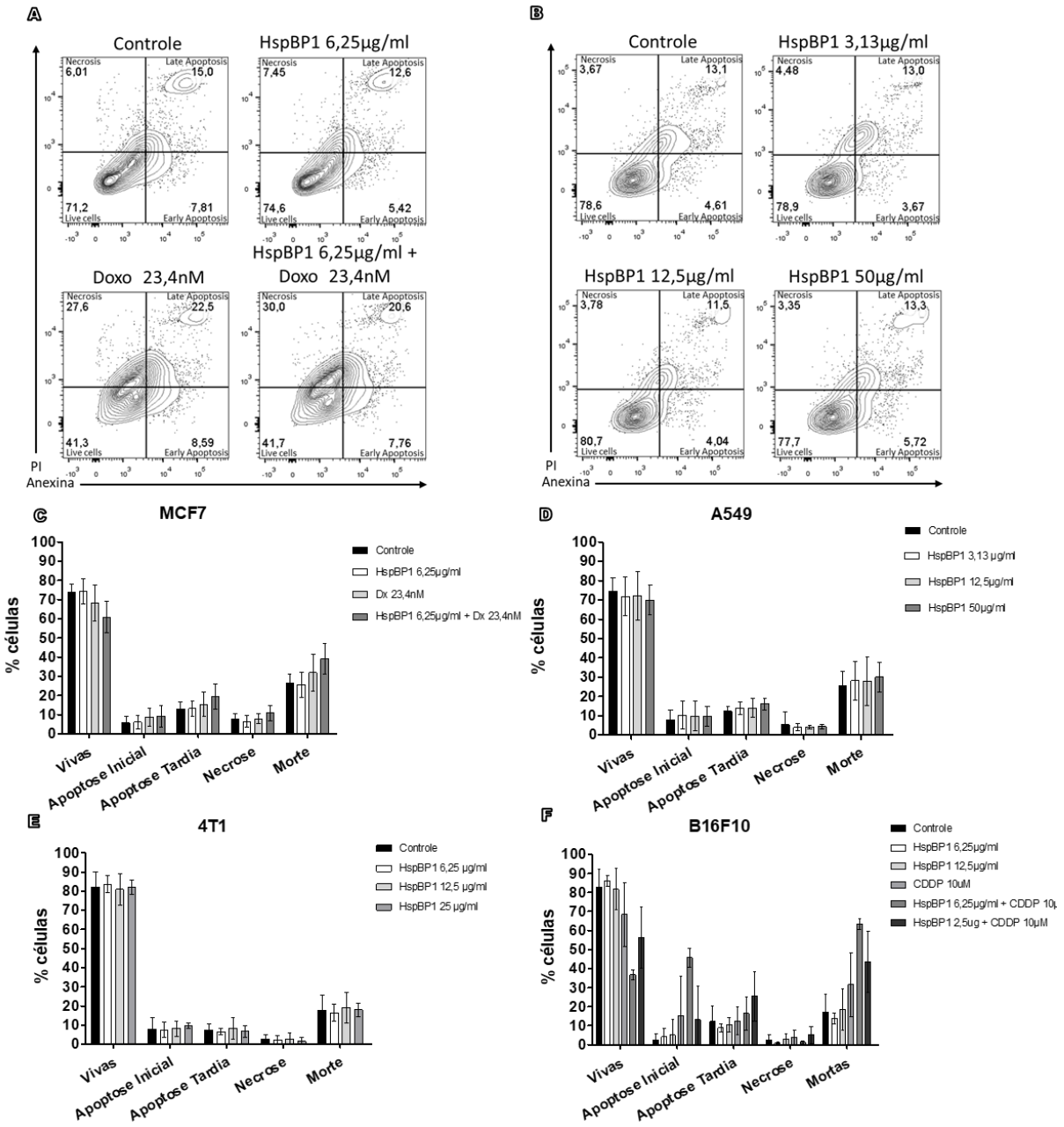

Figura 2.5 Análise de Anexina V/PI por citometria. A e B mostrando *dot plot* representativos de MCF7 (A) e A549 (B) após tratamentos. C-G gráficos em barras mostrando percentual de células em cada estado (vivas, apoptose inicial, apoptose tarde, necrose e soma de todas as mortes).

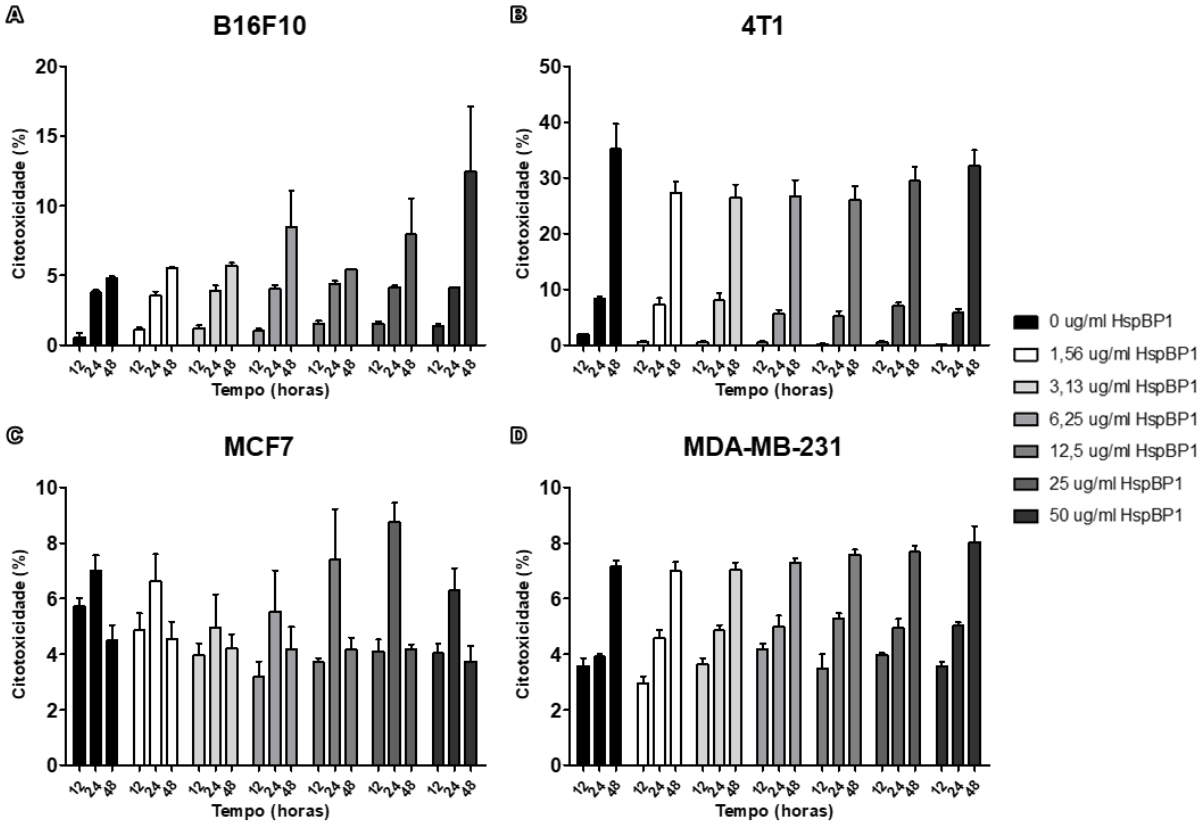

Figura 2.6 Análise de morte celular por LDH. Após tratamento das linhagens de mama e melanoma com HspBP1 por 12, 24 e 48 h, não foi possível ver diferença significativa entre grupos.

CAPÍTULO 3

ARTIGO CIENTÍFICO

Comparison of 2D and 3D cell culture models for cell growth, gene expression and drug resistance

Authors: Julia C. Fontoura [a,b]; Christian Viezzer [a]; Fabiana G. dos Santos [c]; Rosane A. Ligabue [c]; Dyeison Antonow [d]; Patricia Severino [e]; Cristina Bonorino [a,f] *

[a] Cellular and Molecular Immunology Laboratory, Pontifical Catholic University of Rio Grande do Sul (PUCRS), Porto Alegre, RS, Brazil

[b] Cellular and Molecular Biology Graduate Program, PUCRS, Porto Alegre, RS, Brazil

[c] Materials Characterization Laboratory, PUCRS, Porto Alegre, RS, Brazil

[d] Institute of Petroleum and Natural Resources (IPR), Tecnopuc, PUCRS, Porto Alegre, RS, Brazil

[e] Instituto Israelita de Ensino e Pesquisa Albert Einstein, HIAE, São Paulo, SP, Brazil

[f] Department of Surgery, School of Medicine, University of California at San Diego

*Corresponding author at: Basic Health Sciences Department, Universidade Federal de Ciências da Saúde de Porto Alegre (UFCSPA), Porto Alegre, RS, Brazil

Email: cristinabcb@ufcspa.edu.br; cbonorino@ucsd.edu

3.1. INTRODUCTION

Cancer is estimated to have caused over 9.6 million deaths in 2018, still being considered one of the major causes of death worldwide [1]. Tumor types and tumor infiltrating cells are highly heterogeneous, adding to the complexity of the disease. Thus, development of new treatments is a constant, crucial and challenging struggle. One logistic problem in these efforts is that most drug screenings are performed in two-dimensional (2D) *in vitro* cultures, which disregard the complexity of interactions seen in tumors *in vivo*. When in 2D, cells have more surface area in contact with the plastic and culture media than with other cells [2] forcing them into a polarization that does not reflect physiological conditions. A more realistic model of *in vitro* cancer cell cultures is the use of three-dimensional (3D) cultures. They are generally either scaffold-based models, in which cells interact with a substrate, or scaffold-free models, in which cells are unable to attach to a surface, thus forcing cell aggregation and spheroid formation.

In scaffold-based 3D cultures, cells are grown on a substrate that mimics the extracellular matrix (ECM). They are usually further classified into hydrogels or solid scaffolds, and may be either of natural or synthetic origin (Reviewed in: SANYAL, 2014 [3]; TIBBITT; ANSETH, 2010 [4]). One of the most widely accepted 3D cultures is a hydrogel made from the extract of

Engelbreth-Holm Swarm (EHS) tumors, being commercially available as Matrigel® (Corning), Geltrex® (Invitrogen) and Cultrex® (Trevigen). EHS tumors produce a high amount of basement membrane proteins, the most abundant being laminin, collagen IV, entactin, fibronectin, and heparin sulfate proteoglycan; also, these extracts contain a great number of growth factors [5,6]. Culturing cells on an EHS gel may not only alter morphology and gene expression patterns [7], but also migration [8], cell cycle and proliferation [9]. Nevertheless, because this basement membrane gel support is obtained from a murine tumor, attention should be given when culturing non-murine cells on such model. Dijkstra et al. observed CD4+ T cells reactivity when they were in contact with the gel or with dendritic cells exposed to Geltrex® [10]. There is also a great concern when using EHS gels regarding batch to batch variations [6,11]. These variations may significantly alter experiments, as the Matrigel® Growth Factor Reduced was shown to have only 53% similarity between batches [6].

Another technique for scaffold-based approaches is producing membranes through electrospinning. This technique produces fiber matts with adjustable diameter and porosity, while having a large surface area and an interconnected pore structure [12]. These scaffolds may be obtained from different types of materials, mostly natural or synthetic polymers, though also ceramics and metals may be used. As such, scaffolds have been used in different fields, being in tissue engineering [13], water filtration, drug development as a delivery system [14,15], and *in vitro* 3D cell culture [16].

Besides electrospinning, another commonly used technique is Solvent-Casting Particle-Leaching (SCPL), which can produce foam-like membranes. It was developed in 1994 [17], and has been used in a number of studies since then, especially on bone tissue engineering [18,19], though also in vascular repair [20]. SCPL is an approach much simpler than electrospinning, as the polymer solution is mixed with a porogen (usually salt) and left to dry, followed by leaching in order to remove the porogen used, being relatively easy to adjust pore size.

Among the different materials used for scaffold fabrication, polyhydroxybutyrate (PHB) is a very promising one. It is a natural polymer from the polyhydroxyalkanoate family and was first discovered in bacteria. In these organisms, PHB is stored as long chains and used as a source of energy, though it has already been found in various organisms. Because of PHB's highly flexible structure, biocompatibility and biodegradability [21], it has been used in many different areas, be it as bio-implanted patches [22], drug delivery carriers [23], wound dressing

[24], scaffolds for cell growth for tissue engineering [25,26] and as a 3D cell culture model [27].

Considering the need to develop and characterize the usefulness of novel 3D cell culture models for different applications, and that differences in interactions between cells, or between cells and the extracellular matrix, may be related to the selected culture model, we test here two different scaffold producing techniques, electrospinning and SCPL, using the same polymer, PHB. The scaffold topography is compared with EHS gel cell culture, the mostly commonly used 3D model. Cell morphology, gene expression and response to drug treatment were also assessed and compared between the three systems, as well as 2D conventional cultures.

3.2. MATERIALS AND METHODS

3.2.1 Membrane production

3.2.1.1 Electrospinning

PHB (Sigma Aldrich) was solubilized in chloroform at 60 ºC for 45 min, treated with dimethylformamide (20% v/v) for 30 minutes at room temperature and bathed in a steady ultrasound pulse of 40 kHz for 20 minutes. A glass syringe with the polymer solution was attached to an infusion bomb and to its needle was applied an electric current of +14 kV and -1 kV. The polymer was collected on a static collector, and membranes were kept in a vacuum chamber for chloroform evaporation for 48 h, after which the membranes were kept frozen at -20 ºC.

3.2.1.2 Solvent-Casting Particle-Leaching (SCPL)

After solubilizing the polymer as described above, the solution was poured in a casting mold. Then, sieved salt particles below 53 µm were added and the chloroform was left to evaporate for 72 h in an exhaustion hood. The membrane was then kept in deionized water for an ultrasonic bath of 40 kHz for 1 hour, washed and then kept in an ultrasonic bath for another hour. It was then placed for 72 h in a vacuum chamber to dry, followed by storage at -20 ºC.

3.2.2 Scaffold characterization

Solid EHS gel 10mg/ml was fixed with Karnovski solution, followed by a gradual dehydration with acetone and critical point dried. EHS gel, electrospun and SCPL membranes were mounted on stubs and sputter-coated with gold for Field Emission Gun Scanning Electron Microscopy (FESEM, Inspect 50 FEI) analysis. Pore and fiber diameters were measured using

the ImageJ software by using the set scale and measurement functions, for each group was considered a minimum of 4 images and on average 20 measurements per image.

3.2.3 Membrane preparation and cell seeding

Before each experiment, the electrospun and SCPL membranes were sterilized by washing three times in ethanol 70%, followed by three washes in phosphate buffer saline (PBS), being at least 10 minutes for each wash. The membranes were then placed on a 96-well culture plate at 37 ºC and 5% CO_2 for up to 24 hours. For the EHS gel cultures, Geltrex® LDEV free (Invitrogen) at a concentration of 10 mg/ml was added to the wells and left to solidify at 37 ºC, 5% CO_2 for 1 h. The medium used for the culture was supplemented with 2% of EHS gel. The gel solution was manipulated in ice to avoid premature gelling.

Mouse melanoma B16F10 GFP cells (kindly provided by Dr. Martim Bonamino from the Brazilian National Cancer Institute, INCA) were grown in DMEM High glucose (Gibco) supplemented with 10% of Fetal Bovine Serum (FBS). Cultures were kept in a humidified atmosphere of 5% CO_2 and 37 ºC until use. Each of these models had a different cell growth surface, which may alter proliferation rates. We thus performed pilot experiments, in order to determine the most adequate number of cells to be inoculated in each model, so that we could comparatively analyze, in the same amount of culture time, growth both in presence or absence of chemotherapy drugs. Thus, for the experiments, cells at 80% confluence in 2D cultures were detached with trypsin solution and seeded at 10^2 cells/well for 2D cultures; $2{,}5*10^4$ cells/well for EHS gel; 10^4 cells/well on electrospun membranes; and $2{,}5*10^4$ cells/well for SCPL cultures. For the electrospun and SCPL groups, cells were seeded on top of each membrane in 30 µl and left to adhere at 37 ºC and 5% CO_2 for 1 h, after which the medium was completed to 200 µl. After 24 hours, the membranes were carefully washed with PBS and changed to another well. Cultures were kept for 7 days and medium was changed twice.

3.2.4 In vivo experiments

C57BL/6 mice between 6-8 weeks old and 15-20 g were obtained and housed at the Centro de Modelos Biológicos e Experimentais (CEMBE PUC-RS, Brazil), where they had food and water *ad libitum*. Animals were inoculated subcutaneously with 10^6 B16F10 GFP cells on the left flank. After 10 days, the animals were euthanized and tumors were harvested. Each tumor was cut in two pieces, one was kept in a Karnovski solution for FESEM analysis (section 3.2.5) and the other was minced for RNA extraction (section 3.2.7). All animal procedures used were approved by PUC-RS university's animal ethic committee (CEUA), having the protocol ID CEUA 8466.

3.2.5 Scanning Electron Microscopy

At the end of the 7 days of culture, samples were fixed with a Karnovski solution, followed by post-fixation with osmium tetroxide for 1 hour, and a slow and gradual dehydration with acetone. Samples were critical point dried, mounted in stubs and sputter-coated with gold. Visualizations were done through FESEM (Inspect 50 FEI).

3.2.6 Cell Viability (MTT)

After 7 days in culture, cells were treated with either 100 or 200 µM of cisplatin and incubated for 48 h. Then, 20 µl of MTT solution (5 mg/ml) was added to each well, including blank samples, which were composed of the respective model with medium and no cells. The plate was then kept on an incubator at 37 ºC and 5% CO_2. After 3 h the plate was centrifuged at 1500 RPM, 4 ºC, and medium was discarded carefully while on ice. Formazan crystals were dissolved with 100 µl of DMSO and the plate was kept lightly shaking for 20 min, followed by optical density reading on Anthos Zenyth 340r microplate reader between 570 and 620 nm. Readings were normalized to their respective control without cisplatin and data analyzed on GraphPad prism 5.

3.2.7 Microarray

RNA was extracted from samples using the PureLink® RNA Mini Kit (Thermo Fisher). Briefly, cells were washed with ice-cold PBS, lysis buffer was added directly to cells and the protocol was carried out according to the manufacturer's instructions. Gene expression was analyzed through microarray assays (SurePrint G3 Human GE 8x60K Kit, Agilent, USA). Manufacturer's instructions were used in order to label, hybridize and wash the microarrays (LowInput QuickAmp Labeling Kit Two-Color, Agilent, USA), which were then scanned using the SureScan (Agilent, USA) according to default parameters. Experiment quality, background correction, and the identification of expressed genes were carried out with the Feature Extraction software (Agilent, USA). After this initial processing, Genespring software (Agilent, USA) was used for data analysis. For the fluorescence intensity normalization between samples quantile normalization was used, and only probes identified as detected or non-detected in at least 100% of one of the experimental conditions were included in the analysis. Principal Components Analysis (PCA) and Hierarchical Clustering were used to visualize data, and for statistical analysis, One-Way ANOVA was used. Gene expression levels are presented in fold-changes in respect to the *in vivo* data. Results were considered statistically significant if $p<0.05$ after Benjamini-Hochberg False-Discovery Rate (FDR) correction [28,29].

3.3 RESULTS AND DISCUSSION

3.3.1 Scaffold production and characterization

Through electrospinning and SCPL techniques two types of membranes were generated and their topography can be seen on Fig. 1A-C. While gel fibers had small diameters, with a mean of 0.043 ±0.02 μm (Fig. S1A**,** Supporting information), electrospun fibers had larger diameters, with a mean of 1.1 ±0.47 μm (Fig. S1B, Supporting information). SCPL membranes were composed of random shapes, with pore size varying between 0.56-48.36 μm, while electrospun membrane pores and gel pores varied between 0.66-12.07 μm and 0.21-4.35 μm, respectively (Fig. 1D-F, Table 1). Pore size is a very important and discussed issue regarding scaffold models since it can determine how the cells will interact and grow. It has been proposed that in order for cells to grow on a "true 3D" environment, pore sizes should be smaller than the cells. That is important so cells are not growing alongside fibers, thus growing on a 2D curved plane; rather, cells should be completely involved within the membrane [20,30]. Besides, depending on cell type, nanopatterns have been shown to either promote or inhibit cell attachment, exemplifying that small pore scaffolds may act as stimuli and induce spheroid formation [31,32]. The electrospun membrane studied here would be able to provide these stimuli, however, although cells are able to infiltrate the membrane, most are still found growing on top of it. Cells grown on SCPL membranes appear to invade the membrane more easily, showing the importance of larger pore sizes. It is agreed, though, that the pore size should be related to the size of the cells being cultured. As has been seen by Lowery et al, human dermal fibroblasts should be grown on scaffolds with pore sizes between 6-20 μm, as larger ones would promote growth along fibers and decrease ECM production, while in smaller pores although they could bridge the fibers and produce ECM much faster, cells would only grow on top of the membrane [33]. For that, varying pore sizes may promote cell penetration into the scaffold, where it may grow interacting more closely with this ECM mimetic [34].

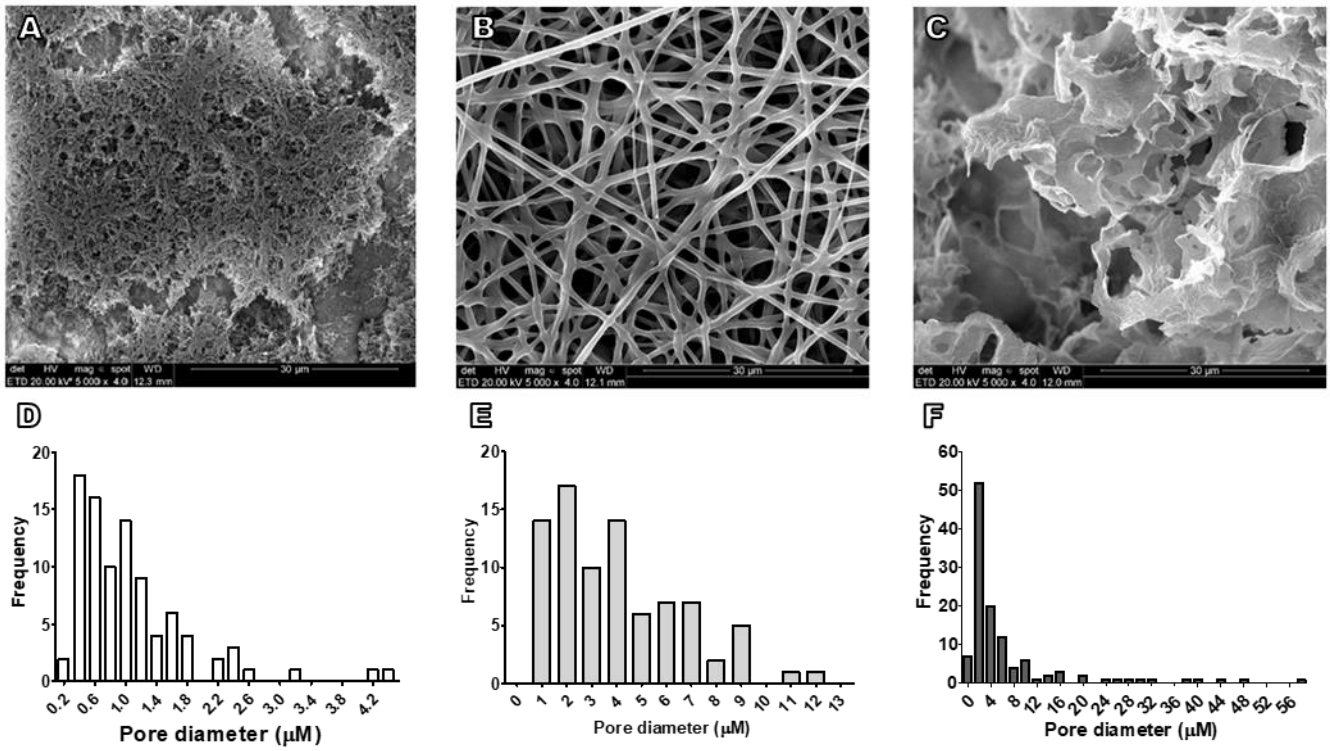

Figure 1. Scaffold structures. FESEM micrographs of the different scaffolds studied, EHS gel (**A**), electrospun (**B**), SCPL membrane (**C**). Magnification of 5,000x, scale bar 30 μM. Pore diameter of the different scaffolds, EHS gel (**D**), electrospun (**E**), SCPL membrane (**F**).

Table 1. Pore size in μM across 3D models

	Min	Max	Mean	Median
EHS gel	0.21	4.35	1.06 ± 0.76	0.89
Electrospun	0.66	12.07	4.04 ± 2.66	3.55
SCPL	0.56	48.36	6.66 ± 9.22	3.04

3.3.2 Cell culture morphology

As has been seen before, cells cultured *in vitro* may alter their morphology according to the conditions in which they are grown in. Triple-negative breast cancer cells (MDA-MB-231) after being cultured on 15% PCL electrospun scaffolds showed a higher elongation factor than cells grown on 2D cultures [16]. Besides, different breast and prostate cancer cell lines showed distinct cell organizations when growing on a 3D environment, as compared with 2D cultures, allowing better drug investigation [7,35]. In order to evaluate cell growth across different culture methods, Field Emission Gun Scanning Electron Microscopy (FESEM) analysis were done after culturing cells for either 7 days *in vitro* or 10 days *in vivo*. As can be seen on Fig. 2, while few cell aggregates may be seen on 2D cultures, those grown on 3D environments were larger. Melanoma cells on 3D cultures also showed a rounder morphology, more closely

resembling *in vivo* than 2D growth. Interestingly, cells on EHS gel (Fig. 2 C and D), electrospun membrane (Fig. 2 G and H) and SCPL membrane (Fig. 2 I and J) showed a variety of morphologies, similarly to B16F10 GFP cells on C57BL/6 (Fig. 2 E and F). Besides, on the SCPL membrane cells tended to grow involving the scaffold, instead of forming spheroids on top of the substrate, as seen on electrospun samples (Fig. 2 H and J). Additionally, cell aggregates on the electrospun membrane had more spherical cells than the other 3D models, and they were also formed on a much higher frequency than on the SCPL membrane (Fig. 3). B16F10 growing on the 3D models also had a number of filopodia, probably used to sense the environment they were growing in.

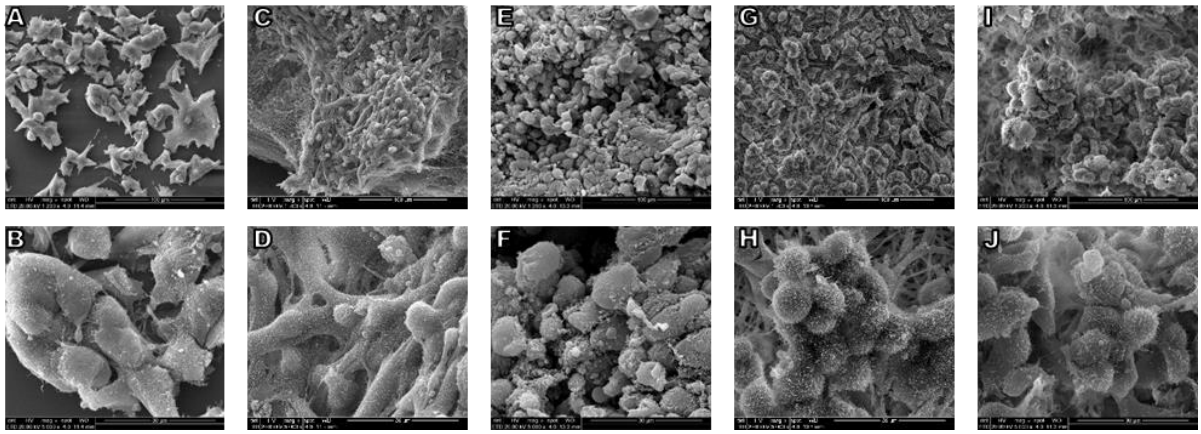

Figure 2. FESEM micrographs of B16F10 GFP cell culture on different models. *In vitro* (7 days culture) 2D **(A,B)**, EHS gel **(C,D)**, Electrospun membrane **(G, H)** and SCPL membrane **(I, J)**. *In vivo* 10 days tumor of B16F10 GFP cells on C57BL/6 **(E, F)**. Magnification of 1,200x **(A,C,E,G,I)** and 5,000x **(B,D,F,H,J)**.

It has already been reported that cells grown on a tissue culture plastic tend to have a more flattened morphology. Human breast cancer cells (MCF7) after growing on 2D were flat with trigonal and polygonal morphologies, while cells grown on a collagen scaffold had a diversity of morphologies, including rounder, spread-out and elongated [36]. Besides, endometrial cell lines when cultured in EHS gels formed glandular and spheroid-like structures, resembling much more closely *in vivo* morphology [37]. In general, the formation of cell aggregates or spheroids has been shown to better simulate tissues, especially when considering that not all cells will get in contact with medium or drugs due to difficulties in nutrient and waste exchange. Depending on the spheroid size, it may be composed of cells on three different stages: cells on the outermost layer will proliferate, while those in the middle layer will be quiescent; if the structure is large enough (usually diameter above 500 µm), it will have a necrotic center due to inaccessibility to nutrients and increase in acidity and wastes products [38]. Thus, the formation of these cell aggregates and spheroids on the 3D cultures studied may bring advantages to the models by providing different microenvironments for the cells. Although spheroids less round in shape may have a different structure than the classical one (since it may develop more than

one necrotic center), it may still provide different microenvironments in the cell culture, thus altering response to signals.

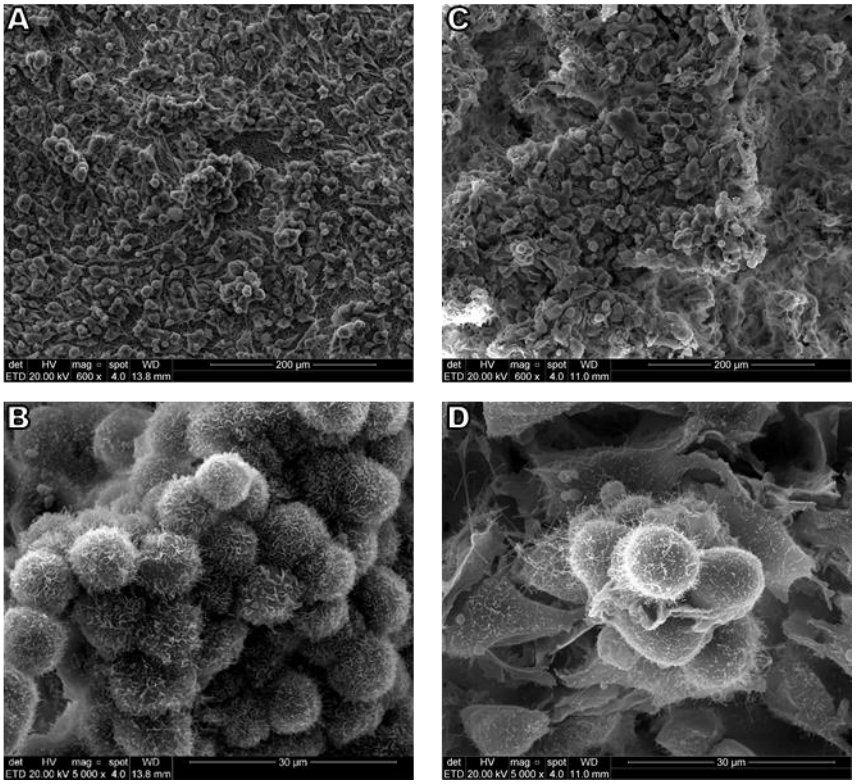

Figure 3. FESEM micrographs of B16F10 GFP growth structure on different models. Cells were grown for 7 days either on Electrospun membranes **(A, B)** or on SCPL membranes **(C, D)**. Cells on the electrospun membrane are shown to form more and larger aggregates than those on the SCPL membrane. Magnification of 600x **(A,C)** and 5,000x **(B,D)**.

3.3.3 Effect of cisplatin on 2D and 3D models

In order to evaluate how the two novel models proposed here, SCPL and electrospun membranes, would affect cell resistance to cisplatin, cultures were treated for 48 h followed by MTT cell viability analysis. As can be seen on Fig. 4, although there is a tendency to drug resistance in 100 µM cisplatin treatment, only cells on the electrospun membrane treated with 200 µM cisplatin were able to withstand drug effects.

Cell interactions in culture conditions may interfere in response to drug treatment. In prostate cancer cell lines, it was found that compounds targeting the mTOR pathway inhibited cancer cells in 2D and 3D cultures, while those targeting the AKT pathway were less effective on 2D [35]. It has also been shown that spheroids on collagen gel had a greater resistance to doxorubicin treatment than cells on 2D and spheroids on a scaffold-free model [39]. In fact, cells cultured on 3D models may display either increased or decreased drug resistance when compared with results from 2D cell cultures. These alterations may vary according to cell culture model and the nature of the drug used [40,41]. As has been described, there are a number

of ways through which resistance can be affected. One was studied by Imamura et al., where dense spheroids had a tendency to be resistant to paclitaxel and doxorubicin treatment when compared to looser spheroids or 2D growth. These denser spheroids showed decreased apoptosis and stained positive for Ki67, while having hypoxic centers [42]. Colorectal cancer cell lines have also been shown to have decreased p53 levels on 3D cultures after CDDP treatment, when compared with 2D treated cultures. Even though these cells would have similar p53 levels on 2D and 3D, after CDDP treatment cells cultured in 3D had decreased sensitivity to the drug. These alterations were attributed to the difference in architecture between 2D and 3D cultures [43]. It is believed that cell morphology and interactions between cells may have a great effect on expression and treatment outcome. As seen on MCF7 breast cancer cells, treatment with CDDP on EHS gel had chromatin reorganization leading to induction of ATR phosphorylation, chk1 activation and REV3L upregulation, leading to increased senescence [39]. These results come to show that depending on the 3D environment and cell-cell and cell-matrix interactions, a culture might become resistant or susceptible to a certain drug treatment.

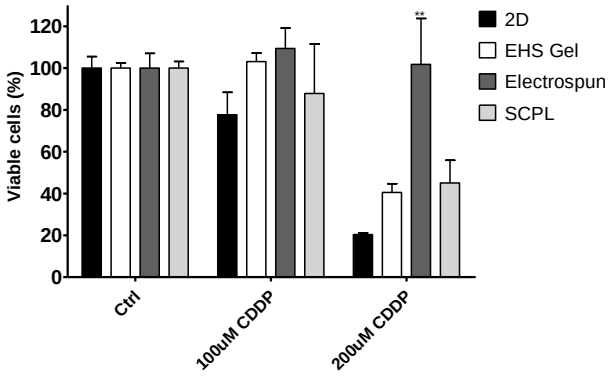

Figure 4. Viability analysis through MTT. B16F10 GFP cells were cultured for 7 days, followed by treatment with Cisplatin (0, 100 or 200 µM) for 48 h. ** $p<0.01$

3.3.4 RNA expression across different culture models

Similar cell morphology was observed for cells grown on EHS Gel, electrospun membranes and SCPL alike, and increased resistance to cisplatin was seen for all four systems. Global gene expression patterns corroborate these findings, as depicted by the PCA plot (Fig. 5A). The PCA plot captures 30% of variability among the conditions and demonstrates that no clear gene expression pattern characterizes each model. In fact, considering a fold-change of 2, only 55 transcripts were differentially expressed among the four conditions. We used hierarchical clustering to visualize this result and this representation highlights that, considering this set of genes, cells grown on 2D and EHS Gel are more similar to each other and cells grown on SCPL

express these genes in a more distinct way (Fig. 5B). It is also interesting to note that only nine transcripts were similarly down regulated in EHS Gel, SCPL and the electrospun models when compared with the 2D cell culture (Fig. 6); none of these transcripts have known functions associated with cell proliferation, differentiation or drug response. Considering the 55 differentially expressed transcripts, 33 correspond to annotated genes, 9 of which are associated with cell signaling (Fig. 7A) and 6 are located at the cell membrane (Fig. 7B).

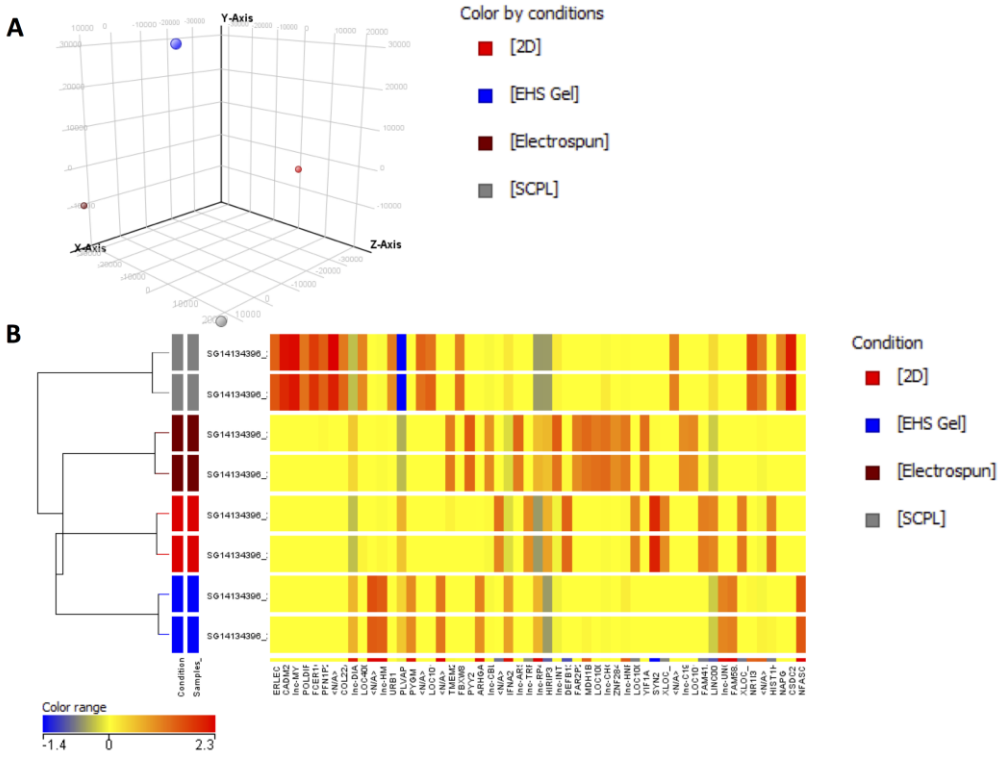

Figure 5 Principal component analysis and hierarchical cluster analysis (A) Principal component analysis depicting global gene expression profiles for the four cell culture models. The first three principal components explain approximately 30% of the variation between the samples, the plot shows no grouping of conditions. **(B)** Hierarchical cluster analysis showing the expression level of the 55 transcripts that showed at least a 2-fold difference (corrected p value < 0.05) in expression levels between any of the four conditions.

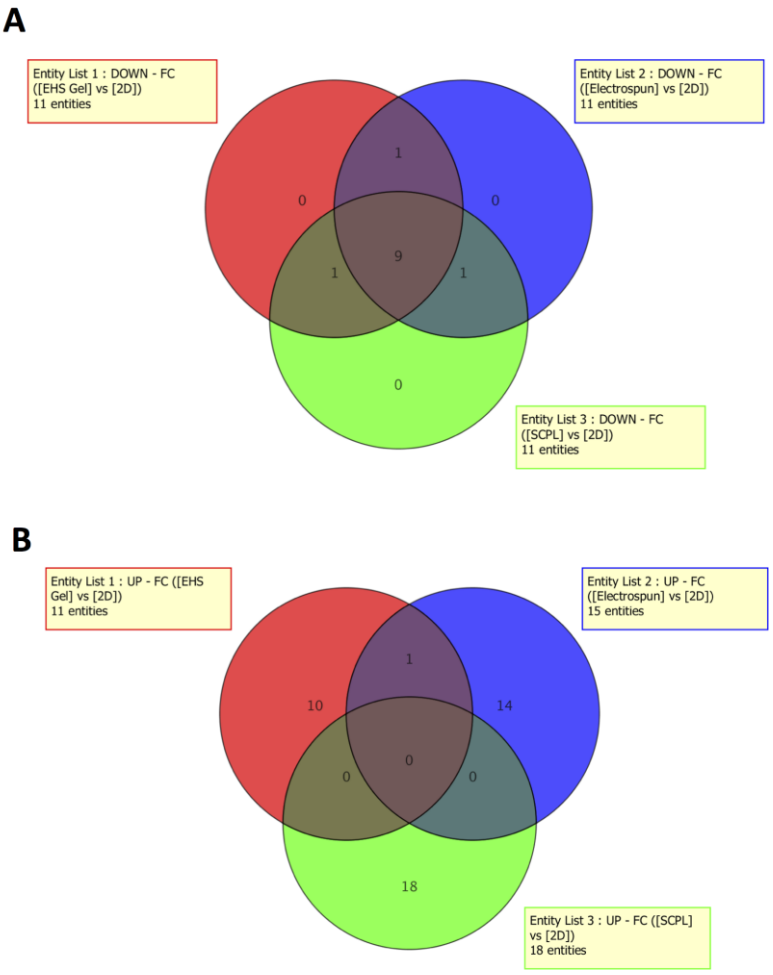

.

Figure 6 Venn diagrams illustrating the significantly differentially expressed genes in each evaluated condition. **(A)** Down regulated genes in EHS Gel, SCPL and electrospun membranes when compared with the 2D cell culture. Nine common genes were down regulated. **(B)** Up regulated genes in EHS Gel, SCPL and electrospun membranes when compared with the 2D cell culture. No common genes were up regulated

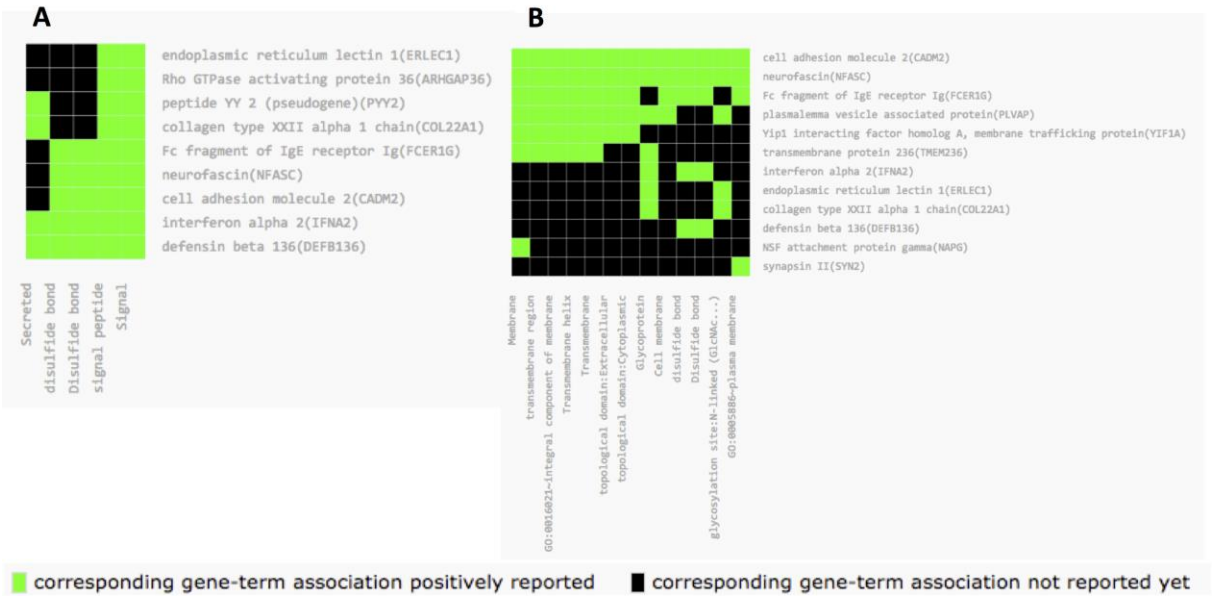

Figure 7 Functional annotation clustering of genes showing at least a 2-fold difference in expression levels between EHS Gel, SCPL or the electrospun membranes against the 2D culture system.

3.4. CONCLUSIONS

All the culture methods analyzed were able to sustain cell growth, and all 3D culture models showed morphologies more similar to *in vivo* growth than to monolayer 2D culture. Both electrospun and SCPL membranes did not induce cell death, and cells grown on them were able to interact with each other and the ECM mimetic. Though there were no substantial differences in response to cisplatin when comparing 2D, EHS gel and SCPL cell culture, when cells were grown on the electrospun membrane even 200 µM of cisplatin was unable to induce significant cell death. Gene expression analysis corroborates with the similarities observed by the biological assays, with relatively few transcripts showing different expression between the models. Further experiments using different conditions such as RNA collection time point and cell stimulation, are necessary to identify differences in molecular mechanisms associated with cell growth and maintenance in each studied model. Even though these 3D models were produced by different techniques, they show many similarities across experiments, demonstrating that the use of animal origin models could be substitute by more ethical platforms. Taken together these results may help to characterize differences between the 3D cell models and the 2D culture, but further experiments, possibly under different conditions, are needed for a better understanding of these differences.

Acknowledgements

Special thanks to MSc. Karina Lima, PhD. Rodrigo Gassen and PhD. Sofia Scomazzon from Pontifical Catholic University of Rio Grande do Sul (PUCRS) for support, as well as Leandro Baum and colleagues from Central Laboratory of Microscopy and Microanalysis (LabCEMM) at the PUCRS for the FESEM technical support. This work was supported by the Brazilian National Program for Support to Oncological Awareness (PRONON) SIPAR 250000.159946/2014-16. J. C. Fontoura is the recipient of a scholarship from CAPES (Coordenação de Aperfeiçoamento de Pessoal de Nível Superior, Brazil)

References

[1] F. Bray, J. Ferlay, I. Soerjomataram, R.L. Siegel, L.A. Torre, A. Jemal, Global Cancer Statistics 2018: GLOBOCAN Estimates of Incidence and Mortality Worldwide for 36 Cancers in 185 Countries, CA. Cancer J. Clin. 68 (2018) 394–424. doi:10.3322/caac.21492.

[2] B.M. Baker, C.S. Chen, Deconstructing the third dimension – how 3D culture microenvironments alter cellular cues, J. Cell Sci. 125 (2012) 3015–3024. doi:10.1242/jcs.079509.

[3] S. Sanyal, Culture and Assay Systems Used for 3D Cell Culture, Corning. (2014).

[4] M.W. Tibbitt, K.S. Anseth, Hydrogel as Extracellular Matrix Mimics for 3D Cell Culture, Biotechnol. Bioeng. 103 (2010) 655–663. doi:10.1002/bit.22361.Hydrogels.

[5] R.D. Simoni, J.B. Hays, T. Nakazawa, S. Roseman, R. Stein, O. Schrecker, H.F. Lauppe, H. Hengstenberg, J. Thompson, H. Towbin, T. Staehelin, J. Gordon, E.B. Waygood, R.L. Mattoo, N. Weigel, M.A. Kukuruzinska, A. Nakazawa, E.G. Waygood, W. Wray, T. Boulikas, V.P. Wray, R.; B. Hancock, Basement Membrane Complexes with Biological Activity, Proc. Natl. Acad. Sci. U.S.A. 25 (1986) 312–318.

[6] C.S. Hughes, L.M. Postovit, G.A. Lajoie, Matrigel: a complex protein mixture required for optimal growth of cell culture., Proteomics. 10 (2010) 1886–1890. doi:10.1002/pmic.200900758.

[7] P.A. Kenny, G.Y. Lee, C.A. Myers, R.M. Neve, J.R. Semeiks, P.T. Spellman, K. Lorenz, E.H. Lee, M.H. Barcellos-Hoff, O.W. Petersen, J.W. Gray, M.J. Bissell, The morphologies of breast cancer cell lines in three-dimensional assays correlate with their profiles of gene expression, Mol. Oncol. 1 (2007) 84–96. doi:10.1016/j.molonc.2007.02.004.

[8] R. Poincloux, O. Collin, F. Lizárraga, M. Romao, M. Debray, M. Piel, P. Chavrier, Contractility of the cell rear drives invasion of breast tumor cells in 3D Matrigel, Proc. Natl. Acad. Sci. 108 (2011) 1943–1948. doi:10.1073/pnas.1010396108.

[9] M. Gargotti, U. Lopez-Gonzalez, H.J. Byrne, A. Casey, Comparative studies of cellular viability levels on 2D and 3D *in vitro* culture matrices, Cytotechnology. 70 (2018) 261–273. doi:10.1007/s10616-017-0139-7.

[10] K.K. Dijkstra, C.M. Cattaneo, F. Weeber, M. Chalabi, J. van de Haar, L.F. Fanchi, M. Slagter, D.L. van der Velden, S. Kaing, S. Kelderman, N. van Rooij, M.E. van Leerdam, A. Depla, E.F. Smit, K.J. Hartemink, R. de Groot, M.C. Wolkers, N. Sachs, P. Snaebjornsson, K. Monkhorst, J. Haanen, H. Clevers, T.N. Schumacher, E.E. Voest, Generation of Tumor-Reactive T Cells by Co-culture of Peripheral Blood Lymphocytes and Tumor Organoids, Cell. 174 (2018) 1586–1598.e12. doi:10.1016/j.cell.2018.07.009.

[11] G. Benton, I. Arnaoutova, J. George, H.K. Kleinman, J. Koblinski, Matrigel: From discovery and ECM mimicry to assays and models for cancer research, Adv. Drug Deliv. Rev. 79–80 (2014) 3–18. doi:10.1016/j.addr.2014.06.005.

[12] L. Jesús Villarreal-Gómez, M. Cornejo-Bravo, R. Vera-Graziano, D. Grande, Electrospinning as a powerful technique for biomedical applications: a critically selected survey, J. Biomater. Sci. 27 (2016) 157–176.

doi:10.1080/09205063.2015.1116885.

[13] J. Ramier, D. Grande, T. Bouderlique, O. Stoilova, N. Manolova, I. Rashkov, V. Langlois, P. Albanese, E. Renard, From design of bio-based biocomposite electrospun scaffolds to osteogenic differentiation of human mesenchymal stromal cells, J. Mater. Sci. Mater. Med. 25 (2014) 1563–1575. doi:10.1007/s10856-014-5174-8.

[14] E. Yan, Y. Fan, Z. Sun, J. Gao, X. Hao, S. Pei, C. Wang, L. Sun, D. Zhang, Biocompatible core-shell electrospun nanofibers as potential application for chemotherapy against ovary cancer, Mater. Sci. Eng. C. 41 (2014) 217–223. doi:10.1016/j.msec.2014.04.053.

[15] S. Chen, S. Kumar Boda, S.K. Batra, X. Li, J. Xie, Emerging Roles of Electrospun Nanofibers in Cancer Research, (2017). doi:10.1002/adhm.201701024.

[16] M. Rabionet, M. Yeste, T. Puig, J. Ciurana, Electrospinning PCL scaffolds manufacture for three-dimensional breast cancer cell culture, Polymers (Basel). 9 (2017) 1–15. doi:10.3390/polym9080328.

[17] A.G. Mikos, A.J. Thorsen, L.A. Czerwonka, Y. Bao, R. Langer, Preparation and characterization o poly(L-lactic acid) foams, Polymer (Guildf). 35 (1994) 1068–1077. doi:10.1002/anie.196904562.

[18] Z.L. Mou, L.M. Duan, X.N. Qi, Z.Q. Zhang, Preparation of silk fibroin/collagen/hydroxyapatite composite scaffold by particulate leaching method, Mater. Lett. 105 (2013) 189–191. doi:10.1016/j.matlet.2013.03.130.

[19] N. Thadavirul, P. Pavasant, P. Supaphol, Fabrication and Evaluation of Polycaprolactone–Poly(hydroxybutyrate) or Poly(3-Hydroxybutyrate-co-3-Hydroxyvalerate) Dual-Leached Porous Scaffolds for Bone Tissue Engineering Applications, Macromol. Mater. Eng. 302 (2017) 1–17. doi:10.1002/mame.201600289.

[20] L. Rogers, S.S. Said, K. Mequanint, The Effects of Fabrication Strategies on 3D Scaffold Morphology, Porosity, and Vascular Smooth Muscle Cell Response, J. Biomater. Tissue Eng. 3 (2013) 300–311. doi:10.1166/jbt.2013.1088.

[21] R.N. Reusch, Physiological Importance of Poly-(R)-3-hydroxybutyrates, Chem. Biodivers. 9 (2012) 2343–2366.

[22] E.C.C. Reis, A.P.B. Borges, C.C. Fonseca, M.M.M. Martinez, R.B. Eleotério, G.O. Morato, P.M. Oliveira, Biocompatibility, osteointegration, osteoconduction, and biodegradation of a hydroxyapatite-polyhydroxybutyrate composite, Brazilian Arch. Biol. Technol. 53 (2010) 817–826. doi:10.1590/S1516-89132010000400010.

[23] X. Wang, S.S. Liow, Q. Wu, C. Li, C. Owh, Z. Li, X.J. Loh, Y.L. Wu, Codelivery for Paclitaxel and Bcl-2 Conversion Gene by PHB-PDMAEMA Amphiphilic Cationic Copolymer for Effective Drug Resistant Cancer Therapy, Macromol. Biosci. 17 (2017) 1–11. doi:10.1002/mabi.201700186.

[24] E.I. Shishatskaya, E.D. Nikolaeva, O.N. Vinogradova, T.G. Volova, Experimental wound dressings of degradable PHA for skin defect repair, J. Mater. Sci. Mater. Med. 27 (2016) 165. doi:10.1007/s10856-016-5776-4.

[25] C. Ye, P. Hu, M.-X. Ma, Y. Xiang, R.-G. Liu, X.-W. Shang, PHB/PHBHHx scaffolds and human adipose-derived stem cells for cartilage tissue engineering, Biomaterials. 30 (2009) 4401–4406. doi:10.1016/j.biomaterials.2009.05.001.

[26] Z. Karahaliloğlu, M. Demirbilek, M. Şam, N. Sağlam, A.K. Mizrak, E.B. Denkbaş, Surface-modified bacterial nanofibrillar PHB scaffolds for bladder tissue repair, Artif. Cells, Nanomedicine Biotechnol. 44 (2016) 74–82. doi:10.3109/21691401.2014.913053.

[27] Y. Wang, X.L. Jiang, S.W. Peng, X.Y. Guo, G.G. Shang, J.C. Chen, Q. Wu, G.Q. Chen, Induced apoptosis of osteoblasts proliferating on polyhydroxyalkanoates, Biomaterials. 34 (2013) 3737–3746. doi:10.1016/j.biomaterials.2013.01.088.

[28] Y. Benjamini, Y. Hochberg, Controlling the False Discovery Rate: A Practical and Powerful Approach to Multiple, 1995.

[29] Y. Benjamini, Discovering the false discovery rate, J. R. Stat. Soc. Ser. B Stat. Methodol. 72 (2010) 405–416. doi:10.1111/j.1467-9868.2010.00746.x.

[30] S. Zhang, F. Gelain, X. Zhao, Designer self-assembling peptide nanofiber scaffolds for 3D tissue cell cultures, Semin. Cancer Biol. 15 (2005) 413–420. doi:10.1016/j.semcancer.2005.05.007.

[31] A.S.G. Curtis, N. Gadegaard, M.J. Dalby, M.O. Riehle, C.D.W. Wilkinson, G. Aitchison, Cells React to Nanoscale Order and Symmetry in Their Surroundings, IEEE Trans. Nanobioscience. 3 (2004) 61–65. doi:10.1109/TNB.2004.824276.

[32] K. Seunarine, D.O. Meredith, M.O. Riehle, C.D.W. Wilkinson, N. Gadegaard, Biodegradable polymer tubes with lithographically controlled 3D micro- and nanotopography, Microelectron. Eng. 85 (2008) 1350–1354. doi:10.1016/j.mee.2008.02.002.

[33] J.L. Lowery, N. Datta, G.C. Rutledge, Effect of fiber diameter, pore size and seeding method on growth of human dermal fibroblasts in electrospun poly(3-caprolactone) fibrous mats, Biomaterials. 31 (2010) 491–504. doi:10.1016/j.biomaterials.2009.09.072.

[34] A. Timnak, J.A. Gerstenhaber, K. Dong, Y. El Har-El, P.I. Lelkes, Gradient porous fibrous scaffolds: A novel approach to improving cell penetration in electrospun scaffolds, Biomed. Mater. 13 (2018). doi:10.1088/1748-605X/aadbbe.

[35] V. Härmä, J. Virtanen, R. Mäkelä, A. Happonen, J.P. Mpindi, M. Knuuttila, P. Kohonen, J. Lötjönen, O. Kallioniemi, M. Nees, A comprehensive panel of three-dimensional models for studies of prostate cancer growth, invasion and drug responses, PLoS One. 5 (2010). doi:10.1371/journal.pone.0010431.

[36] L. Chen, Z. Xiao, Y. Meng, Y. Zhao, J. Han, G. Su, B. Chen, J. Dai, The enhancement of cancer stem cell properties of MCF-7 cells in 3D collagen scaffolds for modeling of cancer and anti-cancer drugs, Biomaterials. 33 (2012) 1437–1444. doi:10.1016/j.biomaterials.2011.10.056.

[37] K. Chitcholtan, E. Asselin, S. Parent, P.H. Sykes, J.J. Evans, Differences in growth properties of endometrial cancer in three dimensional (3D) culture and 2D cell monolayer, Exp. Cell Res. 319 (2013) 75–87.

[38] M. Zanoni, F. Piccinini, C. Arienti, A. Zamagni, S. Santi, R. Polico, A. Bevilacqua, A. Tesei, 3D tumor spheroid models for *in vitro* therapeutic screening: A systematic approach to enhance the biological relevance of data obtained, Sci. Rep. 6 (2016). doi:10.1038/srep19103.

[39] D. Yip, C.H. Cho, A multicellular 3D heterospheroid model of liver tumor and stromal cells in collagen gel for anti-cancer drug testing, Biochem. Biophys. Res. Commun. 433 (2013) 327–332. doi:10.1016/j.bbrc.2013.03.008.

[40] C. Shen, G. Zhang, Q. Meng, Evaluation of amiodarone-induced phospholipidosis by *in vitro* system of 3D cultured rat hepatocytes in gel entrapment, Biochem. Eng. J. 49 (2010) 308–316. doi:10.1016/j.bej.2009.12.010.

[41] N. Gomez-Roman, K. Stevenson, L. Gilmour, G. Hamilton, A.J. Chalmers, A novel 3D human glioblastoma cell culture system for modeling drug and radiation responses, Neuro. Oncol. 19 (2017) 229–241. doi:10.1093/neuonc/now164.

Supplementary

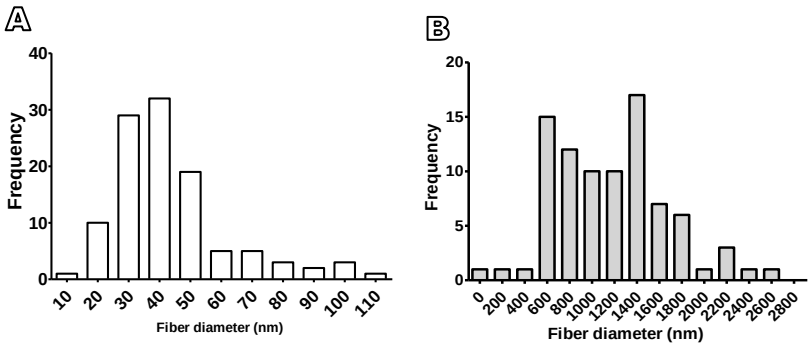

Figure. S1 Fiber diameter frequency distribution of EHS gel (A) and Electrospun membranes (B).

CAPÍTULO 4

4.1 CONSIDERAÇÕES FINAIS

Nesse trabalho foram abordados dois projetos relacionados a biologia tumoral. Primeiramente foi feita a avaliação do efeito antitumoral *in vitro* da cochaperona HspBP1. Experimentos anteriores do laboratório indicavam que HspBP1 estaria agindo de forma a sensibilizar o tumor para quimioterapia ao inibir a chaperona Hsp70. Assim, foram feitas curvas de dose-resposta combinando HspBP1 com um quimioterápico para cada linhagem celular abordada. Avaliamos resposta celular ao tratamento com HspBP1 com/sem quimioterápico por diversas estratégias como: viabilidade por MTT, densidade celular por microscopia e acompanhamento da cultura pelo Incucyte, apoptose por Anexina/PI e morte celular por LDH. Apesar de em algumas das técnicas ser possível ver leves alterações na cultura causadas pelo tratamento com HspBP1, podemos concluir que *in vitro* a proteína não agiu de forma citotóxica, nem citostática. Inclusive, experimentos preliminares de ciclo celular não mostrados aqui, também não apresentaram alterações com a adição de HspBP1 na cultura celular.

Embora não se veja ação antitumoral de HspBP1 *in vitro* pelas técnicas aqui demonstradas, nosso grupo já tem dados mostrando que o tratamento por via intravenosa de tumores *in vivo* tanto de melanoma (B16F10 em C57BL/6) quanto de mama (4T1 em BALB/c) com a proteína HspBP1 levou a redução no volume tumoral. Quando esse experimento foi repetido em animais imunocomprometidos (que apresentavam apenas parte do sistema imune inato funcional), o tratamento de HspBP1 não levou a mesma redução tumoral (Dissertação em processo de conclusão de Lima, K.R. de nosso grupo). Assim, é possível que a ação da proteína seja indireta, o que explica a falta de resposta em modelo *in vitro*.

No segundo projeto abordado, foram feitos experimentos comparando diferentes modelos de cultura celular *in vitro*: 2D, gel EHS, dois tipos de membranas (uma eletrofiada e outra produzida por SCPL), e também com modelo *in vivo*. Em nossos experimentos não foi vista muita diferença entre os tipos de cultura 3D, mesmo quando comparando as membranas com o modelo já estabelecido de gel produzido a partir de extrato de tumor murino EHS. Demonstra-se então o potencial desses modelos que não necessitam de animais para serem produzidos. Também vale salientar, que a escolha do método de cultivo deve ser feita de acordo com os objetivos do trabalho. Cada modelo apresenta vantagens e desvantagens em relação ao seu uso, o gel EHS, por exemplo, é de difícil manipulação, visto que tem de ser feita no gelo. Além disso, a presença de proteínas de origem murina pode complicar seu uso, inclusive

induzindo resposta imune. Apesar da manipulação das membranas ser mais fácil e versátil, visto que é possível cortar no tamanho necessário e o manuseio pode ser feito com uma pinça, a visualização do crescimento celular é difícil. Em geral, não é possível fazer o acompanhamento da cultura nas membranas sem células fluorescentes, por exemplo. Mesmo com algumas dificuldades, a utilização de modelos tridimensionais pode melhorar significativamente experimentos *in vitro*, principalmente por conseguir aproximar a cultura ao *in vivo*. Embora não tenha sido abordado nesse projeto, a utilização de coculturas, ou seja, cultivar mais de um tipo celular em conjunto, também apresenta diversas vantagens. É possível que se fossem repetidos os experimentos de tratamento com HspBP1 em um modelo 3D com células tumorais e do sistema imune, os resultados se mostrassem mais semelhantes aos observados *in vivo*.

REFERÊNCIAS

AL-BADR, Abdullah A.; ALODHAIB, Mansour M. Dacarbazine. [s. l.], v. 41, p. 323–377, 2016.

BENTON, Gabriel et al. Matrigel: From discovery and ECM mimicry to assays and models for cancer research. **Advanced Drug Delivery Reviews**, [s. l.], v. 79–80, p. 3–18, 2014.

BHASKAR, Prajwal et al. Cell response to sterilized electrospun poly(E-caprolactone) scaffolds to aid tendon regeneration *in vivo*. **J Biomed Mater Res Part A**, [s. l.], v. 105A, p. 389–397, 2017.

BORGES, Thiago J. et al. Modulation of alloimmunity by heat shock proteins. **Frontiers in Immunology**, [s. l.], v. 7, n. AUG, 2016.

BOROUGHS, Lindsey K. et al. A unique role for heat shock protein 70 and its binding partner tissue transglutaminase in cancer cell migration. **The Journal of biological chemistry**, [s. l.], v. 286, n. 43, p. 37094–107, 2011.

BRAY, Freddie et al. Global Cancer Statistics 2018: GLOBOCAN Estimates of Incidence and Mortality Worldwide for 36 Cancers in 185 Countries. **CA: a cancer journal for clinicians**, [s. l.], v. 68, p. 394–424, 2018.

BRESLIN, Susan; O'DRISCOLL, Lorraine. **Three-dimensional cell culture: The missing link in drug discoveryDrug Discovery Today**, 2013.

BROQUET, Alexis H. et al. Expression of the molecular chaperone Hsp70 in detergent-resistant microdomains correlates with its membrane delivery and release. **Journal of Biological Chemistry**, [s. l.], v. 278, n. 24, p. 21601–21606, 2003.

BRUNTON LAURENCE L, RANDA HILAL-DANDAN, Bjorn C. Knollman. **Goodman and Gilman's : the pharmacological basis of therapeutics**. 13. ed. New York: McGraw-Hill, 2018.

CALDERWOOD, Stuart K. Molecular Cochaperones: Tumor Growth and Cancer Treatment. **Scientifica**, [s. l.], v. 2013, p. 1–13, 2013.

CALDERWOOD, Stuart K.; PRINCE, Thomas L. **Molecular Chaperones: Methods and Protocols**. [s.l.] : Humana Press, 2011.

CHEE, Jayven et al. Recent advances in the development of biodegradable PHB-based toughening materials: Approaches, advantages and applications. **Materials Science and Engineering C**, [s. l.], v. 92, p. 1092–1116, 2018.

CRAPO, J. D. et al. Cell number and cell characteristics of the normal human lung. **American Review of Respiratory Disease**, [s. l.], v. 126, n. 2, p. 332–337, 1982.

CUKIERMAN, E. et al. Taking cell-matrix adhesions to the third dimension. **Science**, [s. l.], v. 294, n. 5547, p. 1708–1712, 2001.

DEDKOVA, Elena N.; BLATTER, Lothar A. Role of β-hydroxybutyrate, its polymer poly-β-hydroxybutyrate and inorganic polyphosphate in mammalian health and disease. **Frontiers in Physiology**, [s. l.], v. 5, 2014.

ELUSTONDO, Pia A. et al. Polyhydroxybutyrate Targets Mammalian Mitochondria and Increases Permeability of Plasmalemmal and Mitochondrial Membranes. **PLoS ONE**, [s. l.],

2013.

ELUSTONDO, Pia; ZAKHARIAN, Eleonora; PAVLOV, Evgeny. Identification of the polyhydroxybutyrate granules in mammalian cultured cells. **Chemistry and Biodiversity**, [s. l.], v. 9, n. 11, p. 2597–2604, 2012.

FANG, Ye; EGLEN, Richard M. Three-Dimensional Cell Cultures in Drug Discovery and Development. **SLAS Discovery**, [s. l.], v. 22, n. 5, p. 456–472, 2017.

FUTAKI, Sugiko et al. Molecular basis of constitutive production of basement membrane components: Gene expression profiles of Engelbreth-Holm-Swarm tumor and F9 embryonal carcinoma cells. **Journal of Biological Chemistry**, [s. l.], v. 278, n. 50, p. 50691–50701, 2003.

GEHRMANN, Mathias et al. Tumor-Specific Hsp70 Plasma Membrane Localization Is Enabled by the Glycosphingolipid Gb3. **PLoS ONE**, [s. l.], v. 3, n. 4, 2008.

GIRARD, Yvonne K. et al. A 3D Fibrous Scaffold Inducing Tumoroids: A Platform for Anticancer Drug Development. **PLoS ONE**, [s. l.], v. 8, n. 10, 2013.

GOWDA, Naveen K. C. et al. Nucleotide exchange factors Fes1 and HspBP1 mimic substrate to release misfolded proteins from Hsp70. **Nature Structural & Molecular Biology**, [s. l.], v. 25, n. 1, p. 83–89, 2018.

GUY, Gery P. et al. Vital signs: melanoma incidence and mortality trends and projections - United States, 1982-2030. **Morb Mortal Wkly Rep**, [s. l.], v. 64, n. 21, p. 591–596, 2015.

HAIDER, Adnan; HAIDER, Sajjad; KANG, Inn Kyu. A comprehensive review summarizing the effect of electrospinning parameters and potential applications of nanofibers in biomedical and biotechnology. **Arabian Journal of Chemistry**, [s. l.], v. 11, n. 8, p. 1165–1188, 2018.

HANAHAN, Douglas; WEINBERG, Robert A. Hallmarks of cancer: the next generation. **Cell**, [s. l.], v. 144, n. 5, p. 646–74, 2011.

HERVIEU, Alice et al. Dacarbazine-Mediated Upregulation of NKG2D Ligands on Tumor Cells Activates NK and CD8 T Cells and Restrains Melanoma Growth. **Journal of Investigative Dermatology**, [s. l.], v. 133, p. 499–508, 2013.

INCA. **Estimativa 2018. Incidência de câncer no Brasil**. [s.l: s.n.].

JABBAR, Sab; TWENTYMAN, PR; WATSON, JV. **The MTT assay underestimates the growth inhibitory effects of interferonsBr. J. Cancer**. [s.l: s.n.].

JAEGER, Natalia et al. Neuropeptide gastrin-releasing peptide induces PI3K/reactive oxygen species–dependent migration in lung adenocarcinoma cells. **Tumor Biology**, [s. l.], v. 39, n. 3, 2017.

JAGADISH, Nirmala et al. Heat shock protein 70-2 (HSP70-2) overexpression in breast cancer. **Journal of experimental & clinical cancer research : CR**, [s. l.], v. 35, n. 1, p. 150, 2016.

KENNY, Paraic A. et al. The morphologies of breast cancer cell lines in three-dimensional assays correlate with their profiles of gene expression. **Molecular Oncology**, [s. l.], v. 1, n. 1, p. 84–96, 2007.

KHODABAKHSHI, Darioush et al. *In vitro* and *in vivo* performance of a propolis-coated polyurethane wound dressing with high porosity and antibacterial efficacy. **Colloids and**

Surfaces B: Biointerfaces, [s. l.], v. 178, p. 177–184, 2019.

KLEINMAN, Hynda K.; MARTIN, George R. Matrigel: Basement membrane matrix with biological activity. **Seminars in Cancer Biology**, [s. l.], v. 15, n. 5 SPEC. ISS., p. 378–386, 2005.

KOSMAOGLOU, Maria et al. Molecular chaperones and photoreceptor function. **Molecular chaperones and photoreceptor function**, [s. l.], v. 27, p. 434–449, 2008.

LANCASTER, Graeme I.; FEBBRAIO, Mark A. Exosome-dependent trafficking of HSP70: A novel secretory pathway for cellular stress proteins. **Journal of Biological Chemistry**, [s. l.], v. 280, n. 24, p. 23349–23355, 2005.

LIU, Weimin et al. Waste cigarette filter as nanofibrous membranes for on-demand immiscible oil/water mixtures and emulsions separation. **Journal of Colloid and Interface Science**, [s. l.], v. 549, p. 114–122, 2019.

LONGLEY, Daniel B.; HARKIN, D. Paul; JOHNSTON, Patrick G. 5-FLUOROURACIL: MECHANISMS OF ACTION AND CLINICAL STRATEGIES. [s. l.], 2003.

MARYCZ, Krzysztof et al. Biphasic polyurethane/polylactide sponges doped with nano-hydroxyapatite (nHAp) combined with human adipose-derived mesenchymal stromal stem cells for regenerative medicine applications. **Polymers**, [s. l.], v. 8, n. 10, p. 339, 2016.

MCLELLAN, Catherine A.; RAYNES, Deborah A.; GUERRIERO, Vince. HspBP1, an Hsp70 cochaperone, has two structural domains and is capable of altering the conformation of the Hsp70 ATPase domain. **Journal of Biological Chemistry**, [s. l.], v. 278, n. 21, p. 19017–19022, 2003.

MIKOS, Antonios G. et al. Preparation and characterization of poly(L-lactic acid) foams. **POLYMER**, [s. l.], v. 35, n. 5, p. 1068–1077, 1994.

RAYNES, Deborah A.; GUERRIERO, Vince. Inhibition of Hsp70 ATPase activity and protein renaturation by a novel Hsp70-binding protein. **Journal of Biological Chemistry**, [s. l.], v. 273, n. 49, p. 32883–32888, 1998.

REIS, Emily Correna Carlo et al. Biocompatibility, osteointegration, osteoconduction, and biodegradation of a hydroxyapatite-polyhydroxybutyrate composite. **Brazilian Archives of Biology and Technology**, [s. l.], v. 53, n. 4, p. 817–826, 2010.

REUSCH, Rosetta N. Physiological Importance of Poly-(R)-3-hydroxybutyrates. **CHEMISTRY & BIODIVERSITY**, [s. l.], v. 9, p. 2343–2366, 2012.

RIMANN, Markus; GRAF-HAUSNER, Ursula. Synthetic 3D multicellular systems for drug development. **Current Opinion in Biotechnology**, [s. l.], v. 23, n. 5, p. 803–809, 2012.

RISS, Terry L. et al. Cell Viability Assays. In: **Assay Guidance Manual**. [s.l: s.n.]. p. 1–23.

SAIBIL, Helen. Chaperone machines for protein folding, unfolding and disaggregation. **Nature Reviews Molecular Cell Biology**, [s. l.], v. 14, n. 10, p. 630–642, 2013.

SANADA, Masayuki et al. Modes of actions of two types of anti-neoplastic drugs, dacarbazine and ACNU, to induce apoptosis. **Carcinogenesis**, [s. l.], v. 28, n. 12, p. 2657–2663, 2007.

SHALOAM, Dasari; TCHOUNWOU, Paul Bernard. Cisplatin in cancer therapy: Molecular mechanisms of action. **European Journal of Pharmacology**, [s. l.], v. 740, p. 364–378,

2014.

SIM. **Mortalidade - Brasil**. 2017. Disponível em: <http://tabnet.datasus.gov.br/cgi/tabcgi.exe?sim/cnv/obt10uf.def>.

SOUZA, Ana Paula et al. HspBP1 levels are elevated in breast tumor tissue and inversely related to tumor aggressiveness. **Cell stress & chaperones**, [s. l.], v. 14, n. 3, p. 301–10, 2009.

STOCKERT, Juan C. et al. MTT assay for cell viability: Intracellular localization of the formazan product is in lipid droplets. **Acta Histochemica**, [s. l.], v. 114, n. 8, p. 785–796, 2012.

SUBIK, Kristina et al. The expression patterns of ER, PR, HER2, CK5/6, EGFR, KI-67 and AR by immunohistochemical analysis in breast cancer cell lines. **Breast Cancer: Basic and Clinical Research**, [s. l.], v. 4, n. 1, p. 35–41, 2010.

SURIN, A. M. et al. **Disruption of functional activity of mitochondria during MTT assay of viability of cultured neuronsBiochemistry (Moscow)**Pleiades Publishing, , 2017.

SWARM, Richard L. Transplantation of a murine chondrosarcoma in mice of different inbred strains. **Journal of the National Cancer Institute**, [s. l.], v. 31, n. 4, p. 953–975, 1963.

TEO, W. E.; RAMAKRISHNA, S. A review on electrospinning design and nanofibre assemblies. **Nanotechnology**, [s. l.], v. 17, n. 14, 2006.

THORN, Caroline F.; ALTMAN, Russ B. Doxorubicin pathways: pharmacodynamics and adverse effects. **Pharmacogenet Genomics**, [s. l.], v. 21, n. 7, p. 440–446, 2011.

TRAVIS, William D. et al. The 2015 World Health Organization Classification of Lung Tumors. **Journal of Thoracic Oncology**, [s. l.], v. 10, n. 9, p. 1243–1260, 2015.

ULUKAYA, Engin; COLAKOGULLARI, Mukaddes; WOOD, Edward J. Interference by Anti-Cancer Chemotherapeutic Agents in the MTT-Tumor Chemosensitivity Assay. **Chemotherapy**, [s. l.], v. 50, n. 1, p. 43–50, 2004.

VAN TONDER, Alet; JOUBERT, Annie M.; CROMARTY, A. Duncan. Limitations of the 3-(4,5-dimethylthiazol-2-yl)-2,5-diphenyl-2H-tetrazolium bromide (MTT) assay when compared to three commonly used cell enumeration assays. **BMC Research Notes**, [s. l.], v. 8, n. 1, 2015.

WANG, Piwen; HENNING, Susanne M.; HEBER, David. Limitations of MTT and MTS-based assays for measurement of antiproliferative activity of green tea polyphenols. **PLoS ONE**, [s. l.], v. 5, n. 4, 2010.

WANG, Xiaoyuan et al. Codelivery for Paclitaxel and Bcl-2 Conversion Gene by PHB-PDMAEMA Amphiphilic Cationic Copolymer for Effective Drug Resistant Cancer Therapy. **Macromolecular Bioscience**, [s. l.], v. 17, p. 1–11, 2017.

WEAVER, Beth A. How Taxol/paclitaxel kills cancer cells. **Molecular Biology of the Cell**, [s. l.], v. 25, n. 18, p. 2677–2681, 2014.

WEGELE, H.; MÜLLER, L.; BUCHNER, J. Hsp70 and Hsp90--a relay team for protein folding. **Reviews of physiology, biochemistry and pharmacology**, [s. l.], v. 151, n. January, p. 1–44, 2004.

WEINBERG, R. **The Biology of Cancer, Second Edition**. [s.l.] : Taylor & Francis Group,

2013.

WOLFERS, J. et al. Tumor-derived exosomes are a source of shared tumor rejection antigens for CTL cross-priming. **Nature medicine**, [s. l.], v. 7, n. 3, p. 297–303, 2001.

WORLD HEALTH ORGANIZATION. **Global Health Estimates 2016: Deaths by Cause, Age, Sex, by Country and by Region, 2000-2016**, 2018.

XIE, Yan et al. High-performance porous polylactide stereocomplex crystallite scaffolds prepared by solution blending and salt leaching. **Materials Science and Engineering C**, [s. l.], v. 90, p. 602–609, 2018.

YAN, Eryun et al. Biocompatible core-shell electrospun nanofibers as potential application for chemotherapy against ovary cancer. **Materials Science and Engineering C**, [s. l.], v. 41, p. 217–223, 2014.

ZASADIL, Lauren M. et al. Cytotoxicity of paclitaxel in breast cancer is due to chromosome missegregation on multipolar spindles. **Science Translational Medicine**, [s. l.], v. 6, n. 229, 2014.

ANEXO A – Comprovante de submissão do artigo

Gmail — Júlia Crispim da Fontoura <fontoura.julia@gmail.com>

Track your co-authored submission to Materials Science & Engineering C
1 mensagem

Materials Science & Engineering C <EviseSupport@elsevier.com> 16 de fevereiro de 2019 10:56
Responder a: EviseSupport@elsevier.com
Para: fontoura.julia@gmail.com

Dear Miss Crispim da Fontoura,

Submission no: MSEC_2019_572
Submission title: Comparison of 2D and 3D cell culture models for cell growth, gene expression and drug resistance
Corresponding author: Professor Cristina Bonorino
Listed co-author(s): Professor Dyeison Antonow, Dr Christian Viezzer, Dr Patricia Severino, Professor Rosane Ligabue, Miss Fabiana G. Santos, Miss Júlia Crispim da Fontoura

Professor Bonorino has submitted a manuscript to Materials Science & Engineering C and listed you as a co-author. This email is to let you know we will be in contact with updates at each decision stage of the submission process.

The link below takes you to a webpage where you can sign in to our submission system using your existing Elsevier profile credentials or register to create a new profile. You will then have the opportunity to tailor these updates and view reviewer and editor comments once they become available.

http://www.evise.com/profile/api/navigate/MSEC?resourceUrl=%2Fco-author%2F%3Fdgcid%3Dinvite_email_coauthoroutreach09284931%23%2FMSEC%2Fsubmission%2FMSEC_2019_572

ANEXO B – Carta para revisão do manuscrito

Ref: MSEC_2019_572
Title: Comparison of 2D and 3D cell culture models for cell growth, gene expression and drug resistance
Journal: Materials Science & Engineering C

Dear Professor Bonorino,

Thank you for submitting your manuscript to Materials Science & Engineering C. We have completed the review of your manuscript. A summary is appended below. While revising the paper please consider the reviewers' comments carefully. We look forward to receiving your detailed response and your revised manuscript.

Kind regards,
Lijie Grace Zhang
Editor-in-Chief
Materials Science & Engineering C

Comments from the editors and reviewers:
-**Reviewer 1**

-1. Regarding drug resistance, the authors reported only one model drug, cisplatin. It is necessary to expand the study to other common chemotherapeutics, and see if anything varies. Since there is a general trend of drug resistance, why is the exception of electrospun membrane cultures? Authors should have discussed the mechanism behind this phenomenon.

2. In terms of the growth patterns of cells in different 3D models, it is recommended to use a variety of cell lines for validation, instead of just murine melanoma B16F10 cells.

3. For Fig. 2 and Fig. 3, authors used SEM to study cell morphology. However, SEM samples are subjected to a series of sample processing procedures, and the cells for SEM imaging are actually in a “dry state”, which is a lot different from cells under the actual condition. The reviewer consider authors should consider using immunofluorescence staining plus confocal microscopy techniques to reveal the morphological changes of cells under different culture conditions.

4. Why is the number of cell inoculations different in 2D and different 3D models, and does this affect the growth of cells in different models? Please explain.

5. How to define the fiber diameter in Fig. S1, why is there no fiber diameter frequency distribution of SCPL membranes?

6. 3D models are better than 2D models in simulating the in vivo environment. However, it is not enough to only study cell growth, and authors should consider performing more experiments to compare the two models.

7. Minor comments: 1) language needs to be improved. 2) Bar graphs need to be improved.

-**Reviewer 2**

This manuscript introduces two kinds of 3D in vitro models using two different scaffold producing techniques, electrospinning and SCPL. And the scaffold topography was compared with EHS gel cell culture. Cell morphology, gene expression and response to drug treatment were also assessed and compared between the three systems, as well as 2D conventional cultures. In order to make this paper better, author need to pay attention to some inadequate points in the manuscript and some details. As follows:

1. In Section 3.1 “table1 Pore size across 3D models”, the unit is missing and the data is not the same as the test. For example, in Section 3.1, “Considering its different production, SCPL membranes were composed of random shapes, with pore size varying between 0.5-50 μm, while electrospun and gel pores varied between 0.6-12 μm and 0.2-4 μm, respectively (Fig. 1D-F, Table 1)”. However, the pore size of SCPL is 206-4.347. What’s more, the expression of the number should be more standard.

2. As mentioned in this paper, the human dermal fibroblasts should be grown on scaffolds with pore sizes between 6-20 μm, however, the systems used in the paper were not inconformity. The SCPL scaffold had the largest pores

and cell-ECM interactions, while only growth on electrospun membrane was able to induce cisplatin resistance. The reason why it occurred this paper isn't mentioned.

3. In Section 3.4 "RNA expression across different culture models", the PCA plot shows that cells grown on 2D and EHS Gel are more similar to each other and cells grown on SCPL express these genes in a more distinct way. How to explain the result that 3D models had similar RNA expression.

4. Some details should be noticed. For example, the title of Fig 7 is not complete. There are some problems in the typesetting.

All in all, the paper should be improved.

ANEXO C – Resposta aos revisores

Dear Editor,

Please see below a point by point response to the reviewers comments. We are enclosing a new version of the manuscript updated accordingly, with all modifications highlighted in yellow.

- Reviewer 1

1. *Regarding drug resistance, the authors reported only one model drug, cisplatin. It is necessary to expand the study to other common chemotherapeutics and see if anything varies. Since there is a general trend of drug resistance, why is the exception of electrospun membrane cultures? Authors should have discussed the mechanism behind this phenomenon.*

   The reviewer brings an important point. In addition to the previously presented Cisplatin, we have added new experiments using the chemotherapeutic drug Dacarbazine. This new data can be found in **Figure 4** (**page 16**). Cells growing in 3D cultured cells, when incubated with this drug, all showed enhanced resistance when compared with 2D culture, with our membranes performing similarly to the EHS gel. We believe such results support our (an other studies') previous findings that chemotherapeutic drugs toxicity is overestimated in 2D cultures, as well as validates this aspect of our membranes.
   Regarding a possible mechanism behind the general trend of drug resistance and the exception of the electrospun membrane cultures, different explanations have been suggested. We have added that to the Results and Discussion section, **page 16**.
   In terms of the growth patterns of cells in different 3D models, it is recommended to use a variety of cell lines for validation, instead of just murine melanoma B16F10 cells.
   This is also an excellent point. We have performed new experiments using the 4T1 murine breast cancer cell line to add validation to our previous results with B16F10 melanoma cells. The results, added in Results and Discussion **pages 12 through 14**, and in the new **Figure 3**, support our previous findings.

2. *For Fig. 2 and Fig. 3, authors used SEM to study cell morphology. However, SEM samples are subjected to a series of sample processing procedures, and the cells for SEM imaging are actually in a "dry state", which is a lot different from cells under the actual condition. The reviewer consider authors should consider using immunofluorescence staining plus confocal microscopy techniques to reveal the morphological changes of cells under different culture conditions.*

   We have performed additional experiments using confocal microscopy as suggested. For that, we used the B16F10 cell line that expresses GFP. The new results are added in **Figure 2B**, and described in the Results and Discussion, **page 14**.

3. *Why is the number of cell inoculations different in 2D and different 3D models, and does this affect the growth of cells in different models? Please explain.*

Pilot studies were conducted which determined the cell inoculation numbers. Each of these models had a difference surface area for cell growth, and a different proliferation rate was observed in each model, making it impossible to use the same inoculation numbers for the same time of culture without having massive death in one but not all the models. We have now added a paragraph to the methods section on **page 8** explaining this methodological step in more detail.

4. *How to define the fiber diameter in Fig. S1, why is there no fiber diameter frequency distribution of SCPL membranes?*

   We have added the fiber diameter details, analyzed using FESEM and Image J software, in the methods section **page 7**. Because there are no fibers in SCPL membranes, they were not included. This explanation was added to the results section, **page 11**.

5. *3D models are better than 2D models in simulating the in vivo environment. However, it is not enough to only study cell growth, and authors should consider performing more experiments to compare the two models.*

   The reviewer brings and important point. We need to clarify that the aim of this work was to construct and characterize two novel synthetic scaffolds for 3D cultures for tumor models – which is described in the Abstract and now added to the Introduction, **page 6**. We have performed new experiments, and we are adding additional results, as described above (mouse breast cancer cell line (4T1), added results from dacarbazine treatment, and confocal microscopy). Of note, we have performed an *in vivo* experiment, in order to expand our transcriptomics studies. We have added this interesting new data set to **Figure 5**, highlighting molecular similarities between cells grown in 3D systems, compared to *in vivo* and *in vitro* growth. Important transcription data has been added as Supplemental Tables. We hope these new experimental data will satisfy the reviewer.

6. *Minor comments: 1) language needs to be improved. 2) Bar graphs need to be improved.*

   We thank the reviewer for these observations. The latest and revised version of the manuscript has been thoroughly improved both in spelling and grammar as well as clarity of thought. Finally, bar graphs have been adequately standardized.

-Reviewer 2

This manuscript introduces two kinds of 3D in vitro models using two different scaffold producing techniques, electrospinning and SCPL. And the scaffold topography was compared with EHS gel cell culture. Cell morphology, gene expression and response to drug treatment were also assessed and compared between the three systems, as well as 2D conventional cultures. In order to make this paper better, author need to pay attention to some inadequate points in the manuscript and some details. As follows:

1. *In Section 3.1 "table1 Pore size across 3D models", the unit is missing and the data is not the same as the test. For example, in Section 3.1, "Considering its different production, SCPL membranes were composed of random shapes, with pore size varying between 0.5-50 μm, while electrospun and gel pores varied between 0.6-12 μm and 0.2-*

4 μm, respectively (Fig. 1D-F, Table 1)". However, the pore size of SCPL is 206-4.347. What's more, the expression of the number should be more standard.

We thank the reviewer for the observation. This has been corrected, unit has been added to table title, and numbers have been standardized to the US model. The revisions are highlighted in yellow in Table 1.

2. *As mentioned in this paper, the human dermal fibroblasts should be grown on scaffolds with pore sizes between 6-20 μm, however, the systems used in the paper were not in conformity. The SCPL scaffold had the largest pores and cell-ECM interactions, while only growth on electrospun membrane was able to induce cisplatin resistance. The reason why it occurred this paper isn't mentioned.*

   We appreciate the reviewer's observation. We have repeated the cisplatin resistance experiments, adjusting the time in culture. In all of the experiments, except the former set of cisplatin experiments, the total time of culture was 7 days (we were adding cisplatin on day 7, resulting in a final 9 days of culture. This is possibly the reason for variation in these results. We now adjusted the time course of the drug resistance experiments, to 5 days of culture, and two days of treatment, resulting in a 7 days total. This has been changed in Methods, **page 9**.
   Our new results, in new **Figure 4**, show that culture in SCPL cultures there is resistance to cisplatin.
   We have also added another chemotherapeutic drug, Dacarbazine. For this drug, all 3D scaffolds resulted in enhanced resistance (**Fig 4**).
   We mentioned the fibroblast paper as a reference, however these cells are tumor cells, and not fibroblasts. We wanted to test if tumor cell growth in our scaffolds would depend on pore size. However, our results indicate that they have been able to grow in both scaffolds successfully.
   Finally, we have added new experiments with a different cell line (4T1 murine breast cancer) and the results, seen on the new **Figure 3**, indicate this cell line also grows on both SCPL and electrospun membranes.
   We hope the reviewer will be satisfied with this new set of data.

3. *In Section 3.4 "RNA expression across different culture models", the PCA plot shows that cells grown on 2D and EHS Gel are more similar to each other and cells grown on SCPL express these genes in a more distinct way. How to explain the result that 3D models had similar RNA expression.*

   This is a very good point. In fact, we have largely redone the RNA expression studies increasing sample sizes and adding an *in vivo* control, which can be found on Results and discussion **pages 15 through 17**. Our results, now presented in figure 5, show that all 3D scaffolds are more similar among them. They are also more similar to the in vivo cells, and all of them are more distinct from the 2D grown cells.

   Some details should be noticed. For example, the title of Fig 7 is not complete. There are some problems in the typesetting.
   All in all, the paper should be improved.

We thank the reviewer for the thorough revision. **Figure 7** is no longer in the manuscript, and all the new transcriptomics data are in the new **Figure 5**. The article has been revised, both text and figures have been updated accordingly and we hope the improvements will be satisfactory.

ANEXO D – Versão atualizada do artigo (09/2019)

Comparison of 2D and 3D cell culture models for cell growth, gene expression and drug resistance

Authors: Julia C. Fontoura [a,b]; Christian Viezzer [a]; Fabiana G. dos Santos [c]; Rosane A. Ligabue [c]; Ricardo Weinlich [d]; Renato D. Puga [d]; Dyeison Antonow [e]; Patricia Severino [d]; Cristina Bonorino [b,f] *

[a] Laboratório de Imunologia Celular e Molecular, Pontifícia Universidade Católica do Rio Grande do Sul (PUCRS), Porto Alegre, RS, Brasil

[b] Departamento de Ciências Básicas da Saúde, Universidade Federal de Ciências da Saúde, Porto Alegre, RS, Brasil

[c] Laboratório de Caracterização de Materiais, PUCRS, Porto Alegre, RS, Brazil

[d] Hospital Israelita Albert Einstein, São Paulo, SP, Brasil

[e] Institute of Petroleum and Natural Resources (IPR), Tecnopuc, PUCRS, Porto Alegre, RS, Brazil

[f] Department of Surgery, School of Medicine, University of California at San Diego

*Corresponding author at: Departamento de Ciências Básicas da Saúde, Universidade Federal de Ciências da Saúde, Porto Alegre, RS, Brasil

Email: cristinabcb@ufcspa.edu.br; cbonorino@ucsd.edu

1. Introduction

Cancer is estimated to have caused over 9.6 million deaths in 2018, still being considered one of the major causes of death worldwide [1]. Tumor types and tumor infiltrating cells are highly heterogeneous, adding to the complexity of the disease. Thus, development of new treatments is a constant, crucial and challenging struggle. One logistic problem in these efforts is that most drug screenings are performed in two-dimensional (2D) *in vitro* cultures, which disregard the complexity of interactions seen in tumors *in vivo*. When in 2D, cells have more surface area in contact with the plastic and culture media than with other cells [2] forcing them into a polarization that does not reflect physiological conditions. A more realistic model of *in vitro* cancer cell cultures is the use of three-dimensional (3D) cultures. They are generally either scaffold-based models, in which cells interact with a substrate, or scaffold-free models, in which cells are unable to attach to a surface, thus forcing cell aggregation and spheroid formation.

In scaffold-based 3D cultures, cells are grown on a substrate that mimics the extracellular matrix (ECM). They are usually further classified into hydrogels or solid scaffolds, and may be either of natural or synthetic origin (Reviewed in: SANYAL, 2014; TIBBITT; ANSETH, 2010). One of the most widely accepted 3D cultures is a hydrogel made from the extract of

Engelbreth-Holm Swarm (EHS) tumors, being commercially available as Matrigel® (Corning), Geltrex® (Invitrogen) and Cultrex® (Trevigen). EHS tumors produce a high amount of basement membrane proteins, the most abundant being laminin, collagen IV, entactin, fibronectin, and heparin sulfate proteoglycan; also, these extracts contain a great number of growth factors [5,6]. Culturing cells on an EHS gel may not only alter morphology and gene expression patterns [7], but also migration [8], cell cycle and proliferation [9]. Nevertheless, because this basement membrane gel support is obtained from a murine tumor, attention should be given when culturing non-murine cells on such model. Dijkstra et al. observed CD4+ T cells reactivity when they were in contact with the gel or with dendritic cells exposed to Geltrex® [10]. There is also a great concern when using EHS gels regarding batch to batch variations [6,11]. These variations may significantly alter experiments, as the Matrigel® Growth Factor Reduced was shown to have only 53% similarity between batches [6].

Another technique for scaffold-based approaches is producing membranes through electrospinning. This technique produces fiber matts with adjustable diameter and porosity, while having a large surface area and an interconnected pore structure [12]. These scaffolds may be obtained from different types of materials, mostly natural or synthetic polymers, though also ceramics and metals may be used. As such, scaffolds have been used in different fields, being in tissue engineering [13], water filtration, drug development as a delivery system [14,15], and *in vitro* 3D cell culture [16].

Besides electrospinning, another commonly used technique is Solvent-Casting Particle-Leaching (SCPL), which can produce foam-like membranes. It was developed in 1994 [17], and has been used in a number of studies since then, especially on bone tissue engineering [18,19], though also in vascular repair [20]. SCPL is an approach much simpler than electrospinning, as the polymer solution is mixed with a porogen (usually salt) and left to dry, followed by leaching in order to remove the porogen used, being relatively easy to adjust pore size.

Among the different materials used for scaffold fabrication, polyhydroxybutyrate (PHB) is a very promising one. It is a natural polymer from the polyhydroxyalkanoate family and was first discovered in bacteria. In these organisms, PHB is stored as long chains and used as a source of energy, though it has already been found in various organisms. Because of PHB's highly flexible structure, biocompatibility and biodegradability [21], it has been used in many different areas, be it as bio-implanted patches [22], drug delivery carriers [23], wound dressing

[24], scaffolds for cell growth for tissue engineering [25,26] and as a 3D cell culture model [27].

The aim of this work was to construct and characterize two novel synthetic scaffolds for 3D cultures for tumor models. We test here two different scaffold producing techniques, electrospinning and SCPL, using the same polymer, PHB. The scaffold topography is compared with EHS gel cell culture, one of the most commonly used 3D models. Cell morphology, gene expression and response to drug treatment were also assessed and compared between the three systems, as well as 2D conventional cultures. Our results indicate that the two synthetic systems developed by us are similar to the classic EHS gel model, highlighting their potential application as cost effective substitutes for drug screening,

2. Materials and methods

2.1. Membrane production

2.1.1. Electrospinning

PHB (Sigma Aldrich) was solubilized in chloroform at 60 ºC for 45 min, treated with dimethylformamide (20% v/v) for 30 minutes at room temperature and bathed in a steady ultrasound pulse of 40 kHz for 20 minutes. A glass syringe with the polymer solution was attached to an infusion bomb and to its needle was applied an electric current of +14 kV and -1 kV. The polymer was collected on a static collector, and membranes were kept in a vacuum chamber for chloroform evaporation for 48 h, after which the membranes were kept frozen at -20 ºC.

2.1.2. Solvent-Casting Particle-Leaching (SCPL)

After solubilizing the polymer as described above, the solution was poured in a casting mold. Then, sieved salt particles below 53 µm were added and the chloroform was left to evaporate for 72 h in an exhaustion hood. The membrane was then kept in deionized water for an ultrasonic bath of 40 kHz for 1 hour, washed and then kept in an ultrasonic bath for another hour. It was then placed for 72 h in a vacuum chamber to dry, followed by storage at -20 ºC.

2.2. Scaffold characterization

Solid EHS gel 10mg/ml was fixed with Karnovski solution, followed by a gradual dehydration with acetone and critical point dried. EHS gel, electrospun and SCPL membranes were mounted on stubs and sputter-coated with gold for Field Emission Gun Scanning Electron Microscopy (FESEM, Inspect 50 FEI) analysis. Pore and fiber diameters were measured using the ImageJ software by using the set scale and measurement functions, for

each group was considered a minimum of 4 images and on average 20 measurements per image.

2.3. Membrane preparation and cell seeding

Before each experiment, the electrospun and SCPL membranes were sterilized by washing three times in ethanol 70%, followed by three washes in phosphate buffer saline (PBS), being at least 10 minutes for each wash. The membranes were then placed on a 96-well culture plate at 37 ºC and 5% CO_2 for up to 24 hours. For the EHS gel cultures, Geltrex® LDEV free (Invitrogen) at a concentration of 10 mg/ml was added to the wells and left to solidify at 37 ºC, 5% CO_2 for 1 h. The medium used for the culture was supplemented with 2% of EHS gel. The gel solution was manipulated in ice to avoid premature gelling.

Mouse melanoma B16F10 GFP cells (kindly provided by Dr. Martim Bonamino from the Brazilian National Cancer Institute, INCA) and mouse breast cancer 4T1 cells (ATCC CRL-2539) were grown in DMEM High glucose (Gibco) and RPMI-1640, respectively, both supplemented with 10% of Fetal Bovine Serum (FBS). Cultures were kept in a humidified atmosphere of 5% CO_2 and 37 ºC until use. Each of these models had a different cell growth surface, which may alter proliferation rates. We thus performed pilot experiments, in order to determine the most adequate number of cells to be inoculated in each model, so that we could comparatively analyze, in the same amount of culture time, growth both in presence or absence of chemotherapy drugs. Thus, for the experiments, cells at 80% confluence in 2D cultures were detached with trypsin solution and seeded at 10^2 cells/well for 2D cultures; $2{,}5*10^4$ cells/well for EHS gel; 10^4 and $2{,}5*10^4$ cells/well for B16F10 GFP and 4T1 cells on electrospun membranes; and $2{,}5*10^4$ cells/well for SCPL cultures. For the electrospun and SCPL groups, cells were seeded on top of each membrane in 30 µl and left to adhere at 37 ºC and 5% CO_2 for 1 h, after which the medium was completed to 200 µl. After 24 hours, the membranes were carefully washed with PBS and changed to another well. Cultures were kept for 7 days and medium was changed twice.

2.4. In vivo tumor model

C57BL/6 and BALB/c mice between 6-8 weeks old and 15-20 g were obtained and housed at the Centro de Modelos Biológicos e Experimentais (CEMBE PUC-RS, Brazil), where they had food and water *ad libitum*. C57BL/6 animals were inoculated subcutaneously with 10^6 B16F10 GFP cells on the left flank, while BALB/c were inoculated with 10^5 4T1 cells in the third left mammary fat pad. After 10 and 17 days for B16F10 GFP and 4T1 cells, respectively, the animals were euthanized and tumors were harvested. Both tumors were cut and kept in a

Karnovski solution for FESEM analysis (section 2.5), while half of the B16F10 GFP tumor was minced for RNA extraction (section 2.8). All animal procedures used were approved by PUC-RS university's animal ethic committee (CEUA), having the protocol ID CEUA 8466.

2.5. Scanning Electron Microscopy

After 7 days of culture, samples were fixed with a Karnovski solution, followed by post-fixation with osmium tetroxide for 1 hour, and a slow and gradual dehydration with acetone. Samples were critical point dried, mounted in stubs and sputter-coated with gold. Visualizations were done through FESEM (Inspect 50 FEI).

2.6. Confocal Microscopy

B16F10 GFP samples were fixed with 4% paraformaldehyde, quenched with NH_4Cl 50 mM for 5 min, permeabilized with 0,2% PBS-Triton for 5 min and blocked with 1% PBS-bovine serum albumin (BSA) for 30 min. B16F10 GFP cells were then incubated with Hoechst for 5 min, followed by 3 washes with PBS, 5 min each. Samples were kept on PBS-Glycerol (1:1) until imaging on a confocal laser scanning microscope (Zeiss LSM 710), images were analyzed by Photoshop.

2.7. Cell Viability (MTT)

After 5 days in culture, cells were treated with either cisplatin (100 and 200 µM) or dacarbazine (1000 and 2000 µM), doses chosen from dose-dependent curves done on 2D cultures (data not shown). At the end of the 48 h incubation, 20 µl of MTT solution (5 mg/ml) was added to each well, including blank samples composed of the respective model with medium and no cells. The plate was then kept on an incubator at 37 ºC and 5% CO_2. After 3 h the plate was centrifuged at 1500 RPM, 4 ºC, and medium was discarded carefully while on ice. Formazan crystals were dissolved with 200 µl of DMSO and the plate was kept lightly shaking for 10 min, followed by optical density reading on Anthos Zenyth 340r microplate reader between 570 and 620 nm. Readings were normalized to their respective control without drug treatment and data analyzed on GraphPad prism 5.

2.8. Microarray

RNA was extracted from samples using the PureLink® RNA Mini Kit (Thermo Fisher). Briefly, cells were washed with ice-cold PBS, lysis buffer was added directly to cells and the protocol was carried out according to the manufacturer's instructions. RNA integrity was assessed using the Agilent 2100 Bioanalyzer and the RNA 6000 Nano Kit (Agilent Technologies, Santa Clara, CA, USA) and total RNA was stored at -80°C until use. Gene

expression was analyzed using DNA microarrays SurePrint G3 8x60K (Agilent, USA). Cyanine-3 labeled RNA from samples and cyanine-5 labeled reference RNA (Universal Reference RNA, Agilent Technologies) were combined and hybridized to microarrays following manufacturer's protocols (LowInput QuickAmp Labeling Kit Two-Color, Agilent, USA). Microarrays were scanned using the SureScan (Agilent, USA), according to default parameters, and experiment quality, background correction, and the identification of expressed genes were carried out with the Feature Extraction software v12 (Agilent, USA). From the data set, probes were mapped to the reference *Mus musculus* genome (mm9, available at http://hgdownload.cse.ucsc.edu/downloads.html#mouse) using the software package Burrows-Wheeler Aligner (BWA). Based on this alignment, a total of 4598 probes were used in this work (Table S1, Supporting information). Data analysis was carried out using GeneSpring software v12.6 (Agilent). We used quantile normalization for fluorescence intensity normalization between samples, and only probes identified as detected or not detected in at least 100% of one of the experimental conditions were selected for the identification of differentially expressed genes (ANOVA, cut-off for significance p-value <0.05). Gene expression levels are presented in fold-changes in respect to cells cultivated in monolayer (2D). The overall structure of the dataset was visualized with the unsupervised method principal components analysis (PCA) (GeneSpring, Agilent). Hierarchical clustering of differential gene expression is presented in the form of heat maps using Euclidean distance and Ward's or complete linkage (GeneSpring, Agilent, and Morpheus software) and a Venn diagram was used to illustrate differences and similarities between the datasets [28]. Gene Ontology (GO) term and KEGG pathways enrichment analysis were carried out using DAVID Bioinformatics Resources 6.8 and results were considered statistically significant if p-value <0.05 after Benjamini-Hochberg False-Discovery Rate (FDR) correction [29].

3. Results and Discussion

3.1. Scaffold production and characterization

Through electrospinning and SCPL techniques two types of membranes were generated and their topography can be seen on Fig. 1A-C. While gel fibers had small diameters, with a mean of 0.043 ±0.02 µm (Fig. S1A**,** Supporting information), electrospun fibers had larger diameters, with a mean of 1.1 ±0.47 µm (Fig. S1B, Supporting information). Since SCPL membranes had a different production approach from electrospun membranes, it was only possible to measure its pore diameter, as they are not composed of fibers. Instead, these SCPL membranes were composed of random shapes, with pore sizes varying between 0.56-48.36 µm, while electrospun membrane pores and gel pores varied between 0.66-12.07 µm and 0.21-4.35 µm, respectively (Fig. 1D-F, Table 1). Pore size is a very important and discussed issue regarding scaffold models since it can determine how the cells will interact and grow. It has been proposed that in order for cells to grow on a "true 3D" environment, pore sizes should be smaller than the cells. This way, cells may interact more closely with the scaffold. Small pore diameters can also prevent cells from growing alongside fibers, which may be no different than a 2D curved plane [30]. Besides, depending on cell type, nanopatterns have been shown to either promote or inhibit cell attachment [31], or even affect differentiation of myoblasts [32]. It is agreed, though, that the pore diameter should be related to the size of the cells being cultured. As has been seen by Lowery et al, human dermal fibroblasts grew better on scaffolds with pore sizes between 6-20 µm. Larger pores would promote growth along fibers and decrease ECM production, and though smaller ones allowed cells to bridge fibers and produce ECM much faster, they would only grow on top of the membrane [33]. For that, varying pore sizes may promote cell penetration into the scaffold, where it may grow interacting more closely with this ECM mimetic [34].

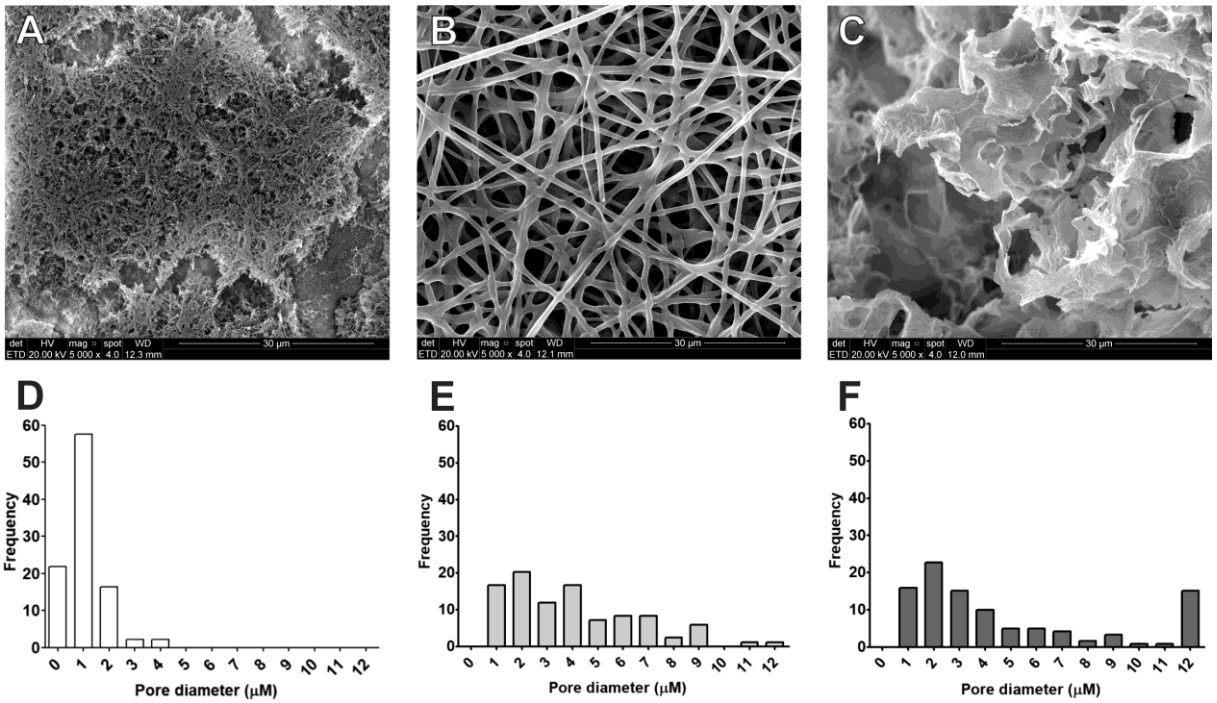

Figure 1. Scaffold structures. FESEM micrographs of the different scaffolds studied, **(A)** EHS gel, **(B)** electrospun, **(C)** SCPL membrane. Magnification of 5,000x, scale bar 30 μM. Pore diameter of the different scaffolds, **(D)** EHS gel, **(E)** electrospun, **(F)** SCPL membrane.

Table 1. Pore size in μM across 3D models

	Min	Max	Mean	Median
EHS gel	0.21	4.35	1.06 ± 0.76	0.89
Electrospun	0.66	12.07	4.04 ± 2.66	3.55
SCPL	0.56	48.36	6.66 ± 9.22	3.04

3.2. Cell culture morphology

As has been seen before, cells cultured *in vitro* may alter their morphology according to the conditions in which they are grown in. Triple-negative breast cancer cells (MDA-MB-231) after being cultured on 15% PCL electrospun scaffolds showed a higher elongation factor than cells grown on 2D cultures [16]. Besides, different breast and prostate cancer cell lines showed distinct cell organizations when growing on a 3D environment, as compared with 2D cultures, allowing better drug investigation [7,35]. In order to evaluate cell growth across different culture methods, we employed two approaches: Field Emission Gun Scanning Electron Microscopy (FESEM) and confocal microscopy analysis. Both were performed after culturing cells for either 7 days *in vitro* or 10 days for B16F10 GFP melanoma cells on C57BL/6 and 14 days for 4T1 breast cancer cells on Balb/c mice. As can be seen by FESEM on Fig. 2 for B16F10 GFP, while there are few cell aggregates on 2D cultures (2A), cells grown on 3D environments were organized in slightly larger aggregates. Melanoma cells on 3D cultures sometimes showed a rounder morphology, viewed by FESEM in the larger magnification detail (2A), more closely resembling *in vivo* than 2D growth. Interestingly, cells on EHS gel, electrospun membrane and

SCPL membrane showed a variety of morphologies, similarly to B16F10 GFP cells on C57BL/6 mice. Morphological differences can also be observed by confocal microscopy (Fig. 2B), where round and elongated cells are seen in more detail. While all cells are elongated in 2D cultures, 3D systems showed both round and elongated cells in the aggregates. Though melanoma cells on both SCPL and electrospun membranes were able to infiltrate the scaffolds, those on the SCPL membrane tended to grow involving the scaffold structure instead of forming spheroids on top of the substrate, as seen on electrospun samples (Fig. 2C, lower panels). Additionally, cell aggregates on the electrospun membrane had more spherical cells than the other 3D models, and they were also formed on a much higher frequency than on the SCPL membrane (Fig. 2C, upper panels). B16F10 growing on the 3D models also had a number of filopodia, traditionally interpreted as interaction with a 3D structure.

As expected, B16F10 GFP cells and 4T1 cells showed different growth characteristics. While B16F10 cultured on EHS gel usually grows spheroids that will merge and form large irregular spheroids, 4T1 tended to have smaller, better-defined round spheroids, which even if merged together, would retain its round conformation. Besides, B16F10 GFP cells when grown on 3D models form cell aggregates and have a rounder morphology than what is seen on 2D, however, the same cannot be said about 4T1 cells. These breast cancer cells, when grown on membranes, seem to mostly maintain their elongated morphology (Fig. 3A). Still, although 4T1 cells don’t appear to readily form cell aggregates, they can easily be seen infiltrating the electrospun membrane, which might allow them to interact more, providing an environment similar to spheroids. Especially on the SCPL membrane, cells were able to grow and envelop the scaffold (Fig 3B). Still, each model has its own structure and characteristics, leading to different cell-cell and cell-ECM interactions. Different cell lines may also react differently to the same stimuli.

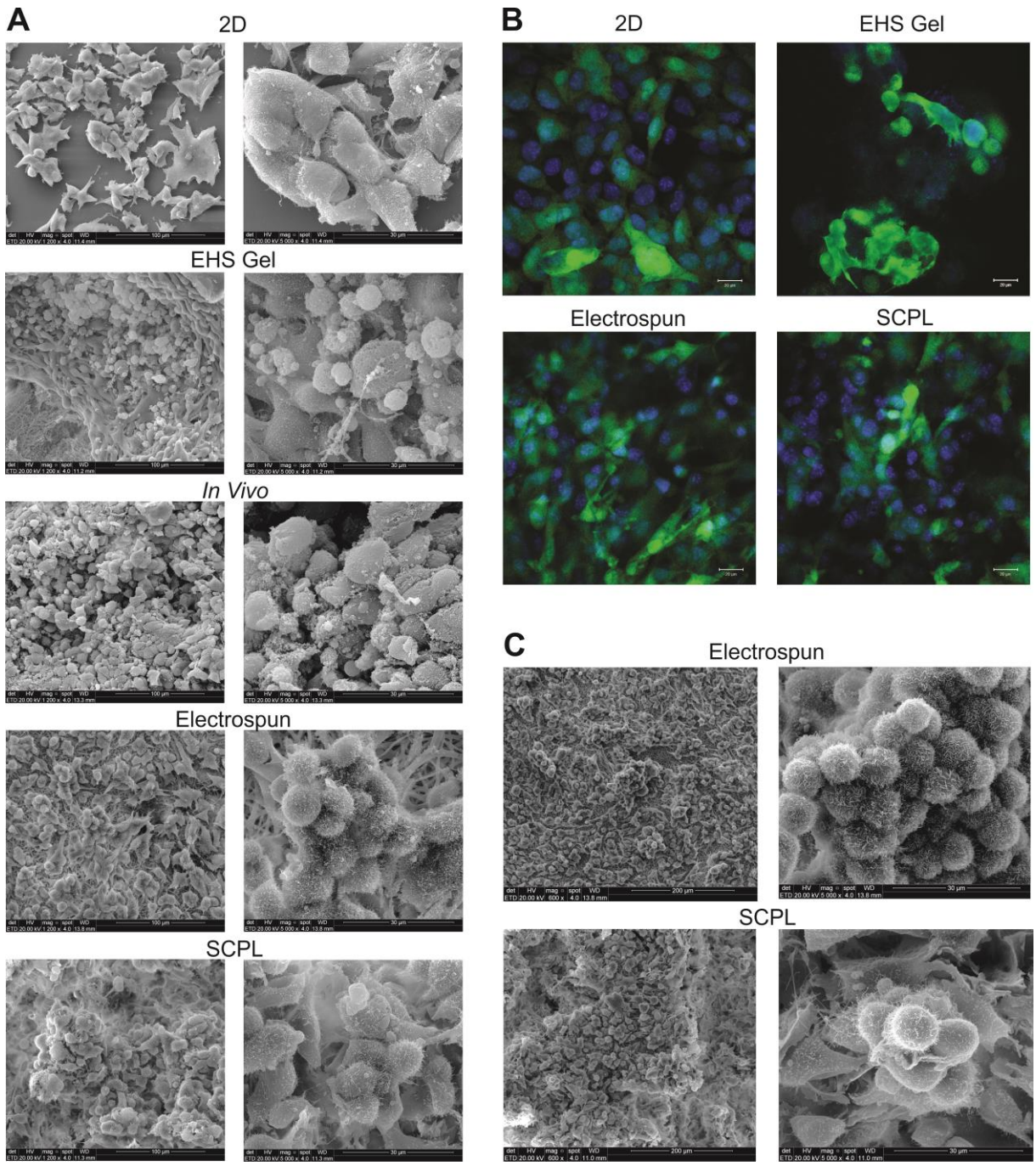

Figure 2. Morphological differences in B16F10 GFP cell cultures grown in different scaffolds (A) FESEM micrographs comparing culture *In vitro* for 7 days and *In vivo* 10 days tumor of B16F10 GFP cells on C57BL/6 mice. Left panel, 1200x; right panel, detail of the upper panel with magnification 5000x. **(B)** Confocal images showing growth *in vitro* after 7 days in culture, where nuclei are stained in blue, and in green GFP produced by the melanoma cells. **(C)** FESEM micrographs of B16F10 GFP growth structures on electrospun and SCPL membranes after 7 days in culture. Left panel, magnification 600x; Right panel, detail with magnification 5000x.

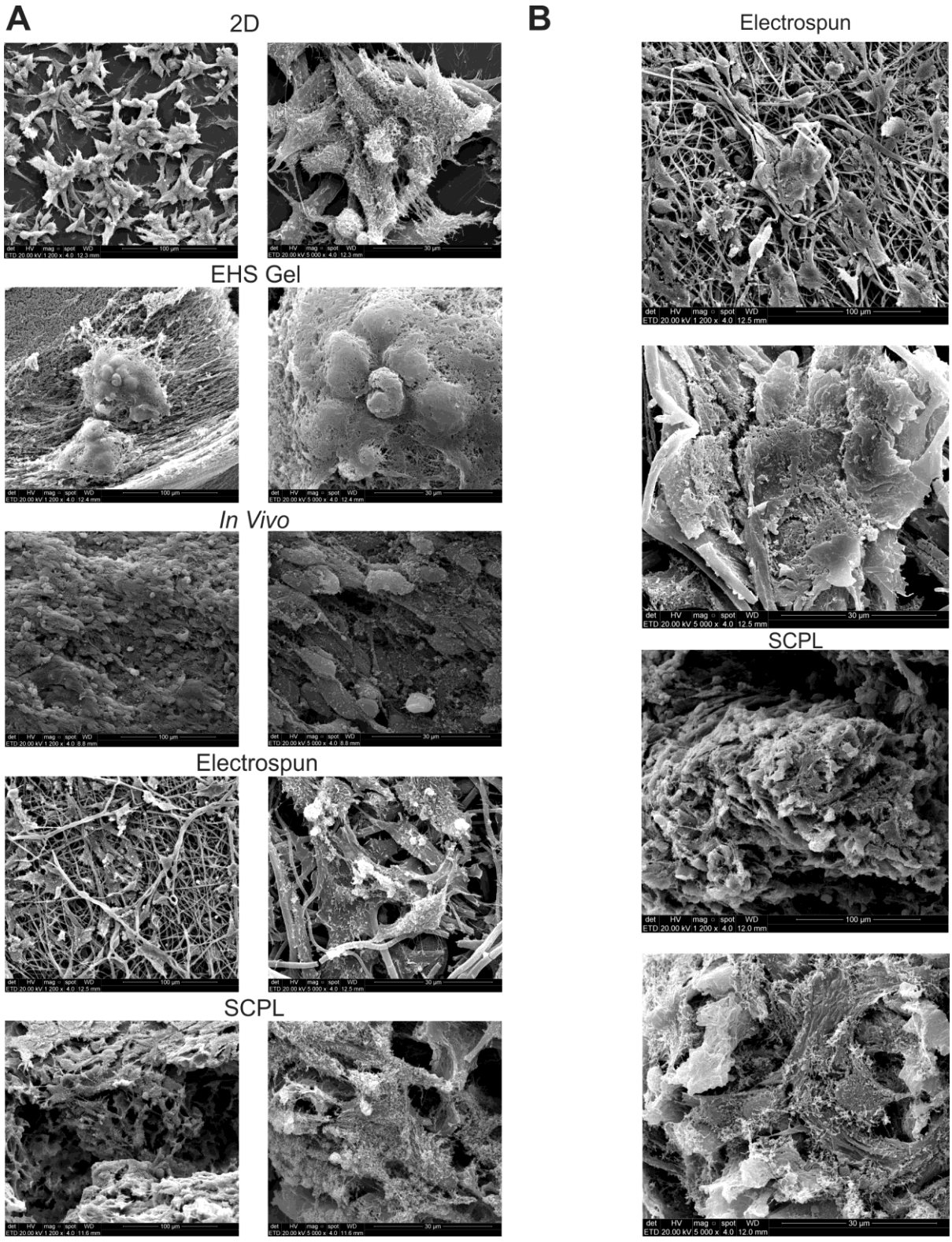

Figure 3. 4T1 breast cancer cell culture in different cell culture systems. FESEM micrographs of **(A)** comparison of cell culture on different models, where cells *in vitro* were grown for 7 days and *In vivo* on Balb/c mice for 14 days. **(B)** Cells grown on electrospun and SCPL scaffolds for 7 days, showing spheroid formation and thorough membrane embracing, respectively.

It has already been reported that cells grown on a tissue culture plastic tend to have a more flattened morphology. Human breast cancer cells (MCF7), after growing on 2D were flat with trigonal and polygonal morphologies, while cells grown on a collagen scaffold had a diversity of morphologies, including rounder, spread-out and elongated [36]. Besides, endometrial cell lines when cultured in EHS gels formed glandular and spheroid-like structures, resembling much more closely *in vivo* morphology [37]. In general, the formation of cell aggregates or spheroids has been shown to better simulate tissues, especially when considering that not all cells will get in contact with medium or drugs due to difficulties in nutrient and waste exchange. Depending on the spheroid size, it may be composed of cells on three different stages: cells on the outermost layer will proliferate, while those in the middle layer will be quiescent; if the structure is large enough (usually diameter above 500 μm), it will have a necrotic core due to nutrient inaccessibility and increased acidity and waste products [38]. Thus, the formation of these cell aggregates and spheroids on the 3D cultures studied may bring advantages to the models by providing different microenvironments for the cells. Although spheroids less round in shape may have a different structure than the classical ones (since it may develop more than one necrotic center), it may still provide different microenvironments in the cell culture, hence altering response to signals.

3.3. Effect of chemotherapeutics on 2D and 3D models

In order to evaluate how the two novel models proposed here, SCPL and electrospun membranes, would affect cell response to chemotherapy, cultures were treated for 48 h with either cisplatin (CDDP) or dacarbazine (DTIC) followed by MTT cell viability analysis. As can be seen on Fig. 4, cells grown on EHS gel showed increased resistance in all drug concentrations used. Such response is expected, as there have been various reports regarding this phenomena [39,40]. Similar to EHS gel cultures, cells on membranes were able to better withstand DTIC treatment than control, however, they only showed a tendency towards CDDP resistance.

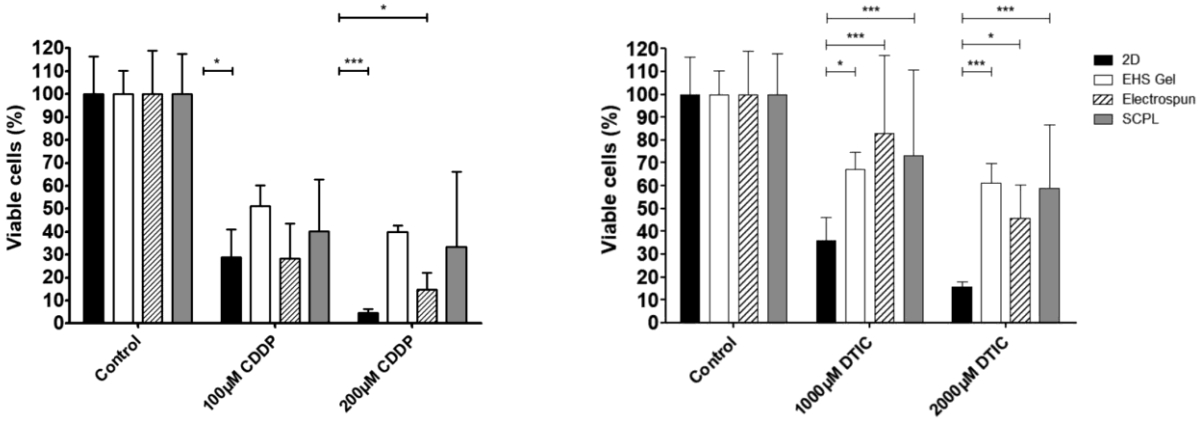

Figure 4. Viability analysis through MTT. B16F10 GFP cells were cultured for 7 days, followed by treatment with either Cisplatin, CDDP (100 or 200 µM) or Dacarbazine, DTIC (1000 or 2000 µM) for 48 h. * for $p < 0.05$ and *** for $p < 0.001$.

Cells cultured on 3D models may display either increased or decreased drug resistance when compared with results from 2D cell cultures. In prostate cancer cell lines, it was found that compounds targeting the mTOR pathway inhibited cancer cells in 2D and 3D cultures, while those targeting the AKT pathway were less effective on 2D [35]. It has also been shown that spheroids on collagen gel showed greater resistance to doxorubicin treatment than cells on 2D and spheroids on a scaffold-free model [41]. These results come to show that depending on the 3D environment and cell-cell and cell-matrix interactions, a culture might become resistant or susceptible to a certain drug treatment. In fact, a number of ways through which resistance can be affected has been described. One was studied by Imamura et al., where dense spheroids had a tendency to be resistant to paclitaxel and doxorubicin treatment when compared to looser spheroids or 2D growth. These denser spheroids showed decreased apoptosis and stained positive for Ki67, while having hypoxic centers [42]. Colorectal cancer cell lines have also been shown to have decreased p53 levels on 3D cultures after CDDP treatment, when compared with 2D treated cultures. Even though these cells would have similar p53 levels on 2D and 3D, after CDDP treatment cells cultured in 3D had decreased sensitivity to the drug. These alterations were attributed to the difference in architecture between 2D and 3D cultures [43]. It is believed that cell morphology and interactions between cells may have a great effect on expression and treatment outcome. As seen on MCF7 breast cancer cells, treatment with CDDP on EHS gel had chromatin reorganization leading to induction of ATR phosphorylation, chk1 activation and REV3L upregulation, leading to increased senescence [39].

Interestingly, both CDDP and DTIC mainly act by crosslinking with DNA (with a platinum or alkyl group, respectively)[44], and both had at least a tendency for drug resistance, not seen

on 2D cultures. These differences are probably due to distinct pathways being activated after treatment. Still, all 3D cultures were able to provide an environment with a scaffold to which cells were able to adhere. Cells treated with cisplatin and cultured on SCPL membrane might have had in general a higher resistance due to increased penetration and interaction of cells with the scaffold, when compared with culture on electrospun membranes.

3.4. RNA expression across different culture models

We compared global gene expression profiles of exponentially growing B16F10 GFP cells in monolayer (2D) with the 3D culture conditions (ElMb, SCPL and EHS gel) and cells collected *in vivo*. The PCA plot indicates that the majority of the variability in the dataset is associated with cell source (2D, 3D or *in vivo*): samples from each culture model grouped together (Fig. 5A).

The tree view representing the variation in gene expression highlights that cells cultivated *in vivo* showed the most significant differences when compared with the 2D cell culture, followed by EHS gel (Fig. 5B, for a complete list of differentially expressed transcripts, considering a fold-change of 2, see Table S2**,** Supporting information). Gene ontology (GO) term and KEGG pathways gene enrichment analysis were carried out to understand if these changes in gene expression levels were related to biological processes involved in the differences in 3D cultures, such as tissue development and cell adhesion, or in response to radio- and chemotherapy, such as cell proliferation, cell death and DNA repair systems. No such differences were found. However, cells collected *in vivo*, EHS gel, and SCPL showed similar alterations in transcription-related processes (RNA synthesis) when compared with cells cultivated in monolayer, as highlighted by the enrichment of GO term Transcription, DNA Template (GO:0006351) (Table S3, Supporting information). For the electrospun membrane, this enrichment was not as evident (p-value above the significance level), but a group of genes associated with this process was also deregulated (Table S3, Supporting information). A summary of the overlap between the 3D cultivation systems can be visualized in the Venn diagram (Fig. 5C) and specific characteristics of each dataset are available as supporting information (Table S4).

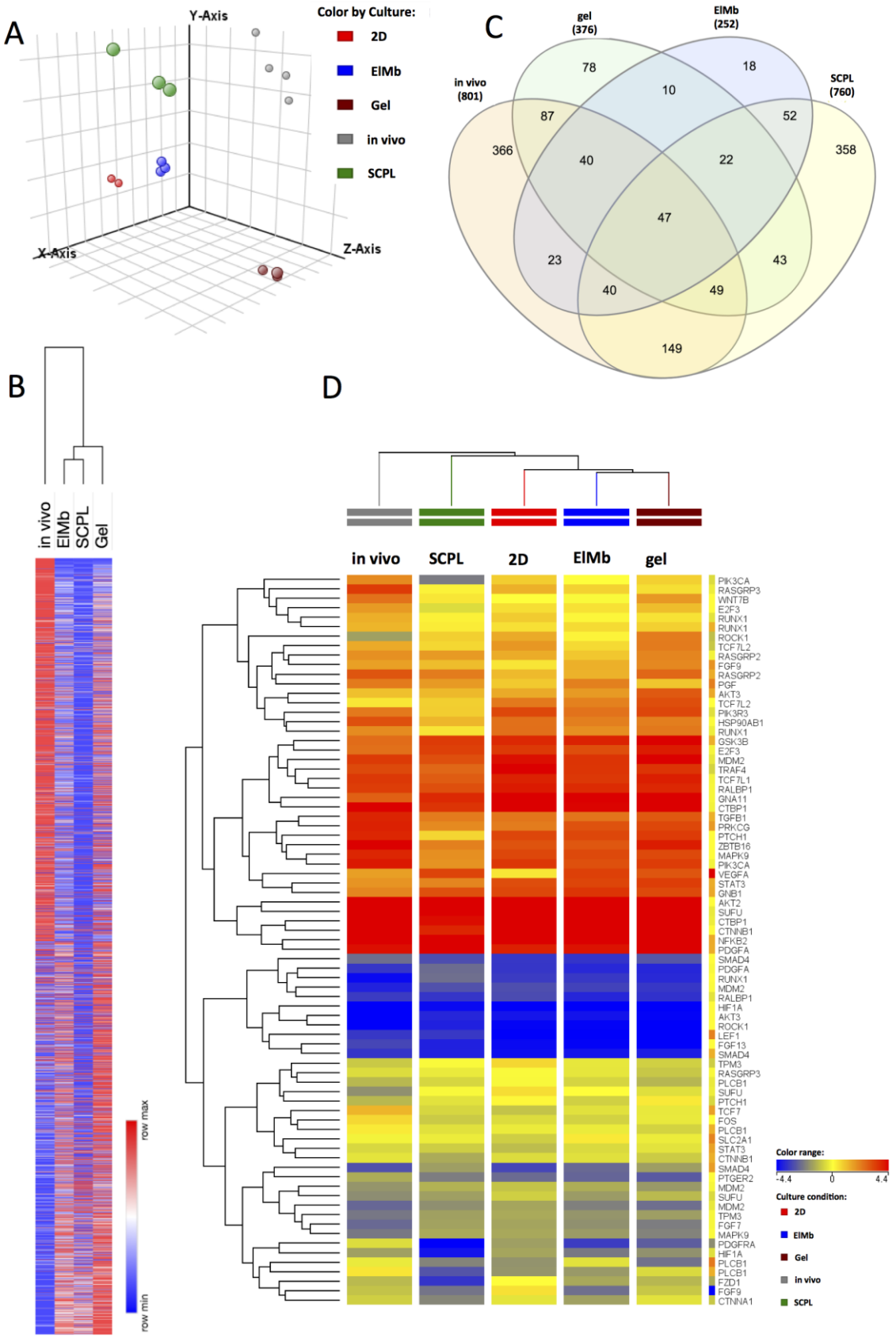
A
Y-Axis
X-Axis
Z-Axis
Color by Culture:
2D
ElMb
Gel
in vivo
SCPL
C
gel (376)
ElMb (252)
in vivo (801)
SCPL (760)
78
18
10
87
52
366
40
22
358
47
23
43
40
49
149
B
in vivo
ElMb
SCPL
Gel
row max
row min
D
in vivo
SCPL
2D
ElMb
gel
PIK3CA
RASGRP3
WNT7B
E2F3
RUNX1
RUNX1
ROCK1
TCF7L2
RASGRP2
FGF9
RASGRP2
PGF
AKT3
TCF7L2
PIK3R3
HSP90AB1
RUNX1
GSK3B
E2F3
MDM2
TRAF4
TCF7L1
RALBP1
GNA11
CTBP1
TGFB1
PRKCG
PTCH1
ZBTB16
MAPK9
PIK3CA
VEGFA
STAT3
GNB1
AKT2
SUFU
CTBP1
CTNNB1
NFKB2
PDGFA
SMAD4
PDGFA
RUNX1
MDM2
RALBP1
HIF1A
AKT3
ROCK1
LEF1
FGF13
SMAD4
TPM3
RASGRP3
PLCB1
SUFU
PTCH1
TCF7
FOS
PLCB1
SLC2A1
STAT3
CTNNB1
SMAD4
PTGER2
MDM2
SUFU
MDM2
TPM3
FGF7
MAPK9
PDGFRA
HIF1A
PLCB1
PLCB1
FZD1
FGF9
CTNNA1
Color range:
-4.4
0
4.4
Culture condition:
2D
ElMb
Gel
in vivo
SCPL

Figure 5.

Figure 5. Microarray analysis comparing gene expression across the different cell culture methods. (**A)** Principal component analysis (PCA) of the source of variation in the gene expression dataset. This is an exploratory statistical method that simplifies the microarray data. Shown here is the average signal of each sample in a three-dimensional space of the first three principal components. Each culture condition clusters separately. (**B**) Hierarchical clustering of gene expression changes between each cultivation system and the monolayer (2D) cell culture. Differentially expressed genes are plotted according to their degree of respective co-expression. Values are represented in log2Foldchange. The cultivation system is indicated at the top, columns represent samples, while rows represent genes. The degree of correlation between genes or samples is plotted in a tree view fashion. (**C**) Venn diagram. Summary the overlap between differentially expressed genes in each dataset. (**D)** Hierarchical clustering of genes belonging to Pathways in Cancer (KEGG Pathways). Values from each culture system are represented in as normalized intensity and include only genes that showed at least a 2-fold change difference when compared with the monolayer culture. 2D: monolayer cell culture; ElMb: electrospun membrane; Gel: EHS gel; SCPL: Solvent-Casting Particle-Leaching membrane.

When the *in vivo* samples were analyzed, differences in the up regulation of genes from immune system processes were noteworthy (LGALS3, HCK, UNC93B1, TFEB, TLR3, SERPING1, LGALS9, BTK, PSMB9, ZAP70, C1RL, NRROS, BCL6, PRDM1, C2, CD79A) as well as in cytoskeleton organization (DLC1, FMNL1, CORO1A, DOCK2, PRR5, TMSB4X, BCL6, IQSEC*3, CAPZB, FLNA, IQSEC2).*

The expression level of gene transcripts previously associated with cancer in the 3D systems was analyzed in more detail, because these models were developed for studies in cancer progression and drug response. We selected genes grouped within KEGG database under the term “Pathways in Cancer” and evaluated the overall gene expression in each system, including genes involved in processes as diverse as cell-cell contact, cell migration, cell death and cell proliferation (a complete scheme for these pathways is available at https://www.genome.jp/kegg-bin/show_pathway?mmu05200). Table 2 lists the genes of the KEGG pathways that showed differential expression between each culture system and cells collected *in vivo* when compared with cells cultivated in monolayer. From a total of 534 genes, 52 were differentially regulated between the 3D systems and the monolayer culture, or among themselves. A comprehensive view of the variation between each system is depicted in Fig. 5D.

Table 2. Differentially expressed genes belonging to KEGG Pathways in Cancer (mmu0520) between 3D cell culture systems and cells collected *in vivo* compared with cells cultivated in monolayer. Only genes showing at least a 2-fold change are listed.

KEGG PATHWAY – Pathways in Cancer: mmu0520		
Cell Source	**Gene Symbol - Up regulated**	**Gene Symbol - Down regulated**
In vivo	TCF7, PTGER2, PGF, LEF1, FGF13, PRKCG, ZBTB16, TGFB1, FOS, WNT7B, RASGRP3, RASGRP2, VEGFA, PDGFRA, PLCB1	E2F3, FGF7, ROCK1, FGF9, GNA11, FZD1, TCF7L2, SUFU, STAT3, TPM3, GNB1, GSK3B, TRAF4, AKT2
EHS gel	WNT7B, PDGFA, VEGFA, RASGRP2, SMAD4, LEF1, ZBTB16, NFKB2, PLCB1, AKT3	FGF9, PDGFRA, FZD1, SUFU, TPM3
Electrospun membrane	PGF, VEGFA, SLC2A1, LEF1	ROCK1, FGF9, PDGFRA, FZD1, CTNNA1, TCF7L2, TPM3
SCPL	RASGRP2, SMAD4, LEF1, VEGFA	HSP90AB1, CTBP1, FGF9, RALBP1, GNA11, FZD1, CTNNA1, TCF7L2, TCF7L1, CTNNB1, HIF1A, RASGRP3, PDGFRA, PIK3CA, MDM2, MAPK9, PTCH1, PIK3R3, PLCB1, RUNX1, TRAF4, AKT2

RNA expression is commonly found altered after modifying cell culture conditions or with tumor development. Lymphoid enhancer binding factor 1 (LEF1), which is associated with the Wnt pathway, had increased expression in all 3D and *in vivo* models when compared with the 2D cell culture. This result is expected, as malignant melanoma patients have been shown to have increased LEF1 when compared with peritumoral tissue and benign nevus [45]. Patients with malignant melanoma have also shown increased serum levels of the Vascular Endothelial Growth Factor (VEGF) in comparison to healthy controls [46]. These results have also been obtained *in vitro*, when T47D breast cancer cells were grown as spheroids and showed increased VEGFA expression [47]. This aspect has also been recapitulated in our experiments, where all 3D cell cultures and *in vivo* model have shown increased expression of VEGFA when compared to 2D cell cultures. As with other genes mentioned, our 3D cultures have been able to approximate to *in vivo* models, exemplifying another way through which they might be better suited for *in vitro* cell culture than the 2D cell culture model.

4. Conclusions

All the culture methods analyzed were able to sustain cell growth, and all 3D cell culture models showed morphologies more similar to *in vivo* growth than to the monolayer cell culture. Both electrospun and SCPL membranes did not induce cell death, and cells grown on them were able to interact with each other and with the ECM mimetic, which was true for both melanoma B16F10 and breast cancer 4T1 cells. After drug treatment with dacarbazine, cells grown in all 3D culture systems showed increased resistance compared to those grown in monolayer, showing at least 30% more viability than the 2D group. After cisplatin treatment,

cells grown on both electrospun and SCPL membranes displayed a tendency for increased drug resistance - though only cells grown on EHS gel had statistically significant increased viability.

Gene expression analysis corroborated the similarities between 3D and *in vivo* groups in relation to 2D, that were observed in the previous biological assays, having relatively few transcripts showing different expression between the models. Even though these 3D models were produced by different techniques, they showed many similarities across experiments, demonstrating that the use of animal origin models such as the EHS gel could be substituted by fully synthetic 3D scaffolds. Further experiments using different conditions such as RNA collection time point and cell stimulation, may identify other differences in molecular mechanisms associated with cell growth and maintenance in each studied model.

Acknowledgements

Special thanks to MSc. Karina Lima, PhD. Rodrigo Gassen and PhD. Sofia Scomazzon from Pontifical Catholic University of Rio Grande do Sul (PUCRS) for support, as well as Leandro Baum and colleagues from Central Laboratory of Microscopy and Microanalysis (LabCEMM) at the PUCRS for the FESEM technical support, and to Thiago P. A. Aloia from Hospital Israelita Albert Einstein for the Confocal Microscopy technical support. This work was supported by the Brazilian National Program for Support to Oncological Awareness (PRONON) SIPAR 250000.159946/2014-16. J. C. Fontoura was the recipient of a scholarship from CAPES (Coordenação de Aperfeiçoamento de Pessoal de Nível Superior, Brazil) and Cristina Bonorino of a fellowship from CNPq.

References

[1] F. Bray, J. Ferlay, I. Soerjomataram, R.L. Siegel, L.A. Torre, A. Jemal, Global Cancer Statistics 2018: GLOBOCAN Estimates of Incidence and Mortality Worldwide for 36 Cancers in 185 Countries, CA. Cancer J. Clin. 68 (2018) 394–424. doi:10.3322/caac.21492.

[2] B.M. Baker, C.S. Chen, Deconstructing the third dimension – how 3D culture microenvironments alter cellular cues, J. Cell Sci. 125 (2012) 3015–3024. doi:10.1242/jcs.079509.

[3] S. Sanyal, Culture and Assay Systems Used for 3D Cell Culture, Corning. (2014).

[4] M.W. Tibbitt, K.S. Anseth, Hydrogel as Extracellular Matrix Mimics for 3D Cell Culture, Biotechnol. Bioeng. 103 (2010) 655–663. doi:10.1002/bit.22361.Hydrogels.

[5] R.D. Simoni, J.B. Hays, T. Nakazawa, S. Roseman, R. Stein, O. Schrecker, H.F. Lauppe, H. Hengstenberg, J. Thompson, H. Towbin, T. Staehelin, J. Gordon, E.B. Waygood, R.L. Mattoo, N. Weigel, M.A. Kukuruzinska, A. Nakazawa, E.G. Waygood, W. Wray, T. Boulikas, V.P. Wray, R.; B. Hancock, Basement Membrane Complexes with Biological Activity, Proc. Natl. Acad. Sci. U.S.A. 25 (1986) 312–318.

[6] C.S. Hughes, L.M. Postovit, G.A. Lajoie, Matrigel: a complex protein mixture required for optimal growth of cell culture., Proteomics. 10 (2010) 1886–1890. doi:10.1002/pmic.200900758.

[7] P.A. Kenny, G.Y. Lee, C.A. Myers, R.M. Neve, J.R. Semeiks, P.T. Spellman, K. Lorenz, E.H. Lee, M.H. Barcellos-Hoff, O.W. Petersen, J.W. Gray, M.J. Bissell, The morphologies of breast cancer cell lines in three-dimensional assays correlate with their profiles of gene expression, Mol. Oncol. 1 (2007) 84–96. doi:10.1016/j.molonc.2007.02.004.

[8] R. Poincloux, O. Collin, F. Lizárraga, M. Romao, M. Debray, M. Piel, P. Chavrier, Contractility of the cell rear drives invasion of breast tumor cells in 3D Matrigel, Proc. Natl. Acad. Sci. 108 (2011) 1943–1948. doi:10.1073/pnas.1010396108.

[9] M. Gargotti, U. Lopez-Gonzalez, H.J. Byrne, A. Casey, Comparative studies of cellular viability levels on 2D and 3D *in vitro* culture matrices, Cytotechnology. 70 (2018) 261–273. doi:10.1007/s10616-017-0139-7.

[10] K.K. Dijkstra, C.M. Cattaneo, F. Weeber, M. Chalabi, J. van de Haar, L.F. Fanchi, M. Slagter, D.L. van der Velden, S. Kaing, S. Kelderman, N. van Rooij, M.E. van Leerdam, A. Depla, E.F. Smit, K.J. Hartemink, R. de Groot, M.C. Wolkers, N. Sachs, P. Snaebjornsson, K. Monkhorst, J. Haanen, H. Clevers, T.N. Schumacher, E.E. Voest, Generation of Tumor-Reactive T Cells by Co-culture of Peripheral Blood Lymphocytes and Tumor Organoids, Cell. 174 (2018) 1586-1598.e12. doi:10.1016/j.cell.2018.07.009.

[11] G. Benton, I. Arnaoutova, J. George, H.K. Kleinman, J. Koblinski, Matrigel: From discovery and ECM mimicry to assays and models for cancer research, Adv. Drug Deliv. Rev. 79–80 (2014) 3–18. doi:10.1016/j.addr.2014.06.005.

[12] L. Jesús Villarreal-Gómez, M. Cornejo-Bravo, R. Vera-Graziano, D. Grande, Electrospinning as a powerful technique for biomedical applications: a critically

selected survey, J. Biomater. Sci. 27 (2016) 157–176. doi:10.1080/09205063.2015.1116885.

[13] J. Ramier, D. Grande, T. Bouderlique, O. Stoilova, N. Manolova, I. Rashkov, V. Langlois, P. Albanese, E. Renard, From design of bio-based biocomposite electrospun scaffolds to osteogenic differentiation of human mesenchymal stromal cells, J. Mater. Sci. Mater. Med. 25 (2014) 1563–1575. doi:10.1007/s10856-014-5174-8.

[14] E. Yan, Y. Fan, Z. Sun, J. Gao, X. Hao, S. Pei, C. Wang, L. Sun, D. Zhang, Biocompatible core-shell electrospun nanofibers as potential application for chemotherapy against ovary cancer, Mater. Sci. Eng. C. 41 (2014) 217–223. doi:10.1016/j.msec.2014.04.053.

[15] S. Chen, S. Kumar Boda, S.K. Batra, X. Li, J. Xie, Emerging Roles of Electrospun Nanofibers in Cancer Research, (2017). doi:10.1002/adhm.201701024.

[16] M. Rabionet, M. Yeste, T. Puig, J. Ciurana, Electrospinning PCL scaffolds manufacture for three-dimensional breast cancer cell culture, Polymers (Basel). 9 (2017) 1–15. doi:10.3390/polym9080328.

[17] A.G. Mikos, A.J. Thorsen, L.A. Czerwonka, Y. Bao, R. Langer, Preparation and characterization o poly(L-lactic acid) foams, Polymer (Guildf). 35 (1994) 1068–1077. doi:10.1002/anie.196904562.

[18] Z.L. Mou, L.M. Duan, X.N. Qi, Z.Q. Zhang, Preparation of silk fibroin/collagen/hydroxyapatite composite scaffold by particulate leaching method, Mater. Lett. 105 (2013) 189–191. doi:10.1016/j.matlet.2013.03.130.

[19] N. Thadavirul, P. Pavasant, P. Supaphol, Fabrication and Evaluation of Polycaprolactone–Poly(hydroxybutyrate) or Poly(3-Hydroxybutyrate-co-3-Hydroxyvalerate) Dual-Leached Porous Scaffolds for Bone Tissue Engineering Applications, Macromol. Mater. Eng. 302 (2017) 1–17. doi:10.1002/mame.201600289.

[20] L. Rogers, S.S. Said, K. Mequanint, The Effects of Fabrication Strategies on 3D Scaffold Morphology, Porosity, and Vascular Smooth Muscle Cell Response, J. Biomater. Tissue Eng. 3 (2013) 300–311. doi:10.1166/jbt.2013.1088.

[21] R.N. Reusch, Physiological Importance of Poly-(R)-3-hydroxybutyrates, Chem. Biodivers. 9 (2012) 2343–2366.

[22] E.C.C. Reis, A.P.B. Borges, C.C. Fonseca, M.M.M. Martinez, R.B. Eleotério, G.O. Morato, P.M. Oliveira, Biocompatibility, osteointegration, osteoconduction, and biodegradation of a hydroxyapatite-polyhydroxybutyrate composite, Brazilian Arch. Biol. Technol. 53 (2010) 817–826. doi:10.1590/S1516-89132010000400010.

[23] X. Wang, S.S. Liow, Q. Wu, C. Li, C. Owh, Z. Li, X.J. Loh, Y.L. Wu, Codelivery for Paclitaxel and Bcl-2 Conversion Gene by PHB-PDMAEMA Amphiphilic Cationic Copolymer for Effective Drug Resistant Cancer Therapy, Macromol. Biosci. 17 (2017) 1–11. doi:10.1002/mabi.201700186.

[24] E.I. Shishatskaya, E.D. Nikolaeva, O.N. Vinogradova, T.G. Volova, Experimental wound dressings of degradable PHA for skin defect repair, J. Mater. Sci. Mater. Med. 27 (2016) 165. doi:10.1007/s10856-016-5776-4.

[25] C. Ye, P. Hu, M.-X. Ma, Y. Xiang, R.-G. Liu, X.-W. Shang, PHB/PHBHHx scaffolds and human adipose-derived stem cells for cartilage tissue engineering, Biomaterials. 30

(2009) 4401–4406. doi:10.1016/j.biomaterials.2009.05.001.

[26] Z. Karahaliloğlu, M. Demirbilek, M. Şam, N. Sağlam, A.K. Mizrak, E.B. Denkbaş, Surface-modified bacterial nanofibrillar PHB scaffolds for bladder tissue repair, Artif. Cells, Nanomedicine Biotechnol. 44 (2016) 74–82. doi:10.3109/21691401.2014.913053.

[27] Y. Wang, X.L. Jiang, S.W. Peng, X.Y. Guo, G.G. Shang, J.C. Chen, Q. Wu, G.Q. Chen, Induced apoptosis of osteoblasts proliferating on polyhydroxyalkanoates, Biomaterials. 34 (2013) 3737–3746. doi:10.1016/j.biomaterials.2013.01.088.

[28] H. Heberle, V.G. Meirelles, F.R. da Silva, G.P. Telles, R. Minghim, InteractiVenn: A web-based tool for the analysis of sets through Venn diagrams, BMC Bioinformatics. 16 (2015) 169. doi:10.1186/s12859-015-0611-3.

[29] Y. Benjamini, Discovering the false discovery rate, J. R. Stat. Soc. Ser. B Stat. Methodol. 72 (2010) 405–416. doi:10.1111/j.1467-9868.2010.00746.x.

[30] S. Zhang, F. Gelain, X. Zhao, Designer self-assembling peptide nanofiber scaffolds for 3D tissue cell cultures, Semin. Cancer Biol. 15 (2005) 413–420. doi:10.1016/j.semcancer.2005.05.007.

[31] K. Seunarine, D.O. Meredith, M.O. Riehle, C.D.W. Wilkinson, N. Gadegaard, Biodegradable polymer tubes with lithographically controlled 3D micro- and nanotopography, Microelectron. Eng. 85 (2008) 1350–1354. doi:10.1016/j.mee.2008.02.002.

[32] L.M. Murray, V. Nock, J.J. Evans, M.M. Alkaisi, The use of substrate materials and topography to modify growth patterns and rates of differentiation of muscle cells, J. Biomed. Mater. Res. - Part A. 104 (2016) 1638–1645. doi:10.1002/jbm.a.35696.

[33] J.L. Lowery, N. Datta, G.C. Rutledge, Effect of fiber diameter, pore size and seeding method on growth of human dermal fibroblasts in electrospun poly(3-caprolactone) fibrous mats, Biomaterials. 31 (2010) 491–504. doi:10.1016/j.biomaterials.2009.09.072.

[34] A. Timnak, J.A. Gerstenhaber, K. Dong, Y. El Har-El, P.I. Lelkes, Gradient porous fibrous scaffolds: A novel approach to improving cell penetration in electrospun scaffolds, Biomed. Mater. 13 (2018). doi:10.1088/1748-605X/aadbbe.

[35] V. Härmä, J. Virtanen, R. Mäkelä, A. Happonen, J.P. Mpindi, M. Knuuttila, P. Kohonen, J. Lötjönen, O. Kallioniemi, M. Nees, A comprehensive panel of three-dimensional models for studies of prostate cancer growth, invasion and drug responses, PLoS One. 5 (2010). doi:10.1371/journal.pone.0010431.

[36] L. Chen, Z. Xiao, Y. Meng, Y. Zhao, J. Han, G. Su, B. Chen, J. Dai, The enhancement of cancer stem cell properties of MCF-7 cells in 3D collagen scaffolds for modeling of cancer and anti-cancer drugs, Biomaterials. 33 (2012) 1437–1444. doi:10.1016/j.biomaterials.2011.10.056.

[37] K. Chitcholtan, E. Asselin, S. Parent, P.H. Sykes, J.J. Evans, Differences in growth properties of endometrial cancer in three dimensional (3D) culture and 2D cell monolayer, Exp. Cell Res. 319 (2013) 75–87.

[38] M. Zanoni, F. Piccinini, C. Arienti, A. Zamagni, S. Santi, R. Polico, A. Bevilacqua, A. Tesei, 3D tumor spheroid models for *in vitro* therapeutic screening: A systematic

approach to enhance the biological relevance of data obtained, Sci. Rep. 6 (2016). doi:10.1038/srep19103.

[39] L.R. Gomes, C.R.R. Rocha, D.J. Martins, A.P.Z.P. Fiore, G.S. Kinker, A. Bruni-Cardoso, C.F.M. Menck, ATR mediates cisplatin resistance in 3D-cultured breast cancer cells via translesion DNA synthesis modulation, Cell Death Dis. 10 (2019) 459. doi:10.1038/s41419-019-1689-8.

[40] K. Rea, F. Roggiani, L. De Cecco, F. Raspagliesi, M.L. Carcangiu, J. Nair-Menon, M. Bagnoli, I. Bortolomai, D. Mezzanzanica, S. Canevari, A. Kourtidis, P.Z. Anastasiadis, A. Tomassetti, Simultaneous E-cadherin and PLEKHA7 expression negatively affects E-cadherin/EGFR mediated ovarian cancer cell growth, J. Exp. Clin. Cancer Res. 37 (2018). doi:10.1186/s13046-018-0796-1.

[41] D. Yip, C.H. Cho, A multicellular 3D heterospheroid model of liver tumor and stromal cells in collagen gel for anti-cancer drug testing, Biochem. Biophys. Res. Commun. 433 (2013) 327–332. doi:10.1016/j.bbrc.2013.03.008.

[42] Y. Imamura, T. Mukohara, Y. Shimono, Y. Funakoshi, N. Chayahara, M. Toyoda, N. Kiyota, S. Takao, S. Kono, T. Nakatsura, H. Minami, Comparison of 2D- and 3D-culture models as drug-testing platforms in breast cancer, Oncol. Rep. 33 (2015) 1837–1843. doi:10.3892/or.2015.3767.

[43] J. He, X. Liang, F. Luo, X. Chen, X. Xu, F. Wang, Z. Zhang, P53 is involved in a three-dimensional architecture-mediated decrease in chemosensitivity in colon cancer, J. Cancer. 7 (2016) 900–909. doi:10.7150/jca.14506.

[44] B.C.K. Brunton Laurence L, Randa Hilal-Dandan, Goodman and Gilman's : the pharmacological basis of therapeutics, 13th ed., McGraw-Hill, New York, 2018. doi:10.1017/CBO9781107415324.004.

[45] S. Xu, Z. Yang, J. Zhang, Y. Jiang, Y. Chen, H. Li, X. Liu, D. Xu, Y. Chen, Y. Yang, Y. Zhang, D. Li, J. Xia, Increased levels of β-catenin, LEF-1, and HPA-1 correlate with poor prognosis for acral melanoma with negative BRAF and NRAS mutation in BRAF exons 11 and 15 and NRAS exons 1 and 2, DNA Cell Biol. 34 (2015) 69–77. doi:10.1089/dna.2014.2590.

[46] S. Verykiou, R. Ellis, P. Lovat, Established and Emerging Biomarkers in Cutaneous Malignant Melanoma, Healthcare. 2 (2014) 60–73. doi:10.3390/healthcare2010060.

[47] C. Wenzel, B. Riefke, S. Gründemann, A. Krebs, S. Christian, F. Prinz, M. Osterland, S. Golfier, S. Räse, N. Ansari, M. Esner, M. Bickle, F. Pampaloni, C. Mattheyer, E.H. Stelzer, K. Parczyk, S. Prechtl, P. Steigemann, 3D high-content screening for the identification of compounds that target cells in dormant tumor spheroid regions, Exp. Cell Res. 323 (2014) 131–143. doi:10.1016/j.yexcr.2014.01.017.

[48] A. Riedl, M. Schlederer, K. Pudelko, M. Stadler, S. Walter, D. Unterleuthner, C. Unger, N. Kramer, M. Hengstschläger, L. Kenner, D. Pfeiffer, G. Krupitza, H. Dolznig, Comparison of cancer cells in 2D vs 3D culture reveals differences in AKT–mTOR–S6K signaling and drug responses, J. Cell Sci. 130 (2017) 203–218. doi:10.1242/jcs.188102.

Appendix A. Supplementary data

Figure S1. Fiber diameter frequency distribution of **(A)** EHS gel and **(B)** Electrospun membranes.

Table S1. List of all probes used for data analysis.

Table S2. Complete list of differentially expressed transcripts of each model when compared with cells grown on a monolayer, considering fold-change of 2.

Table S3. Gene ontology (GO) term analysis, comparing each 3D and *in vivo* cell culture models with the 2D monolayer cell culture.

Table S4. Additional information regarding the overlapping of significantly altered transcripts in 3D and *in vivo* models when compared to the 2D.